Divide and convert: a decoupled mechanism for hair cell regeneration in the zebrafish inner ear

Marielle O. Beaulieu

A dissertation

submitted in partial fulfillment of the

requirements for the degree of

Doctor of Philosophy

University of Washington

2024

Reading Committee:

David Raible, Chair

Jennifer Stone

Cecilia Moens

Program Authorized to Offer Degree:

Molecular and Cellular Biology

University of Washington

Abstract

Divide and convert: a decoupled mechanism for hair cell regeneration in the zebrafish inner ear

Marielle O. Beaulieu

Chair of the Supervisory Committee:

Professor David Raible

Departments of Otolaryngology – Head and Neck Surgery and Biological Structure

Loss of hearing and balance in humans presents a massive and increasing global health burden. In humans and other mammals, dysfunction of the auditory and vestibular systems is often caused by the death of mechanosensory hair cells in the inner ear, which adult mammals have a limited ability to regenerate. In contrast, non-mammalian vertebrates including zebrafish can robustly regenerate functional hair cells throughout life. Zebrafish hair cell regeneration has been studied extensively in the lateral line, an external sensory system with hair cells and associated supporting cells that are analogous to cells of the inner ear. In comparison, the zebrafish inner ear has been understudied, despite being a highly tractable and regenerative model system that is highly conserved with the inner ear of other vertebrates. The work presented in this dissertation aims to characterize cell types in the zebrafish inner ear and determine when and how zebrafish inner ear hair cells are regenerated. First, single-cell RNA sequencing was used to describe multiple hair and supporting cell subtypes in the zebrafish inner ear, and fluorescent in situ hybridization was used to validate the identities of these cell types in vivo. Addition during growth and regeneration of both hair cell subtypes was then quantified during the larval phase of growth. Finally, by using a marker of cell division, the broad mechanism of regeneration was determined to be a two-step, decoupled process in which supporting cells divide to produce hair cell precursors and,

independently, transdifferentiate into new hair cells. This work has substantially advanced the zebrafish inner ear as a model system for studying hair cell regeneration that will be of immense value in the effort to facilitate hearing and vestibular restoration in mammals.

TABLE OF CONTENTS

LIST OF FIGURES AND TABLES

ACKNOWLEDGEMENTS

So many people have supported me on my journey towards and through graduate school. These are a few people for whom I'd like to express my gratitude.

First, thank you to the past and present mentors who encouraged in me a passion for biology: Meghan Shuff, my high school AP biology teacher, who modeled enthusiasm for science and inspired me to pursue biology as a major in college. Dr. Russ Fernald, in whose lab I first got a taste of scientific research and was first exposed to exciting interdisciplinary scientific discussion. All the folks – instructors and peers – at Friday Harbor Labs, where I got to play field biologist for a couple months and was surrounded by people having so much fun doing science. Dr. Doug Vollrath and Dr. Melissa Calton, who mentored me while I worked as a lab technician after college and helped me develop professional and laboratory skills that would be immensely helpful in graduate school.

Thank you to my graduate supervisor and mentor Dr. David Raible. I joined the Raible lab in the summer of 2019, not knowing that less than nine months later we would be under stay-at-home orders at the beginning of a global pandemic. Through the worst of the pandemic, Dave managed the lab with compassion and understanding and genuinely cared for the health and safety of lab members. Dave supported my ideas for experiments, created a fun and caring lab environment, dedicated time and energy to improving the culture of our departments, and refrained from re-writing any of my important written proposals. At first, the idea of others reading my own scientific writing was absolutely terrifying and a persistent source of perfectionist tendencies. But by not over-editing, Dave pushed me to become so much more confident as a writer, and I think this was one of my biggest areas of growth during graduate school.

Thank you to all the past and present members of the Raible lab: Dr. Andrea McQuate trained me while I was rotating in the lab. She has been such a knowledgeable and caring mentor, always providing encouragement and ready to listen and give support. Tor Linbo provided a wealth of zebrafish and experimental knowledge, and Dr. Robin Gibson kept us and our lab organized and was lightning fast with administrative support. Dr. Francisco Barros-Becker was a cheerleader for fun lab activities and led the charge for our flower-planting wellness activity. Dr. Iván Cruz organized happy hours and trivia and was always available for a chat or feedback. Dr. Madeleine Hewitt provided fellow grad student support and

served as a role model for me in the lab. Tricia Wu and Dr. Selina Baeza-Loya for just so much support and good times and restaurant recommendations. Thanks especially to Iván, Tricia, and Maddy for working alongside me and forming a support network while we were on the Biological Structure DEI committee. We accomplished more together than we ever could have alone. None of our work would be possible without the UW fish facility managers Dave White and Jessica Knight and veterinarian George Sanders, D.V.M..

Thank you to my advisory committee members: Drs. Cecilia Moens, Emily Hatch, Aakanksha Singhvi, and Ron Kwon and my reading committee Drs. Cecilia Moens and Jennifer Stone. Thanks to Dr. Jennifer Stone, Jeff Rasmussen, and Celeste Berg for thoughtful questions and discussion at supergroup lab meetings and to my training grant advisors Drs. David Raible, Joe Sicneros, and David Perkel. Thank you to our collaborators Tuo Shi, Dr. Gage Crump, and Dr. Neil Segil.

Thank you to my MCB cohort of 2018 – we're almost all done! – especially the cohort friends that have been supportive the whole way through. Thanks to all the local friends who provided much needed distraction and fun and who played board games and trivia and kickball with me.

Thank you to my family for supporting me and loving me and allowing me to pursue science as a career. I feel lucky to have close family members that understand the importance of science and that are also fierce competitors at long-distance Mario Kart. Thanks for fun visits and vacations to distract me from work. Thank you also to my partner's family for being so welcoming and supportive and providing much needed laughs during grad school.

Finally, I'd like to thank my partner, the soon-to-be Dr. Daniel Barrero. He has held me through stressful and anxious times, read my drafts and listened to my practice presentations, watched silly and scary movies with me, fed me, and been such a good cat dad. This PhD program introduced us on the first day of interviews and now we're graduating and moving on together. I'm so proud of us and I love you so much.

Marielle O. Beaulieu

Seattle, 2024

CHAPTER 1: INTRODUCTION

Hair cells are the mechanosensory cells of the inner ear that sense sound and head position. In mammals, these vulnerable cells are susceptible to damage from a variety of insults including exposure to ototoxic drugs, noise over-exposure, and age-related degeneration. Consequently, the incidence of auditory and vestibular dysfunction increases with age, causing significant disability and decreased quality of life and representing an increasing global health burden (Agrawal et al., 2013; GBD 2019 USA Hearing Loss Collaborators et al., 2024; Cunningham and Tucci, 2017). Compared to other vertebrates, mammals experience an outsized impact of vestibular and auditory system damage, due to our limited ability to regenerate hair cells. Unlike mammals, non-mammalian vertebrates can robustly regenerate hair cells throughout life. Aside from differences in regeneration potential, the inner ear is highly structurally and functionally conserved across the vertebrate kingdom.

A major goal of the field of inner ear biology has been to understand how non-mammalian vertebrates generate hair cells in the post-embryonic period, with the thought that these lessons could be applied to therapeutic approaches for hair cell loss in humans. Hair cells can be added during initial development and growth of sensory organs, by removal and replacement over time or ‘turnover’, and in regeneration following tissue damage. Here, I will describe the evidence for hair cell addition in these three contexts in the main vertebrate model systems in which they have been studied. Hair cell regeneration has been studied in a wide variety of vertebrates including amphibians (Avallone et al., 2008; Baird et al., 1996; Jones and Corwin, 1996; Taylor and Forge, 2005), but most recent work has been focused on mammals, birds, and fishes. In this chapter I will first describe the anatomy and cellular composition of the inner ear organs, then I will give an overview of hair cell addition and regeneration in mammals, birds, and fishes with a focus on in vivo models. Finally, I will provide the rationale for the zebrafish inner ear studies discussed in subsequent chapters.

1.1 Conserved anatomy and cell types of the inner ear

The general mechanism of action of hair cells is that mechanical deflection of stereocilia at the apical end of the cell causes ion channels to open. This causes the cell to depolarize, sending an

electrical signal to the central nervous system via afferent neuron synapses on the basal side of the cell. Within the inner ear, hair cells are organized in discrete sensory patches in stereotyped orientations that allow them to sense sound and multiple types of head movement (Figure 2.1). The vestibular system contains three semicircular canals of different orientations for sensing angular rotation of the head in different directions. Hair cells in the semicircular canals are found in organs called cristae. Each canal has an enlarged cavity called an ampulla where the crista is located, and hair cell stereocilia bundles protrude from the ampulla into the fluid-filled canal. Rotation of the head results in inertial lag in the fluid of the canals, causing deflection of the hair cell stereocilia and depolarization. The utricle and saccule are two additional vestibular organs with sensory patches called maculae. These organs are overlaid by a gelatinous matrix and one or more calcified 'ear stones' called otoconia (mammals, birds) or otoliths (fish). Tilt, vibration, and gravitational pull on the head result in inertial lag of the otoconia or otolith, causing hair cell bundles projecting into the matrix to deflect and the hair cell to depolarize. Some vertebrates have additional macular organs. The lagena is a third otolith organ present in non-mammalian vertebrates that functions in audition and balance and is thought to be the evolutionary precursor to the more specialized auditory organ seen in birds and mammals (Gacek, 2009; Khorevin, 2008). Fish also have maculae neglecta, patches of hair cells of likely auditory function that develop later in the larval stage and do not have associated otoliths (Bever and Fekete, 2002; Corwin, 1983, 1981). Finally, mammals and birds have a specialized auditory organ in which hair cells are stimulated by sound waves traveling down a long membrane, resulting in tonotopic encoding of sound frequency. This structure is called the cochlea and the sensory organ is called the organ of Corti in mammals or the basilar papilla (BP) in birds. Importantly, fish do not have a similarly specialized auditory organ. Instead, the utricle, saccule, and lagena are all capable of responding to sound (Favre-Bulle et al., 2020; Popper and Fay, 1993; Yao et al., 2016). Often one of these organs plays a larger role in sound detection than the others, but which organ this is varies across fish species (Ladich and Schulz-Mirbach, 2016).

Within hair cell sensory patches, hair cells can be subdivided into distinct morphological and functional types. Amniote vestibular organs contain type I and type II hair cells, which are organized in to central and peripheral (cristae) or striolar and extrastriolar (maculae) regions (Desai et al., 2005b, 2005a; Fernandez and Goldberg, 1976; Jan et al., 2021; Scheibinger et al., 2022). Type I hair cells are identified

by their flask-like shape and calyx-forming associated afferent neurons, while type II hair cells which have shorter cell bodies and bouton-forming associated afferents (Burns and Stone, 2017; Eatock and Songer, 2011; Wersall, 1956). Fish vestibular organs also have distinguishable striolar/extrastriolar and central/peripheral regions (Bang et al., 2001; Chang et al., 1992; Haddon and Lewis, 1996; Jiang et al., 2017; Liu et al., 2022; Platt, 1993; Shi et al., 2023; Tanimoto et al., 2022; Zhu et al., 2021). Fish do not have hair cells with the morphological dimorphism of type I and II hair cells, though there is some evidence for calyx-like afferent terminals in the cristae of goldfish (Lanford and Popper, 1996). In the cristae, all hair cells in an ampulla have the same polarity, while the macular organs display a line of polarity reversal which allows for higher sensitivity to movement in multiple directions (Popper, 1977; Tanimoto et al., 2022). Hair cell diversity in these forms as well as in stereocilia bundle height, physiology, and afferent projections allow for sensitivity to multiple types of stimuli. For a more in-depth review on vestibular system organization see (Baeza-Loya and Raible, 2023; Eatock and Songer, 2011). Amniote auditory organs also display hair cell variability. In the chick BP, hair cells are taller towards the neural side of the organ and shorter towards the abneural side (Rubel and Ryals, 1982; Tanaka and Smith, 1978). In the highly structured mammalian organ of Corti there is one row of inner hair cells juxtaposed with three rows of outer hair cells. Importantly, some subtypes of hair cells are more susceptible to ototoxin damage than others. Striolar hair cells and type I hair cells are more likely to die from aminoglycoside exposure (Forge et al., 1993; Lindeman, 1969; Weisleder and Rubel, 1992; Yan et al., 1997), as are outer hair cells in the organ of Corti (Schacht et al., 2012).

Hair cell production in vertebrates begins during embryogenesis. The developing organs are first comprised of proneural cells. Notch signaling, among other signaling pathways, mediates lateral inhibition that causes proneural cells to differentiate into hair or supporting cells (Atkinson et al., 2015; Daudet and Żak, 2020). Supporting cells are critically important to the function of inner ear sensory organs. These are glia-like cells that maintain ion balance in the surrounding endolymph, phagocytose dying hair cells, and provide physical support to hair cells (Wan et al., 2013). Importantly, supporting cells represent a hair cell precursor population in species that can generate hair cells during regrowth and turnover (Corwin and Cotanche, 1988; Lin et al., 2011; Lopez-Schier and Hudspeth, 2006; Millimaki et al., 2010; Weisleder et

al., 1995). What mechanisms are involved in supporting cell replacement of hair cells is a major area of research and a main motivating question for the work in this thesis.

1.2 Hair cell addition in commonly studied vertebrate systems

Mammals

In the mammalian cristae, developmental hair cell addition begins prenatally, with some continued differentiation and maturation of the organ after birth (Anniko et al., 1979; Nordemar, 1983). Continued proliferation in adulthood is not normally observed in crista support cells in the absence of hair cell damage (Kinoshita et al., 2019). Utricle hair cells also begin to differentiate during gestation, but many peripheral utricular cells continue to divide postpartum, and about half of the total hair cells in the utricle are added in the two weeks after birth (Burns et al., 2012b). The utricle goes on to maintain some ability to add new hair cells under homeostatic conditions. A low level of turnover occurs in the adult mouse utricle (Bucks et al., 2017), and immature hair cells have been observed in older adult guinea pig and human utricles (Forge et al., 1993; Lin and Forge, 1997; Taylor et al., 2015). The window for hair cell addition in the cochlea is earlier and narrower than in the utricle, with terminal mitoses occurring in the mouse between embryonic day 12 and 16 (Ruben, 1967) and differentiation of hair cells between embryonic day 15-17 (Lim and Anniko, 1985; Sher, 1971). Organ of Corti cells remain post-mitotic throughout the life of mammals; no hair cell turnover has been observed in this organ.

Though regeneration potential declines after birth in mammals, there is plasticity in the mammalian auditory and vestibular organs in the late embryonic and early neonatal period. Multiple inducible, genetically encoded methods of hair cell ablation in mice have been developed for studying hair cell regeneration in mammals (Burns et al., 2012a; Golub et al., 2012). When hair cells are ablated in postnatal day 0 (P0) neonates using a transgenic line in which CreER drives production of diphtheria toxin fragment A (DTA) in hair cells, approximately 30% of utricle hair cells die within one to two days of *Cre* recombination. Utricle supporting cell proliferation is subsequently extended by several days postnatally. Hair cells are regenerated over six days post-ablation, with some arising from mitosis of supporting cells and more arising from supporting cell transdifferentiation. If ablation is induced later, at

P5, regeneration is greatly diminished (Burns et al., 2012a). Another study of the neonatal utricle identified a subset of Lgr5-expressing striolar supporting cells that proliferated in response to neomycin or genetically induced hair cell death (Wang et al., 2015). This study used a *Pou4f3*-driven diphtheria toxin receptor (DTR) transgenic mouse line (Golub et al., 2012) as opposed to the CreER-DTA mouse line. In this case, when diphtheria toxin was administered at P1, hair cells were lost gradually until P15. Hair cell numbers recovered significantly but not completely by P30. Both type I and II hair cells were regenerated by a combination of proliferation and transdifferentiation of supporting cells (Wang et al., 2015). Though hair cells were regenerated and reinnervated, the extent to which function is recovered in the utricle after postnatal hair cell ablation is not well understood.

In the perinatal organ of Corti, certain cells can be regenerated with retention of organ function. When certain differentiated supporting cells are ablated in the neonatal mouse cochlea, they can be regenerated over the course of a few days and the animals develop with normal hearing. If these cells are ablated after the onset of hearing or if hair cells are also killed, no regeneration occurs (Mellado Lagarde et al., 2014). When hair cells in the organ of Corti are ablated at P0 either in the *Pou4f3*^{DTR} system or another CreER-DTA model, hair cells are regenerated by direct transdifferentiation of supporting cells (Cox et al., 2014). A small number of new hair cells were also produced by supporting cells that reentered the cell cycle. Though regenerated hair cells follow normal developmental maturation and express markers of mature hair cells, only a fraction of the hair cells lost are replaced and most of those new hair cells do not survive past P15 (Cox et al., 2014). The ability of support cells to transdifferentiate also wanes quickly after birth. Support cells from P6 mice are unable to transdifferentiate and are unresponsive to inhibition of notch signaling (Maass et al., 2015), which generally increases hair cell differentiation. Several possible explanations for this precipitous decrease in regeneration potential have been suggested, including structural (Burns and Corwin, 2014; Collado et al., 2011) and epigenetic (Jen et al., 2019; Tao et al., 2021) changes that occur with organ maturation.

In adult mammals, regeneration is possible but limited in the vestibular organs and nonexistent in the cochlea. In the utricle and cristae, supporting cells can proliferate following aminoglycoside toxicity (Kinoshita et al., 2019; Lopez et al., 1998; Rubel et al., 1995; Warchol et al., 1993). When hair cells are regenerated, a small number arise from supporting cells that divide in response to hair cell death, but the

majority arise from direct transdifferentiation of supporting cells (Bucks et al., 2017; Kawamoto et al., 2009). In the cristae, proliferation is sufficient to maintain support cell numbers during regeneration (Kinoshita et al., 2019; Lopez et al., 1998), but in the utricle few supporting cells divide, resulting in an overall decrease in their number (Golub et al., 2012). Regenerated type II hair cells have active mechanotransduction and are innervated but do not have mature bundle morphology (Golub et al., 2012). For unknown reasons, only type II hair cells are regenerated in the mammalian vestibular organs (Forge et al., 1993; Kawamoto et al., 2009; Lopez et al., 1998). However, production of type I hair cells can be achieved in the adult mouse by deleting *Sox2*, a transcription factor found in type II hair cells (Stone et al., 2021). In contrast to the vestibular organs, the organ of Corti loses potential for proliferation regeneration shortly after birth (Cox et al., 2014; Maass et al., 2015; Roberson and Rubel, 1994; Sobkowicz et al., 1997), and any subsequent hair cell death is permanent. Nevertheless, certain cells from the cochlea and utricle when isolated and cultured regain the ability to proliferate and differentiate into cells that express hair cell markers (Li et al., 2003; White et al., 2006), suggesting that in vivo proliferation could be reinitiated with the right treatment or genetic manipulation. Altering the Notch signaling pathway in the mammalian inner ear confers some extended flexibility to regenerate hair cells (Atkinson et al., 2014; Lin et al., 2011; Liu et al., 2012; Sayyid et al., 2019; Staecker et al., 2007). However, there is evidence that Notch signaling is not required to maintain post-embryonic organ patterning, suggesting that Notch pathway inhibition may not be an effective means of promoting regeneration in cases of acquired hearing loss (Maass et al., 2015).

Birds

The majority of developmental hair cell addition in the chicken utricle occurs between embryonic day 7 and post-hatch day 16, with most of that addition occurring pre-hatch (Goodyear et al., 1999). After this initial population expansion, hair cells continue to be produced via mitosis of support cells to replace older hair cells (Jørgensen, 1991; Jørgensen and Mathiesen, 1988; Roberson et al., 1992; Stone et al., 1999), with a rate of approximately 2% of hair cells turning over per day (Goodyear et al., 1999). Utricular hair cells are estimated to have a half-life of 20-30 days (Goodyear et al., 1999; Kil et al., 1997). When treated with proliferation markers, labeled support cell-type II hair cell pairs are frequently observed,

suggesting that support cells divide asymmetrically to produce new hair cells (Goodyear et al., 1999; Jørgensen and Mathiesen, 1988; Roberson et al., 1992). These divisions are not terminal mitoses, as indicated by the fact that support cells can be dual-labeled after application of two rounds of different markers of proliferation (Jørgensen and Mathiesen, 1988; Stone et al., 1999). In contrast to the utricle, the chick BP undergoes a wave of terminal mitosis over the course of several days during development (Katayama and Corwin, 1989), and hair cells are not added or removed by turnover later-on (Cruz et al., 1987; Jørgensen and Mathiesen, 1988; Mason et al., 1995).

Robust regeneration occurs in the avian vestibular system. Proliferation of support cells is elevated above normal levels in all vestibular epithelia in the chick inner ear following aminoglycoside toxicity in chicks (Kil et al., 1997; Stone et al., 1999; Weisleder and Rubel, 1992). After cessation of aminoglycoside treatment, type I hair cells were completely ablated in the vestibular organs, and type II hair cell numbers were significantly decreased. By 2-3 weeks post-treatment, type II hair cells were present throughout the vestibular organs and few type I cells were observed, and by 8-9 weeks post-treatment the number and patterning of type I and II hair cells showed near complete recovery (Warchol and Speck, 2007; Weisleder and Rubel, 1992). As type I hair cell numbers increase, the number of type II hair cells decreases in the absence of cell death, suggesting that some type II hair cells further differentiate into type I hair cells in the vestibular organs (Weisleder et al., 1995). Vestibular reflexes return to normal following regeneration (Boyle et al., 2002; Dickman and Lim, 2004; Goode et al., 1999).

Despite the lack of homeostatic proliferation and turnover, the adult avian BP can still regenerate hair cells after noise and ototoxin-induced damage (Cotanche, 1987; Ryals and Rubel, 1988). Support cell proliferation is re-initiated after hair cell death (Corwin and Cotanche, 1988; Girod et al., 1989; Ryals and Rubel, 1988; Stone et al., 1999), as is proliferation of hyaline cells along the abneural edge of the sensory epithelium (Girod et al., 1989). However, proliferation is not required for regeneration of some hair cells (Adler and Raphael, 1996). Continuous infusion of the cell division marker BrdU during regeneration in the chick ear has demonstrated that while the majority of regenerated hair cells are produced by mitotic division and differentiation of support cells, the earliest wave of regenerated hair cells is produced by direct transdifferentiation, or fate conversion without de-differentiation and division (Roberson et al., 2004). Regeneration in the avian BP occurs over the span of days to weeks and results

in correct reinnervation of new hair cells and recovery of hearing (Bermingham-McDonogh and Rubel, 2003; Sato et al., 2024). As in other model systems, single cell-RNA sequencing of avian hair and supporting cells during regeneration is beginning to elucidate the underlying signaling pathways at work (Benkafadar et al., 2021; Janesick and Heller, 2019; Matsunaga et al., 2023).

Fishes

Fish inner ear organs grow by adding new cells and expanding in area as the animal grows larger throughout its life. Post-embryonic hair cell addition in the ear has been documented in a wide variety of both cartilaginous and bony fishes, including sharks (Corwin, 1981), rays (Corwin, 1983), and teleost fishes such as cichlids (Popper and Hoxter, 1984), goldfish (Platt, 1977), and zebrafish (Bang et al., 2001; Haddon and Lewis, 1996). In the oscar, a cichlid species, hair cell number increases 34-fold in the saccule as fish grow from 2 cm in length to 17 cm (Popper and Hoxter, 1984). Zebrafish experience a 10-fold increase in hair cells between one month and one year of age (Bang et al., 2001; Higgs et al., 2002). Proliferation of support cells continues across the macular organs into adulthood (Lombarte and Popper, 1994; Popper and Hoxter, 1984). A recent study used proliferation and apoptosis as proxies for hair cell turnover and found low rates of both processes in adult zebrafish (Coffin et al., 2024). Regeneration experiments have also looked at apoptosis in adult zebrafish and goldfish inner ears and show low levels of cell death in undamaged otic organs (Jimenez et al., 2021; Smith et al., 2006). Together these results suggest that adult inner ear hair cells may be long-lived, and that turnover does not occur at high rates in the fish inner ear.

Regeneration of hair cells has historically been understudied in the fish inner ear. A handful of studies have used noise exposure as a means of damaging hair cells. In one study, adult goldfish exposed to loud noise for 48 hours showed temporary auditory threshold shifts and decreased hair cell bundle density in the first two days post-exposure. By one-week post-exposure, auditory thresholds recovered and bundle density showed partial recovery (Smith et al., 2006). A similar study in zebrafish found that proliferation increased in the saccule following damage and recovery of hair cell bundle density by 14 days post-exposure (Schuck and Smith, 2009). More recent work has shown that both the saccule and lagena of zebrafish experience damage as a result of noise overexposure (Lau and Vasconcelos,

2023). Fish inner ear hair cells are susceptible to aminoglycosides delivered by injection, which causes death of striolar cells in the macular organs and auditory threshold shifts (Uribe et al., 2013; Yan et al., 1997). After gentamicin injections in the oscar, approximately half of the hair bundles in the striola of the utricle and lagena were lost, but hair cell bundle density returned to normal within days of cessation of drug administration (Lombarte et al., 1993). Finally, laser ablation has been used to ablate hair cells in the utricle of embryonic zebrafish. This study used lineage tracing to show that after ablation of a small number of hair cells, support cells differentiate into new hair cells without dividing (Millimaki et al., 2010).

More recently, genetically encoded methods have been developed that allow for more effective and widespread ablation of inner ear hair cells. Specifically, a DTR zebrafish line similar to that developed in mice (Golub et al., 2012) has been used to ablate hair cells in the adult zebrafish maculae (Jimenez et al., 2022, 2021). These transgenic fish express DTR under the regulation of the myo6b promoter, which is expressed exclusively in hair cells. Administration of diphtheria toxin results in near complete hair cell loss in the utricle and saccule over the course of five days, accompanied by a vestibular phenotype. After 10 days of recovery in the saccule and 13 days in the utricle, hair cell numbers recover to near-control levels. This ablation paradigm has been used to conduct single-cell RNA sequencing of cells during hair cell regeneration (Jimenez et al., 2022). This study and others in the future will help to clarify gene regulatory networks and molecular mechanisms of hair cell regeneration in the fish inner ear.

In addition to inner ear hair cells, fish and amphibians have an external organ system called the lateral line with hair and support cells that are analogous to those of the ear. Most existing work on hair cell regeneration in fishes has been conducted in the zebrafish lateral line, which has been a powerful model system due to its accessibility for genetic manipulation and imaging (Pickett and Raible, 2019; Sheets et al., 2021). In neuromasts, the sensory organs of the lateral line, hair cells are added in pairs by support cells that divide and symmetrically differentiate into daughter cells of opposing polarity (Lopez-Schier and Hudspeth, 2006; Mackenzie and Raible, 2012; Romero-Carvajal et al., 2015; Wibowo et al., 2011). Neuromast hair cells exhibit a high rate of turnover normally, with a half life of about one week (Cruz et al., 2015). Lateral line hair cells can be easily ablated by incubating fish in ototoxins in the water and regenerate within days (Harris et al., 2003). The source of new hair cells during lateral line regeneration is also support cells, which have spatially and functionally distinct subtypes (Lush et al.,

2019; Thomas and Raible, 2019). Neuromasts in the lateral line exhibit remarkable plasticity and regenerative abilities and can regenerate at least 10 successive times without a decrease in regenerated hair cell number (Cruz et al., 2015). Though the lateral line has been an extremely useful tool, it is ultimately not as comparable to the ear of other vertebrates as the fish inner ear. This has prompted an increasing focus on the zebrafish inner ear as a promising model system for regeneration.

1.3 Advancing the zebrafish inner ear as a model for hair cell regeneration

The mammalian and avian inner ears both have limitations as model organisms in terms of accessibility and manipulability. Both reside within a bony skull, making injections, surgery, and in-vivo imaging invasive and difficult. Currently, explants can only be cultured from very young, pre-hearing animals and do not yet have good longevity. Though the zebrafish inner ear is farther removed evolutionarily from the human ear, zebrafish provide many advantages as a model system. The genetic toolkit available in zebrafish allows for relatively quick and inexpensive production of transgenic lines, and the zebrafish inner ear is still highly conserved with that of other vertebrates. Furthermore, the ear of zebrafish is located superficially, allowing for greater accessibility for injections and live imaging. Zebrafish embryos are optically transparent, and pigment mutants can extend live imaging potential well into the larval stage, when inner ear organs become functional. Our understanding of zebrafish hair cell regeneration in the inner ear is limited compared to the wealth of information that has been generated from lateral line studies. My thesis work focused on characterizing hair cell types and addition in the larval zebrafish inner ear and understanding how the zebrafish ear compares to other model systems, particularly the lateral line. Chapter 2 presents a collaboration using single-cell RNAseq analysis to identify cell subtypes in the zebrafish inner ear and computationally compare them to cells of the lateral line and mammalian ear. In Chapter 3, I take a quantitative approach to characterizing hair cell addition during growth and regeneration in the zebrafish inner ear and identify a previously unrecognized mechanism of hair cell regeneration. Finally, in Chapter 4 I summarize the impact of this work and describe future avenues of potential research.

CHAPTER 2: SINGLE-CELL TRANSCRIPTOMIC PROFILING OF THE ZEBRAFISH INNER EAR REVEALS MOLECULARLY DISTINCT HAIR CELL AND SUPPORTING CELL SUBTYPES

The contents of this chapter have been published in the following journal article:

Shi T*, Beaulieu MO*, Saunders LM, Fabian P, Trapnell C, Segil N, Crump JG, Raible DW. Single-cell transcriptomic profiling of the zebrafish inner ear reveals molecularly distinct hair cell and supporting cell subtypes. Elife. 2023 Jan 4;12:e82978. doi: 10.7554/eLife.82978. PMID: 36598134; PMCID: PMC9851615.

The following authors contributed to the contents of this chapter:

Tuo Shi: Conceptualization, Data curation, Formal analysis, Validation, Investigation, Visualization, Methodology, Writing - original draft, Writing – review and editing; Contributed equally with Marielle O. Beaulieu

Marielle O. Beaulieu: Conceptualization, Data curation, Formal analysis, Validation, Investigation, Visualization, Methodology, Writing - original draft, Writing – review and editing; Contributed equally with Tuo Shi

Lauren M. Saunders: Resources, Software, Methodology

Peter Fabian: Resources, Methodology

Cole Trapnell: Resources, Software, Funding acquisition

Neil Segil: Conceptualization, Funding acquisition

J. Gage Crump: Conceptualization, Supervision, Funding acquisition, Project administration, Writing – review and editing

David W. Raible: Conceptualization, Resources, Formal analysis, Supervision, Funding acquisition, Investigation, Project administration, Writing – review and editing

Supplementary files can be accessed at: https://elifesciences.org/articles/82978/figures#files

2.1 Abstract

A major cause of human deafness and vestibular dysfunction is permanent loss of the mechanosensory hair cells of the inner ear. In non-mammalian vertebrates such as zebrafish, regeneration of missing hair cells can occur throughout life. While a comparative approach has the potential to reveal the basis of such differential regenerative ability, the degree to which the inner ears of fish and mammals share common hair cells and supporting cell types remains unresolved. Here we perform single-cell RNA sequencing of the zebrafish inner ear at embryonic through adult stages to catalog the diversity of hair cells and non-sensory supporting cells. We identify a putative progenitor population for hair cells and supporting cells, as well as distinct hair and supporting cell types in the maculae versus cristae. The hair cell and supporting cell types differ from those described for the lateral line system, a distributed mechanosensory organ in zebrafish in which most studies of hair cell regeneration have been conducted. In the maculae, we identify two subtypes of hair cells that share gene expression with mammalian striolar or extrastriolar hair cells. In situ hybridization reveals that these hair cell subtypes occupy distinct spatial domains within the three macular organs, the utricle, saccule, and lagena, consistent with the reported distinct electrophysiological properties of hair cells within these domains. These findings suggest that primitive specialization of spatially distinct striolar and extrastriolar hair cells likely arose in the last common ancestor of fish and mammals. The similarities of inner ear cell type composition between fish and mammals validate zebrafish as a relevant model for understanding inner ear-specific hair cell function and regeneration.

2.2 Introduction

Mechanosensory hair cells of the inner ear are responsible for sensing sound and head position in vertebrates. Hair cells are notoriously susceptible to damage from multiple types of insults, including noise and ototoxic drug exposure. Studies of hair cell physiology in mammals are limited by the location of the inner ear within the temporal bone, which precludes many targeted manipulations and in vivo imaging beyond the neonatal stage. As a result, non-mammalian vertebrates with analogous, more easily accessible hair cells have become useful models for studying hair cell development, death, and

regeneration. Non-mammalian vertebrates such as birds and fish can regenerate hair cells of the auditory and vestibular systems that are lost due to injury (Monroe et al., 2015; Stone and Cotanche, 2007). This differs from mammals, where cochlear hair cell death leads to permanent hearing loss (Corwin and Cotanche, 1988; Yamasoba and Kondo, 2006), and limited regeneration of vestibular hair cells results in minimal recovery of function (Golub et al., 2012). Non-mammalian model systems of hair cell regeneration have the potential to reveal conserved pathways that can be targeted to promote hair cell survival and regeneration in humans. However, the extent of hair cell molecular homology across vertebrates remains unclear.

Due to its accessibility for manipulation and imaging, the zebrafish lateral line system has been widely used to study mechanisms of hair cell physiology (Pickett and Raible, 2019; Sheets et al., 2021). The lateral line is an external sensory system that allows aquatic vertebrates to detect local movement of water. Sensory organs of the lateral line, called neuromasts, contain hair cells and supporting cells that share properties with those of the inner ear. However, relative to the lateral line, cells in the zebrafish inner ear are likely more similar to their mammalian counterparts, raising the potential for it to be a more comparable system in which to study hair cell function.

Zebrafish and mammals share several inner ear sensory organs. Three semicircular canals with sensory end organs called cristae sense angular rotation of the head. Two additional sensory end organs detect linear acceleration and gravity: the utricular and saccular macula each with an associated otolith crystal (Figure 2.1). Fish lack a specific auditory structure such as the mammalian cochlea and instead sense sound through the saccule, utricle, and a third otolith organ, the lagena. Although historically the saccule and utricle were thought to be for vestibular function and the lagena analogous to the cochlea for sound detection, there is now substantial evidence for all three otolith end organs being used for sound detection with diverse specializations across fishes (Popper and Fay, 1993). Zebrafish exhibit behavioral responses to sound frequencies between 100-1200 Hz (Bhandiwad et al., 2013; Zeddies and Fay, 2005), and neural responses up to 4000 Hz (Poulsen et al., 2021). In larval zebrafish, both saccule and utricle hair cells respond to vibration stimuli, with the utricle responding to relatively lower frequencies than the saccule, as well as additive effects when both are stimulated (Favre-Bulle et al., 2020; Yao et al., 2016).

Within the mammalian utricle and saccule, there are both morphological and spatial differences between hair cells (Eatock and Songer, 2011; Lysakowski and Goldberg, 2004). Hair cells are broadly classified by their morphology and innervation, with Type I hair cells having calyx synapses surrounding the hair cell body and Type II hair cells having bouton synapses. Both Type I and Type II cells can be found within the central region of the macular organs known as the striola and in the surrounding extrastriolar zones. Although the role of spatial segregation into striolar versus extrastriolar zones has not been fully elucidated, hair cells across these regions vary in morphology, electrophysiology, and synaptic structure (Desai et al., 2005b; Li et al., 2008). The striola is characterized by hair cells with taller ciliary bundles and encompasses a line of polarity reversal where hair cells change their stereocilia orientation (Figure 2.1E). Whereas distinct Type I and Type II hair cells, and in particular the calyx synapses typical of Type I cells, have not been identified in fishes, spatial heterogeneity in the maculae, including those of zebrafish, has been previously noted (Chang et al., 1992; Liu et al., 2022; Platt, 1993; Popper, 2000). However, the homologies of cells at the cellular and molecular levels have remained unknown.

Recent single-cell and single-nucleus RNA-sequencing efforts have generated a wealth of transcriptomic data from hair cells in several model systems, facilitating more direct comparison of cell types and gene regulatory networks between species. Although single-cell transcriptomic data have recently been published for the zebrafish inner ear (Jimenez et al., 2022; Qian et al., 2022), the diversity of hair cell and supporting cell subtypes has not been thoroughly analyzed. In order to better understand the diversification of cell types in the zebrafish inner ear, and their relationships to those in mammals, here we perform single-cell and single-nucleus RNA sequencing of the zebrafish inner ear from embryonic through adult stages. We find that hair and supporting cells from the zebrafish inner ear and lateral line are transcriptionally distinct, and that hair and supporting cells differ between the cristae and maculae. All of these distinct cell types are present during larval development and are maintained into adulthood. In situ hybridization reveals that these hair cell subtypes occupy distinct spatial domains within the utricle, saccule, and lagena, and computational comparison of hair cell types reveals homology with striolar and extrastriolar hair cell types in mammals. These findings point to an origin of striolar and extrastriolar hair cell types in at least the last common ancestor of fish and mammals.

2.3 Results

Inner ear hair cells and supporting cells are distinct from those of the lateral line

To assess differences between inner ear and lateral line cells, we analyzed a subset of cells from a large single-nucleus RNA-seq dataset of whole zebrafish at embryonic and larval stages (24-96 hours post-fertilization (hpf)), which was prepared by single-nucleus combinatorial indexing and sequencing ("sci-Seq"; (Saunders et al., 2023)). Within an initial dataset of 1.25 million cells from 1233 embryos spanning 18 timepoints between 18 and 96 hours (see Saunders et al., 2022 for more detail), a total of 16,517 inner ear and lateral line cells were isolated, combined, and re-processed using Monocle 3 (Figure 2.2A-B). Initially, otic vesicle and lateral line cell clusters were identified by *eya1* expression (Sahly et al., 1999) in combination with the following known marker genes. Inner ear nonsensory cells were identified by expression of the transcription factor gene *sox10* (Dutton et al., 2009) in combination with inner ear supporting cell genes *(stm*, *otog*, *otogl*, *otomp*, *tecta*, and *oc90*; Figure 2.2C) (Kalka et al., 2019; Petko et al., 2008; Söllner et al., 2003; Stooke-Vaughan et al., 2015). Lateral line nonsensory cells were identified by expression of known markers *fat1b*, *tfap2a, tnfsf10l3, lef1, cxcr4b, fgfr1a*, and *hmx3a* (Figure 2.2D) (Feng and Xu, 2010; Haas and Gilmour, 2006; Lee et al., 2016; McGraw et al., 2011; Steiner et al., 2014; Thomas and Raible, 2019). We identified hair cells by expression of the pan-hair cell genes *otofb*, *cdh23, pcdh15a, ush1c, myo7aa, slc17a8*, and *cacna1da* (Figure 2.2E) (Chatterjee et al., 2015; Ernest, 2000; Obholzer et al., 2008; Phillips et al., 2004; Seiler et al., 2005; Sheets et al., 2012; Söllner et al., 2004). To distinguish between inner ear and lateral line hair cells, we queried expression of previously described markers for inner ear (*gpx2*, *kifl*, *strc*, and *lhfpl5a*) and lateral line (*strc1*, *lhfpl5b*, and *s100t*) (Erickson et al., 2020; Erickson and Nicolson, 2015). Although many of these markers are at low abundance, these populations are marked distinctly by *strc* and *s100t* (Figure 2.2F). We used Monocle3 to identify differentially expressed genes (Supplementary File 1) and to generate modules of co-expressed genes (Figure 2.2.S1, Supplementary File 2).

Both hair cells and nonsensory supporting cells from the inner ear and lateral line formed distinct clusters, with nonsensory cells from the two mechanosensory organs showing greater distinction than hair cells (Figure 2.2B, Figure 2.2.S2A). To confirm the relative differences between inner ear and lateral line hair cells and nonsensory cells, Partition-based Graph Abstraction (PAGA) analysis was used to

measure the connectivity of clusters (Wolf et al., 2019). PAGA analysis revealed strong connectivity within inner ear supporting cell clusters and within lateral line supporting cell clusters but little connectivity between them (Figure 2.2.S2A, Supplementary File 3).

The inner ear nonsensory cluster includes structural cells forming the otic capsule, identified by expression of the extracellular matrix protein-encoding genes *collagen type 2 a1a* (*col2a1a*) and *matrilin 4* (*matn4*) (Xu et al., 2018), as well as sensory supporting cells expressing *lfng* (Figure 2.3D; Figure 2.2.S2B). Inner ear and lateral line supporting cells remain as distinct clusters even when structural *matn4*+ cells are excluded from analysis (Figure 2.2.S2C). Thus, both hair cells and supporting cells have distinct gene expression profiles between the inner ear and lateral line at embryonic and larval stages.

Single-cell RNA-seq reveals distinct hair cell and supporting cell populations in the juvenile and adult inner ear of zebrafish

To identify distinct subtypes of inner ear hair cells and supporting cells from larval through adult stages, we first re-analyzed single-cell RNA sequencing (scRNA-seq) datasets from larval stages (72 and 120 hpf) (Fabian et al., 2022), in which otic placode cells and their descendants were labeled with *Sox10*:Cre to induce recombination of an ubiquitous *ubb*:LOXP-EGFP-STOP-LOXP-mCherry transgene (Kague et al., 2012). We also performed additional scRNA-seq using these transgenic lines by dissecting ears from juvenile (14 days post-fertilization (dpf)), and adult (12 months post-fertilization (mpf)) animals. Following cell dissociation and fluorescence-activated cell sorting (FACS) to purify mCherry+ cells, we constructed scRNA-seq libraries using 10x Chromium technology. For all datasets, hair cells and supporting cells were identified for further analysis based on the expression of hair cell markers *myo6b* and *strc* and supporting cell markers *stm* and *lfng*; structural cells were removed from further analysis based on expression of *matn4* and *col2a1a* (Figure 2.3.S1). Using Seurat, we integrated this dataset with the sci-Seq embryonic and larval dataset (36-96 hpf) (Figure 2.3A,B). The combined dataset comprises 3246 inner ear cells separated into 10 groups based on unsupervised clustering, with differentially expressed genes for each cluster shown in Figure 2.3E and Supplementary File 4. We identified 6 clusters of hair cells based on shared expression of *myo6b*, *strc*, *lhfpl5a*, and *gfi1aa* (Yu et al., 2020), a nascent hair cell cluster based on expression of *atoh1a* (Millimaki et al., 2007)and the Notch ligand *dla*

(Riley et al., 1999), and two clusters of supporting cells based on expression of *lfng* and *stm* (Figure 2.3C,D, Figure 2.3.S2). An additional putative progenitor cluster (cluster 0), enriched for cells from embryonic stages, is characterized by expression of genes such as *fgfr2* (Rohs et al., 2013), *fat1a* (Down et al., 2005), *igsf3*, and *pard3bb* (Figure 2.3.S3). Although these marker genes are differentially expressed in the putative progenitor cluster, some of them (e.g. *fat1a* and *pard3bb*) retain a lower expression level in supporting cell populations (Figure 2.3.S3F). This is further demonstrated by gene modules of these clusters (Figure 2.3.S4, Supplementary File 5), where the progenitor signature module genes (Module 1) are expressed in lower levels in the supporting cell clusters. This transcriptional relatedness between progenitors and supporting cells may underlie the role of supporting cells as a resident stem cell population during zebrafish hair cell regeneration.

Developmental trajectories in the inner ear

To understand potential lineage relationships between clusters, we performed pseudotime trajectory analysis using Monocle3. We anchored the pseudotime projection at the putative progenitor cell cluster. Analysis revealed two major trajectories toward hair cells and supporting cell clusters for both maculae and cristae (Figure 2.4A,B, Figure 2.4.S1), with distinct patterns of gene expression along each trajectory (Supplementary File 6). We find that average gene expression of the putative progenitor (Cluster 0) markers follow two patterns: decreasing along both hair cell and supporting cell trajectories (*fgfr2* and *igsf3*) and decreasing only along the hair cell trajectory (*fat1a* and *pard3bb*) (Figure 2.4C,D, Figure 2.4.S1B,C). The hair cell trajectory progresses first through a stage marked by expression of *dla* and then *atoh1a* (Cluster 2, Figure 2.4E, Figure 2.4.S1D). Concurrent with decreasing expression of nascent hair cell genes, we observe increasing expression of mature hair cell genes *gfi1aa* and *myo6b* (Figure 2.4F, Figure 2.4.S1E). Along the supporting cell trajectory we observed upregulation of supporting cell-specific markers, including *stm* and *lfng* (Figure 2.4G, Figure 2.4.S1F). These bifurcating lineage trajectories from Cluster 0 (Figure 2.4A) to hair and supporting cell clusters are consistent with the identification of Cluster 0 as a population of bipotent progenitors regulated by Notch signaling during early development (Haddon et al., 1998; Riley et al., 1999). To localize these developmental stages in vivo, we examined *dla* expression by in situ hybridization (Figure 2.4.S2). We find that *dla* is expressed in

supporting cells adjacent to myo6:GFP hair cells in both cristae and maculae, consistent with peripheral addition of new cells at the margins of the sensory patches.

Distinct supporting cell types in the cristae versus maculae

Supporting cells comprise two major clusters that can be distinguished by expression of *tectb* and *zpld1a* among other genes (Figure 2.3C, see Supplementary File 7 for differentially expressed genes). The *tectb* gene encodes Tectorin beta, a component of the tectorial membrane associated with cochlear hair cells in mammals (Goodyear et al., 2017), and a component of otoliths in zebrafish (Kalka et al., 2019). The z*pld1a* gene, encoding Zona-pellucida-like domain containing protein 1a, is expressed in the cristae in fish (Dernedde et al., 2014; Yang et al., 2011) and mouse (Vijayakumar et al., 2019). Using fluorescent in situ hybridization, we find that *tectb* is expressed in the macular organs but not cristae, and *zpld1a* is expressed in cristae but not maculae (Figure 2.5C,D). Neither were detected in lateral line neuromasts (Figure 2.5C,D), showing they are inner ear-specific genes. Both *tectb* and *zpld1a* are expressed primarily in supporting cells, as they show little overlap in expression with the hair cell marker *myo6b*:GFP, similar to expression of the supporting cell marker *lfng* (Figure 2.5B-D, Figure 2.5.S1). These results demonstrate the presence of distinct supporting cell subtypes for the maculae and cristae.

Distinct types of hair cells in the zebrafish inner ear

While inner ear and lateral line hair cells share many structural and functional features, we sought to determine if these cells also have distinct molecular signatures. We compared published datasets of lateral line hair cells (Baek et al., 2022; Kozak et al., 2020; Ohta et al., 2020) to our data, restricting analysis to datasets generated by 10x Chromium preparation to avoid technical batch effects across studies. Using Scanorama for alignments (Hie et al., 2019), hair cells from the inner ear and lateral line form distinct clusters, with a number of differentially expressed genes (Figure 2.2.S3), including the known markers for lateral line (*s100t*) and inner ear (*strc*) (Figure 2.2). This analysis suggests that inner ear hair cells of the maculae and cristae are more similar to each other than to lateral line hair cells.

Within the maculae and cristae, we find that hair cells can be subdivided into two major groups (clusters 1 and 3 versus cluster 4). These clusters are distinguished by differential expression of a

number of genes including two calcium binding protein genes, *cabp1b* and *cabp2b* (Di Donato et al., 2013) (Figure 2.3E). Hair cell cluster 5 has a mixed identity with co-expression of a number of genes shared between these two groups, including *cabp1b* and *cabp2b*.

We next tested the in vivo expression of genes in each cluster using in situ hybridization, choosing *cabp1b* and *cabp2b* as representative markers for each cluster (Figure 2.6A). In the larval cristae, utricle, and saccule, *cabp1b* and *cabp2b* mark *myo6b*+ hair cells in largely non-overlapping zones (Figure 2.6B-D). By adult stages, complementary domains of *cabp1b*+ and *cabp2b*+ hair cells become clearly apparent (Figure 2.6E-K). In the adult utricle, a central crescent of *cabp2b+; myo6b*+ hair cells is surrounded by a broad domain of *cabp1b*+; *myo6b*+ hair cells. In the saccule and lagena, a late developing sensory organ, central *cabp2b+; myo6b*+ hair cells are surrounded by peripheral *cabp1b+; myo6b*+ hair cells. We also find several genes that are specific for hair cells in the cristae, utricle, or saccule (Figure 2.7A). These include the calcium binding protein gene *cabp5b* in the cristae, the transcription factor *skor2* in the utricle, and the deafness gene *loxhd1b* in the saccule (Figure 2.7B-D, Figure 2.7.S1).

The domain organization of hair cells in the adult macular organs resembles that of striolar and extrastriolar hair cells in the mammalian utricle. We therefore examined expression of *pvalb9*, the zebrafish ortholog of the mouse striolar hair cell marker *Ocm* (Hoffman et al., 2018; Jiang et al., 2017) (Figure 2.8, Figure 2.8.S1). In the larval utricle, we observe near complete overlap of *pvalb9* with *cabp2b* (Figure 2.8B-D). In the adult utricle, there is substantial overlap of *pvalb9* with *cabp2b* expression (except for a thin strip of *pvalb9*+; *cabp2b*- cells), and little overlap with *cabp1b* expression (Figure 2.8F,G). In addition, anti-Spectrin staining of hair bundles reveals a line of polarity reversal within the *cabp2b*+ domain of the utricle (Figure 2.8H,I), consistent with polarity reversal occurring within the striolar domains of mammalian macular organs (Li et al., 2008). Cluster 1/3 (*cabp1b*+) and Cluster 4 (*cabp2b*+) populations also differentially express genes related to stereocilia tip link and mechanotransduction channel components (Figure 2.8.S2, Supplementary File 8) and various calcium and potassium channels (Figure 2.8.S3, Supplementary File 8). We also note that the utricle marker *skor2* labels primarily extrastriolar hair cells within this end organ, with *loxhd1b* labeling striolar hair cells within the saccule. These findings suggest that zebrafish Cluster 4 (*cabp2b*+) and Cluster 1/3 (*cabp1b*+) hair cells largely

correspond to striolar and extrastriolar hair cells, respectively, with distinct mechanotransduction and synaptic properties.

Global homology of striolar and extrastriolar hair cells between fish and mice

To further probe similarities between zebrafish Cluster 4 (*cabp2b*+) and Cluster 1/3 (*cabp1b*+) hair cells versus striolar and extrastriolar hair cells in mammals, we utilized the Self-Assembling Manifold mapping (SAMap) algorithm (Musser et al., 2021; Tarashansky et al., 2019) to compare cell types across distant species. A strength of this algorithm is that it compares not only homologous gene pairs but also close paralogs, which is especially useful considering the extensive paralog switching observed between vertebrate clades (Postlethwait, 2007), as well as the extra round of genome duplication in the teleost lineage leading to zebrafish. When comparing adult zebrafish maculae with the postnatal mouse utricle (Jan et al., 2021), we find the highest alignment score between supporting cells (Figure 2.9A). Consistent with the spatial domains revealed by our in situ gene expression analysis, we find that mouse striolar Type I hair cells exclusively map to zebrafish Cluster 4 (*cabp2b*+) hair cells, and mouse extrastriolar Type I and Type II hair cells predominantly to zebrafish Cluster 1/3 (*cabp1b*+) hair cells. In contrast, zebrafish lateral line hair cells (Lush et al., 2019) align exclusively to mouse extrastriolar and not striolar hair cells (Figure 2.9.S1). The small degree of mapping of mouse extrastriolar Type I hair cells to zebrafish Cluster 4 (*cabp2b*+) hair cells suggests that zebrafish Cluster 4 (*cabp2b*+) hair cells may have more of a Type I identity than Cluster 1/3 (*cabp1b*+) cells in general. Gene pairs driving the homology alignment include striolar markers *Ocm*, *Loxhd1*, and *Atp2b2* for zebrafish Cluster 4 (*cabp2b*+) hair cells, and mouse extrastriolar markers *Tmc1*, *Atoh1*, and *Jag2* for zebrafish Cluster 1/3 (*cabp1b*+) hair cells (Supplementary File 9). Thus, zebrafish Cluster 4 (*cabp2b*+) macular hair cells are closely related to striolar cells of the mouse utricle, with zebrafish lateral line and Cluster 1/3 (*cabp1b*+) macular hair cells more closely related to mouse extrastriolar hair cells.

A recent single-cell study revealed distinct central versus peripheral hair cell subpopulations in postnatal mouse cristae, reminiscent of the striolar and extrastriolar populations in the maculae (Wilkerson et al., 2021). As our zebrafish cristae hair cells also separate into distinct clusters, Cluster 9 (*cabp1b*+) and Cluster 8 (*cabp2b*+) (Figure 2.6A,B), we performed SAMap analysis between the crista

cell populations of the two species to investigate cell type homology. Similar to what we observed for the utricle, zebrafish centrally located Cluster 8 crista hair cells predominantly map to mouse central crista hair cells, and zebrafish peripherally located Cluster 9 crista hair cells exclusively map to mouse peripheral crista hair cells (Figure 2.9B, see Supplementary Files 10 and 11 for differentially expressed genes in Cluster 8 and Cluster 9 hair cells and gene pairs driving homology). Conserved types of spatially segregated HCs therefore exist in both the maculae and cristae of zebrafish and mouse.

2.4 Discussion

Our single-cell transcriptomic profiling of the embryonic to adult zebrafish inner ear reveals a diversity of hair cell and supporting cell subtypes that differ from those of the lateral line. As much of our knowledge about zebrafish hair cell regeneration comes from studies of the lateral line, understanding similarities and differences between the lateral line and inner ear has the potential to uncover mechanisms underlying the distinct regenerative capacity of inner ear hair cell subtypes. Recent tools to systematically damage inner ear hair cells in zebrafish (Jimenez et al., 2021) should enable such types of comparative studies.

We identify hair cells and supporting cells specific for maculae versus cristae, as well as two spatially segregated types of zebrafish inner ear hair cells with similarities to mammalian striolar and extrastriolar hair cells. These molecular signatures are conserved across larval and adult stages. However, consistent with other recent work (Jimenez et al., 2022; Qian et al., 2022), we were not able to resolve distinct clusters of hair cells or supporting cells corresponding to the distinct types of maculae: i.e. utricle, saccule, and lagena.

The division of auditory and vestibular function across the otolith organs in zebrafish remains somewhat unclear. The saccule is thought to act as the primary auditory organ of larval zebrafish, as the utricle is not necessary for sound detection above low frequencies (Yao et al., 2016). In the zebrafish adult, excess sound exposure can damage the saccule, while damage to the utricle is unknown (Schuck and Smith, 2009). Conversely, the utricle is critical for larval vestibular function, while input from the saccule is unnecessary (Riley and Moorman, 2000). However, there is contrasting evidence for overlap in function of both saccule and utricle for sound detection in larvae (Favre-Bulle et al., 2020; Poulsen et al., 2021).

Currently we are not able to identify clearly distinct hair cell types in the utricle compared to the saccule that might reflect functional differences; whether such genetic signatures exist remains an important question that will require further in-depth analysis. It is interesting to note that mammalian vestibular end organs are also capable of responding to high-frequency sound stimuli (reviewed in Curthoys, 2017), suggesting that sound detection by hair cells may not be linked to a distinct end organ-specific molecular signature.

Our study supports zebrafish possessing distinct types of striolar and extrastriolar hair cells in the maculae and cristae, with molecular differences between these subtypes implying different physiological properties. Zebrafish striolar and extrastriolar hair cell subtypes express distinct combinations of ion channel genes and mechanotransduction components, consistent with previous reports of distinct current profiles in central versus peripheral hair cells in the zebrafish utricle, saccule, and lagena (Haden et al., 2013; Olt et al., 2014), as well as spatial differences in ciliary bundle morphology and synaptic innervation in the larval zebrafish utricle (Liu et al., 2022). The distinct spatial distribution, channel expression, and hair bundle morphologies in these hair cells resembles the known spatial, electrophysiological, and hair bundle compositional differences seen in the striolar versus extrastriolar hair cells in the amniote vestibular end organs (Holt et al., 2007; Kharkovets et al., 2000; Lapeyre et al., 1992; Meredith and Rennie, 2016; Moravec and Peterson, 2004; Rüsch et al., 1998; Xue and Peterson, 2006).

In each of the zebrafish end organs, striolar and extrastriolar hair cells can be defined by differential expression of calcium binding proteins, in particular *cabp1b* versus *cabp2b*. As these calcium binding proteins closely interact with synaptic calcium channels (Cui et al., 2007; Picher et al., 2017) with potential functionally different consequences (Yang et al., 2018), their differential expression may confer unique electrophysiological properties to each cell type. Mutations in human *CABP2* associated with the autosomal recessive locus DFNB93 result in hearing loss (Picher et al., 2017; Schrauwen et al., 2012), underlining its functional importance. Even though we chose *cabp1b* and *cabp2b* as characteristic markers for zebrafish extrastriolar and striolar regions, it is worth noting that *Cabp2*, but not *Cabp1*, is expressed in all mouse postnatal utricular hair cells with differentially higher expression in the striola (Jan et al., 2021). Of note, lateral line hair cells express higher levels of *cabp2b* than *cabp1b* (Lush et al., 2019), despite our analysis suggesting that they are more closely related to extrastriolar hair cells. These

observations emphasize the importance of examining global patterns of gene expression rather than individual markers when assigning homology of cell types.

By contrast, we found no clear homology of zebrafish inner ear hair cells with mammalian Type I and Type II hair cells. The lack of molecular signatures corresponding to Type I hair cells is consistent with previous reports that one of their major features, calyx synapses, are absent from fishes (Lysakowski and Goldberg, 2004). These findings suggest that the diversification of inner ear hair cells into Type I and Type II cells emerged after the evolutionary split of ray-finned fishes from the lineage leading to mammals.

We recognize that identifying cell type homology across tissues and species through molecular analysis has several potential caveats. Although we have collected transcriptomic data from the zebrafish inner ear from a wide range of developmental stages, we are limited by the fact that the publicly available datasets for zebrafish lateral line and mouse utricle and cristae are restricted to immature stages. Thus, cell maturity could be a confounder in our analyses. However, when we limited the comparison of lateral line hair cells and postnatal mouse vestibular hair cells to 3-5 dpf inner ear hair cells, we see similar alignments as when we used our 12 mpf data (Figure 2.9.S1). In addition, we collected fewer supporting cells from adult zebrafish than expected, skewing cell type representation towards hair cells (Figure 2.3C). Thus, additional optimization may be needed to further interrogate the cell subtypes within zebrafish inner ear supporting cell populations.

Nonetheless, our integrated dataset reveals distinct molecular characteristics of hair cells and supporting cells in the zebrafish inner ear sensory organs, with conservation of these patterns from larval stages to adults. Although not discussed in detail here, our data include additional cell populations of the zebrafish inner ear that express extracellular matrix-associated genes important for otic capsule structure and ion channel-associated genes associated with fluid regulation. These data form a resource that can be further explored to inform molecular aspects of hair cell electrophysiology, mechanotransduction, sound versus motion detection, maintenance of inner ear structure and ionic balance, and inner ear-specific hair cell regeneration.

2.5 Materials and Methods

Zebrafish lines

This study was performed in strict accordance with the recommendations in the Guide for the Care and Use of Laboratory Animals of the National Institutes of Health. The Institutional Animal Care and Use Committees of the University of Southern California (Protocol 20771) and University of Washington (Protocol 2997-01) approved all animal experiments. Experiments were performed on zebrafish (*Danio rerio*) of AB or mixed AB/Tubingen background. For adult stages, mixed sexes of animals were used for constructing single-cell libraries, as well as RNAScope experiments. Published lines include *Tg(Mmu.Sox10-Mmu.Fos:Cre)*^{zf384} (Kague et al., 2012); *Tg(-3.5ubb:LOXP-EGFP-STOP-LOXP-mCherry)*^{cz1701Tg} (Mosimann et al., 2011)*;* and *Tg(myosin 6b:GFP)*^{w186} (Hailey et al., 2017).

In situ hybridization and RNAScope

Hybridization chain reaction in situ hybridizations (Molecular Instruments, HCR v3.0) were performed on 5 dpf *myo6b*:GFP larvae as directed for whole-mount zebrafish embryos and larvae (Choi et al., 2018, 2016). Briefly, embryos were treated with 1-phenyl 2-thiourea (PTU) beginning at 24 hpf. At 5 dpf, larvae were fixed in 4% PFA overnight at 4°C. Larvae were washed with PBS and then stored in MeOH at -20°C until use. Larvae were rehydrated using a gradation of MeOH and PBST washes, treated with proteinase K for 25 min and post-fixed with 4% PFA for 20 min at room temperature. For the detection phase, larvae were pre-hybridized with a probe hybridization buffer for 30 min at 37°C, then incubated with probes overnight at 37°C. Larvae were washed with 5X SSCT to remove excess probes. For the amplification stage, larvae were pre-incubated with an amplification buffer for 30 min at rt and incubated with hairpins overnight in the dark at rt. Excess hair pins were removed by washing with 5X SSCT. Larvae were treated with DAPI and stored at 4°C until imaging. All HCR in situ patterns were confirmed in at least 3 independent animals. Transcript sequences submitted to Molecular Instruments for probe generation are listed in Supplementary File 12. The *cabp1b* probes were tested on 3 separate occasions and imaged in at least 6 animals; *cabp2b* probes were tested on 5 separate occasions and imaged in at least 20 different animals; *cabp5b* probes were tested on 3 separate occasions and imaged in at least 9 different animals; *lfng* probes were tested on two separate occasions and imaged in at least 5 different animals; *loxhd1b* probes were tested on two separate occasions and imaged in at least 7 animals; *pvalb9* probes

were tested on two separate occasions and imaged in at least 6 different animals; *skor2* probes were tested on two separate occasions and imaged in at least 6 different animals; *tectb* probes were tested on 4 separate occasions and imaged in at least 10 different animals; *zpld1a* probes were tested on 3 separate occasions and imaged in at least 9 different animals.

RNAScope samples were prepared by fixation in 4% paraformaldehyde either at room temperature for 2 hours or at 4 °C overnight. Adult (28-33mm) inner ears were dissected and dehydrated in methanol for storage. RNAScope probes were synthesized by Advanced Cell Diagnostics (ACD): Channel 1 probe *myo6b* (1045111-C1), Channel 2 probe *pvalb9* (1174621-C2), and Channel 3 probes *cabp1b* (1137731-C3) and *cabp2b* (1137741-C3). Whole inner ear tissues were processed through the RNAScope Fluorescent Multiplex V2 Assay (ACD Cat. No. 323100) according to manufacturer's protocols with the ACD HybEZ Hybridization oven. *cabp1b* probe was tested on 4 separate occasions with 6 animals or 12 ears total; *cabp2b* probe was tested on 4 separate occasions with 7 animals or 14 ears total; *pvalb9* probe was tested on 2 separate occasions with 6 animals or 12 ears total. *myo6b* probe was used with each of the above probes.

Immunofluorescence staining

Immediately following the RNAScope protocol, samples were prepared for immunofluorescence staining using mouse anti-β-Spectrin II antibody (BD Bioscience Cat. No. 612562, RRID: AB_399853). Briefly, RNAScope probed zebrafish ears were rehydrated in PBS for 5 min and rinsed in PBDTx (0.5 g bovine serum albumin, 500 µL DMSO, 250 µL 20% Triton-X in 50 mL PBS, pH = 7.4) for 15 min at room temperature. They were then blocked in 2% normal goat serum (NGS) in PBDTx for 3 hours at room temperature, and incubated with 1:500 dilution of mouse anti-β-Spectrin II antibody in PBDTx containing 2% NGS overnight at 4 °C. After 3 washes in PBDTx for 20 min each at room temperature, samples were incubated with 1:1000 dilution of Alexa 647 goat-anti-mouse IgG1 secondary antibody (Invitrogen Cat. No. A-21240, RRID: AB_2535809) for 5 hours at room temperature. They were then washed 2 times in PBSTx (250 µL 20% Triton-X in 50 mL PBS) for 5 min each before imaging. Three animals or 6 ears total were subjected to Spectrin detection on 2 separate occasions.

Imaging

Confocal images of whole-mount RNAScope samples were captured on a Zeiss LSM800 microscope (Zeiss, Oberkochen, Germany) using ZEN software. HCR-FISH imaging was performed on a Zeiss LSM880 microscope (Zeiss, Oberkochen, Germany) with Airyscan capability. Whole larvae were mounted between coverslips sealed with high vacuum silicone grease (Dow Corning) to prevent evaporation. Z-stacks were taken through the ear at intervals of 1.23 µm using a 10X objective or through individual inner ear organs at an interval of 0.32 µm using a 20X objective. 3D Airyscan processing was performed at standard strength settings using Zen Blue software.

Single-cell preparation and analysis

scRNA-seq library preparation and alignment

For 14 dpf animals (n=35), heads from converted *Sox10:Cre; ubb:LOXP-EGFP-STOP-LOXP-mCherry* fish were decapitated at the level of the pectoral fin with eyes and brains removed. For 12 mpf animals (n=6, 27-31mm), utricle, saccule, and lagena were extracted from converted *Sox10:Cre; ubb:LOXP-EGFP-STOP-LOXP-mCherry* fish after brains and otolith crystals were removed. Dissected heads and otic sensory patches were then incubated in fresh Ringer's solution for 5–10 min, followed by mechanical and enzymatic dissociation by pipetting every 5 min in protease solution (0.25% trypsin (Life Technologies, 15090-046), 1 mM EDTA, and 400 mg/mL Collagenase D (Sigma, 11088882001) in PBS) and incubated at 28.5 °C for 20–30 min or until full dissociation. Reaction was stopped by adding 6× stop solution (6 mM CaCl2 and 30% fetal bovine serum (FBS) in PBS). Cells were pelleted (376 × g, 5 min, 4 °C) and resuspended in suspension media (1% FBS, 0.8 mM CaCl2, 50 U/mL penicillin, and 0.05 mg/mL streptomycin (Sigma-Aldrich, St. Louis, MO) in phenol red-free Leibovitz's L15 medium (Life Technologies)) twice. Final volumes of 500 µL resuspended cells were placed on ice and fluorescence-activated cell sorted (FACS) to isolate live cells that excluded the nuclear stain DAPI. For scRNAseq library construction, barcoded single-cell cDNA libraries were synthesized using 10X Genomics Chromium Single Cell 3′ Library and Gel Bead Kit v.3.1 (14 dpf) or Single Cell Multiome ATAC + Gene Expression kit (12 mpf, single library built with all three sensory patches combined prior to library

preparation, ATAC data not shown) per the manufacturer's instructions. Libraries were sequenced on Illumina NextSeq or HiSeq machines at a depth of at least 1,000,000 reads per cell for each library. Read2 was extended from 98 cycles, per the manufacturer's instructions, to 126 cycles for higher coverage. Cellranger v6.0.0 (10X Genomics) was used for alignment against GRCz11 (built with GRCz11.fa and GRCz11.104.gtf) and gene-by-cell count matrices were generated with default parameters.

Data processing of scRNA-seq

Count matrices of inner ear and lateral line cells from embryonic and larval timepoints (18-96 hpf) were analyzed using the R package Monocle3 (v1.0.0) (Cao et al., 2019). Matrices were processed using the standard Monocle3 workflow (preprocess_cds, detect_genes, estimate_size_factors, reduce_dimension(umap.min_dist = 0.2, umap.n_neighbors = 25L)). This cell data set was converted to a Seurat object for integration with 10X Chromium sequencing data using SeuratWrappers. The count matrices of scRNA-seq data (14 dpf and 12 mpf) were analyzed by R package Seurat (v4.1.0) (Hao et al., 2021). Cells of neural crest origins were removed bioinformatically based on our previous study (Fabian et al., 2022). The matrices were normalized (NormalizeData) and integrated with normalized scRNA-seq data from the embryonic and larval time points according to package instruction (FindVariableFeatures, SelectIntegrationFeatures, FindIntegrationAnchors, IntegrateData; features = 3000). The integrated matrices were then scaled (ScaleData) and dimensionally reduced to 30 principal components. The data were then subjected to neighbor finding (FindNeighbors, k = 20) and clustering (FindClusters, resolution = 0.5), and then visualized through UMAP with 30 principal components as input. After data integration and processing, RNA raw counts from all matrices were normalized and scaled according to package instructions to determine gene expression for all sequenced genes, as the integrated dataset only contained selected features for data integration.

Mouse utricle scRNA-seq data (Jan et al., 2021) was downloaded from NCBI Gene Expression Omnibus (GSE155966). The count matrix was analyzed by R package Seurat (v4.1.0). Matrices were normalized (NormalizeData) and scaled for the top 2000 variable genes (FindVariableFeatures and ScaleData). The

scaled matrices were dimensionally reduced to 15 principal components. The data were then subjected to neighbor finding (FindNeighbors, k = 20) and clustering (FindClusters, resolution = 1) and visualized through UMAP with 15 principal components as input. Hair cells and supporting cells were bioinformatically selected based on expression of hair cells and supporting cell markers *Myo6* and *Lfng*, respectively. Hair cells were further subcategorized into striola type I hair cells by co-expression of striola marker *Ocm* and type I marker *Spp*, extrastriola type I hair cells by expression of *Spp* without *Ocm*, and extrastriola type II hair cells by expression of *Anxa4* without *Ocm*.

Mouse crista scRNA-seq data (Wilkerson et al., 2021) was downloaded from NCBI Gene Expression Omnibus (GSE168901). The count matrix was analyzed by R package Seurat (v4.1.0). Matrices were normalized (NormalizeData) and scaled for the top 2000 variable genes (FindVariableFeatures and ScaleData). The scaled matrices were dimensionally reduced to 15 principal components. The data were then subjected to neighbor finding (FindNeighbors, k = 20) and clustering (FindClusters, resolution = 1) and visualized through UMAP with 15 principal components as input. Hair cells and supporting cells were bioinformatically selected based on expression of hair cell and supporting cell markers *Pou4f3* and *Sparcl1*, respectively. Hair cells were further subcategorized into central hair cells by expression of *Ocm* and peripheral hair cells by expression of *Anxa4*.

Pseudotime analysis

We used the R package Monocle3 (v1.0.1) to predict the pseudo temporal relationships within the integrated scRNA-seq dataset of sensory patches from 36 hpf to 12 mpf. Cell paths were predicted by the learn_graph function of Monocle3. We set the origin of the cell paths based on the enriched distribution of 36 to 48 hpf cells. Hair (all macular hair cells, clusters 0-5) and supporting (macular supporting cells clusters 0 and 6) cell paths were selected separately (choose_cells) to plot hair cells and supporting cell marker expression along pseudotime (plot_genes_in_pseudotime).

Differential gene expression

We utilized *presto* package's differential gene expression function to identify differentially expressed genes among the different cell types. Wilcox rank sum test was performed by the function *wilcox usc.* We then filtered for genes with log2 fold change greater than 0.5 and adjusted p-value less than 0.01. To compare inner ear hair cells to lateral line hair cells, we used the following datasets from GEO: 6-7 dpf lateral line hair cells (GSE144827, Kozak et al., 2020), 4 dpf lateral line hair cells (GSE152859, Ohta et al., 2020), and 5 dpf lateral line hair cells and supporting cells (GSE196211, Baek et al., 2022). Hair cells were selected from datasets by expression of *otofb* and integrated along with our 10x Chromium dataset with Scanorama (Hie et al., 2019). Gene modules were computed in Monocle3 (v1.0.1) with a q-value cutoff of 1 x e-50.

SAMap analysis for cell type homology

We used the python package SAMap (v1.0.2)(Tarashansky et al., 2019) to correlate gene expression patterns and determine cell type homology between mouse utricle (GSE155966) (Jan et al., 2021) or crista (GSE168901) (Wilkerson et al., 2021) hair cells and supporting cells and our 12 mpf zebrafish inner ear scRNA-seq data. Zebrafish lateral line hair cell sc-RNA data (GSE123241)(Lush et al., 2019) was integrated with our 12 mpf inner ear data using Seurat in order to compare to mice. First, a reciprocal BLAST result of the mouse and zebrafish proteomes was obtained by performing blastp (protein-protein BLAST, NCBI) in both directions using in-frame translated peptide sequences of zebrafish and mouse transcriptome, available from Ensembl (Danio_rerio.GRCz11.pep.all.fa and Mus_musculus.GRCm38.pep.all.fa). The generated maps were then used for the SAMap algorithm. Raw count matrices of zebrafish and mouse scRNA-seq Seurat objects with annotated cell types were converted to h5ad format using SeuratDisk package (v0.0.0.9020) and loaded into Python 3.8.3. Raw data were then processed and integrated by SAMap. Mapping scores between cell types of different species were then calculated by get_mapping_scores and visualized by sankey_plot. Gene pairs driving cell type homology were identified by GenePairFinder.

Data availability

Single-cell RNA seq datasets are available from the NCBI Gene Expression Omnibus with Gene Set Accession number GSE211728.

2.6 Acknowledgments

This manuscript is dedicated to Neil Segil, who was a wonderful colleague, friend, and mentor to many. We thank Megan Matsutani for fish care, the USC Stem Cell Flow Cytometry Core, and the CHLA Next-Generation Sequencing Core. We also thank David White and the UW Zebrafish Facility staff for fish care.

2.7 Figures

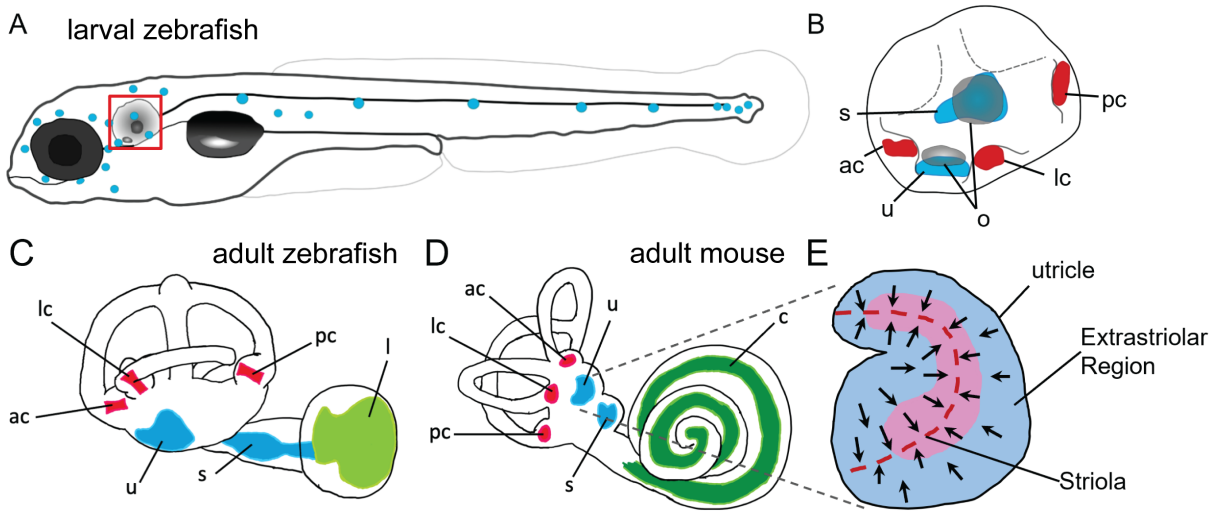

Figure 2.1 Anatomy of zebrafish and mouse inner ears

A) Illustration of the lateral line system of a 5 dpf zebrafish. Blue circles represent individual neuromasts located on the body of the fish. Boxed region indicates location of the ear. B) Enlarged diagram of the 5 dpf zebrafish ear showing cristae (red) and macular (blue) sensory organs. C,D) Illustrations of adult zebrafish and mouse inner ears showing homologous end organs in the semicircular canal crista ampullaris (red) and macula otolith organs (blue). Light green and dark green represent unique end organs of the lagena in zebrafish and cochlea in mice. E) Illustration of the mouse utricle showing striolar and extrastriolar regions of the sensory organ. Arrows represent hair cell planar polarity within the sensory organ and red dashed line represents the line of polarity reversal within the striola. ac: anterior crista, c: cochlea, l: lagena, lc: lateral crista, o: otolith, pc: posterior crista, s: saccule, u: utricle.

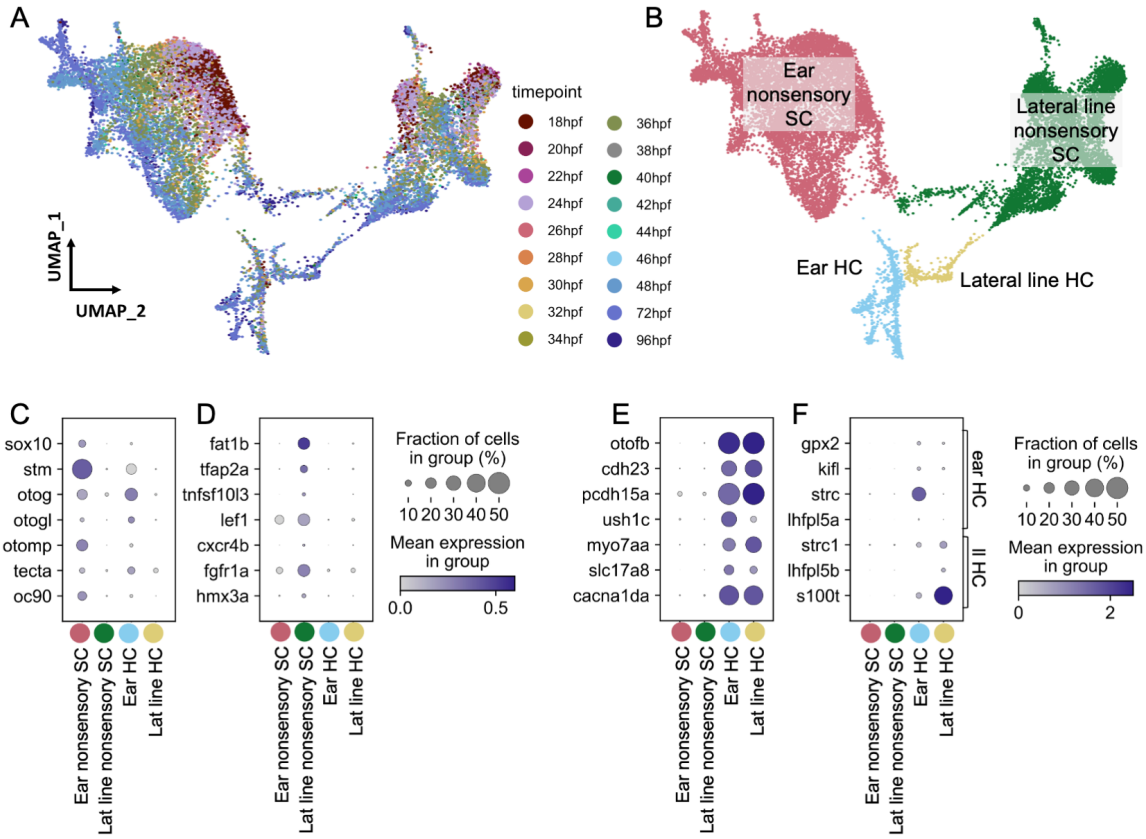

Figure 2.2 Molecularly distinct cell types between the zebrafish inner ear and lateral line

Ear and lateral line cells were selected from a whole-embryo single-nucleus RNA-seq dataset from animals between 18 and 96 hpf using known marker genes for hair cells and supporting cells. A-B) UMAP projection of inner ear and lateral line cells grouped by A) developmental timepoint and B) broad cell type: ear nonsensory SC (red), lateral line nonsensory SC (green), ear HC (blue), and lateral line HC (yellow). Clusters in B) correspond to columns of following gene expression plots. Widely accepted marker genes for C) inner ear nonsensory cells, D) lateral line nonsensory cells, and E) hair cells show enriched expression in the corresponding clusters from B, confirming their identity. F) Expression of previously identified marker genes for inner ear or lateral line hair cells was used to identify hair cell origin.

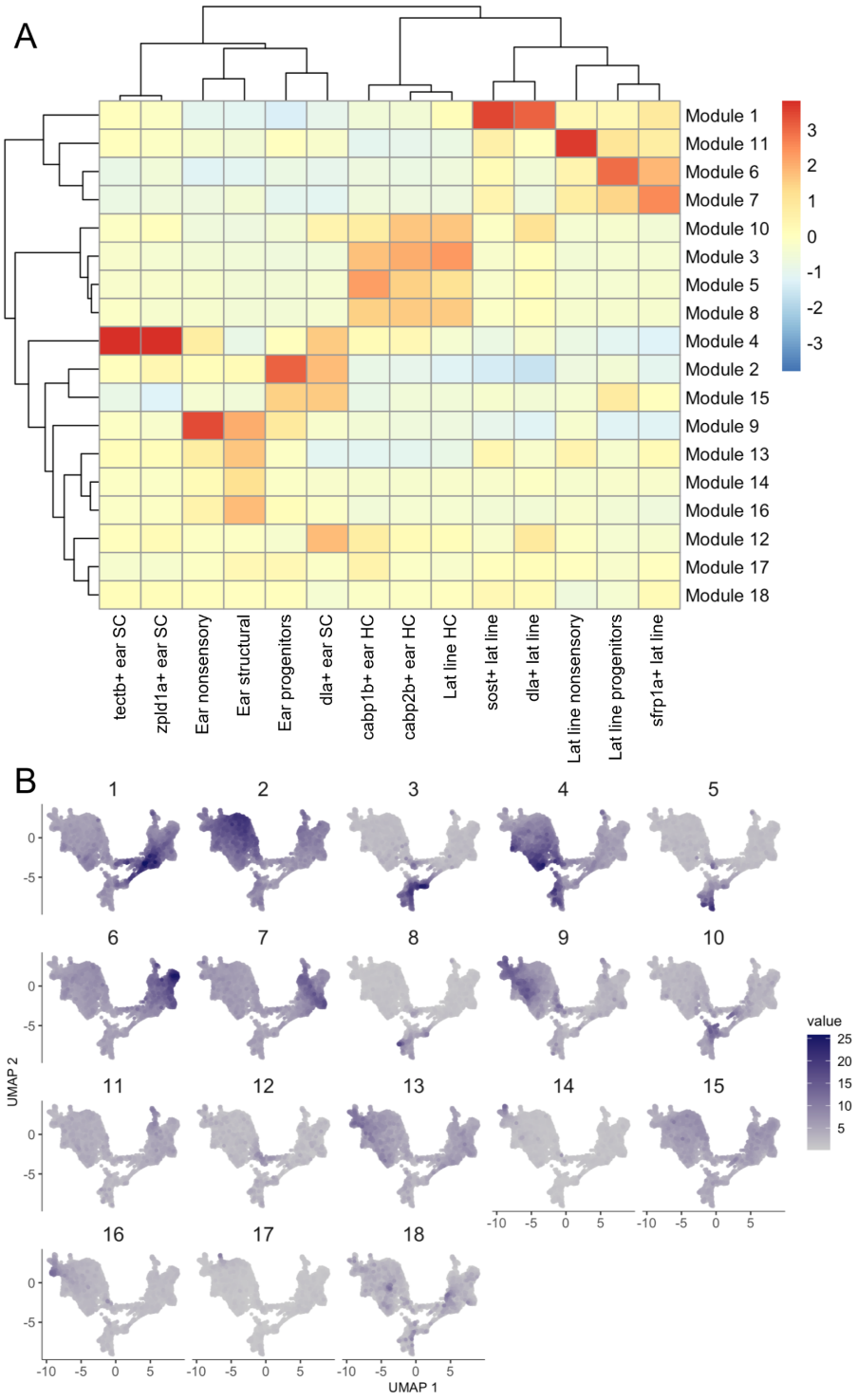

Figure 2.2.S1 Gene modules for embryonic to larval inner ear and lateral line dataset

Gene modules calculated in Monocle 3 for the embryonic to larval inner ear and lateral line dataset displayed as A) a heatmap of module gene enrichment by cluster where red indicates higher enrichment

and blue indicates de-enrichment and B) module expression across the UMAP for the dataset. Module genes with statistical values are listed in Supplementary File 2.

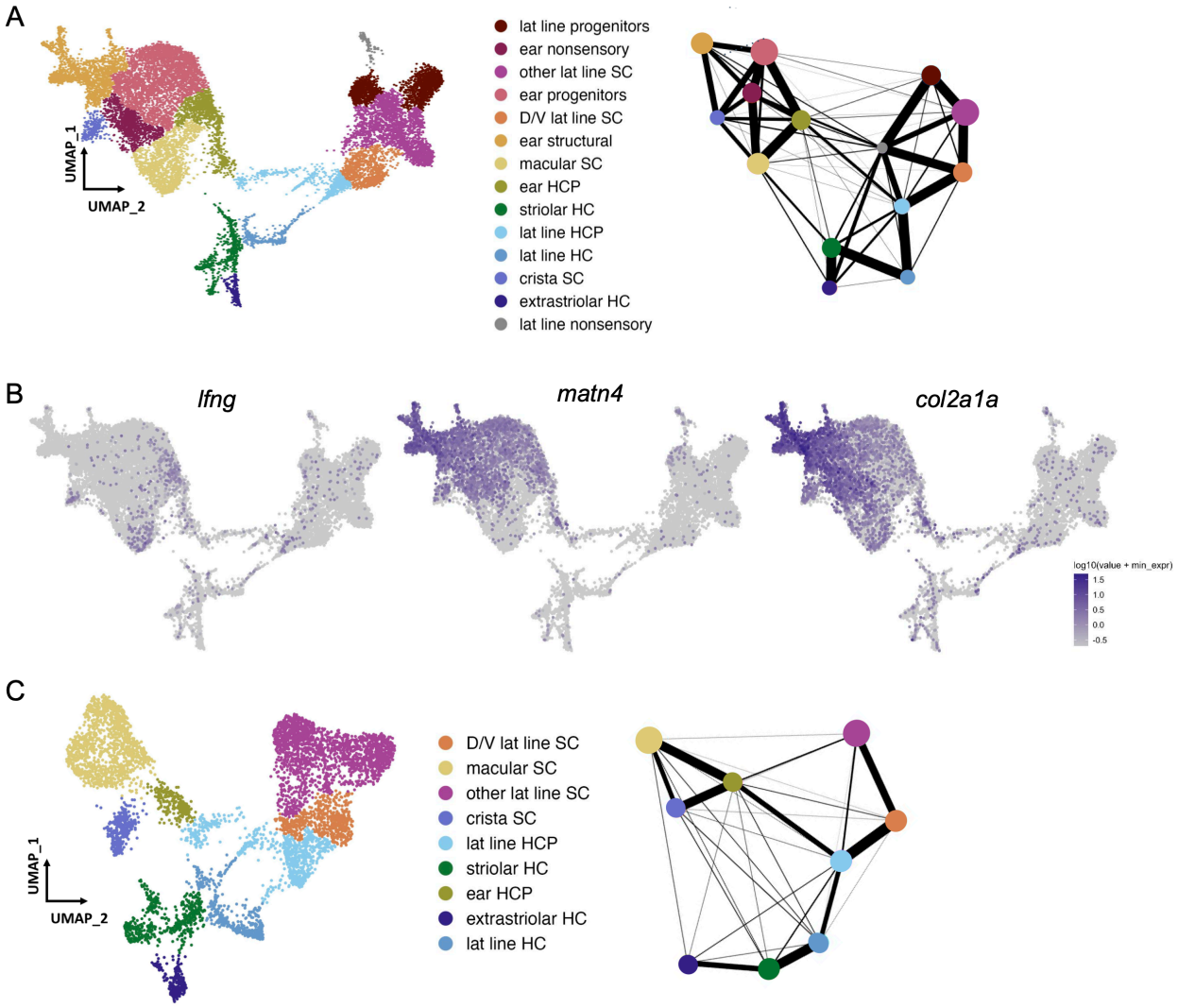

Figure 2.2.S2 Selection of otic sensory cells from snRNA-seq dataset

A) Clustering of 18 hpf to 96 hpf dataset to illustrate cell subtypes. PAGA analysis of this dataset shows strong connectivity among ear nonsensory cells and among lateral line nonsensory cells, but weak interconnectivity between these two groups. B) Feature plots show expression of the supporting cell marker *lfng*, and markers of structural otic cells *matn4* and *col2a1a*. C) UMAP of sensory patch cells from 36-96hpf are-clustered without structural and early otic vesicle cells. PAGA analysis again shows strong connectivity within hair cells and supporting cell groups andd weak connectivity between lateral line and inner ear supporting cells. PAGA connectivity scores are listed in Supplementary File 1.

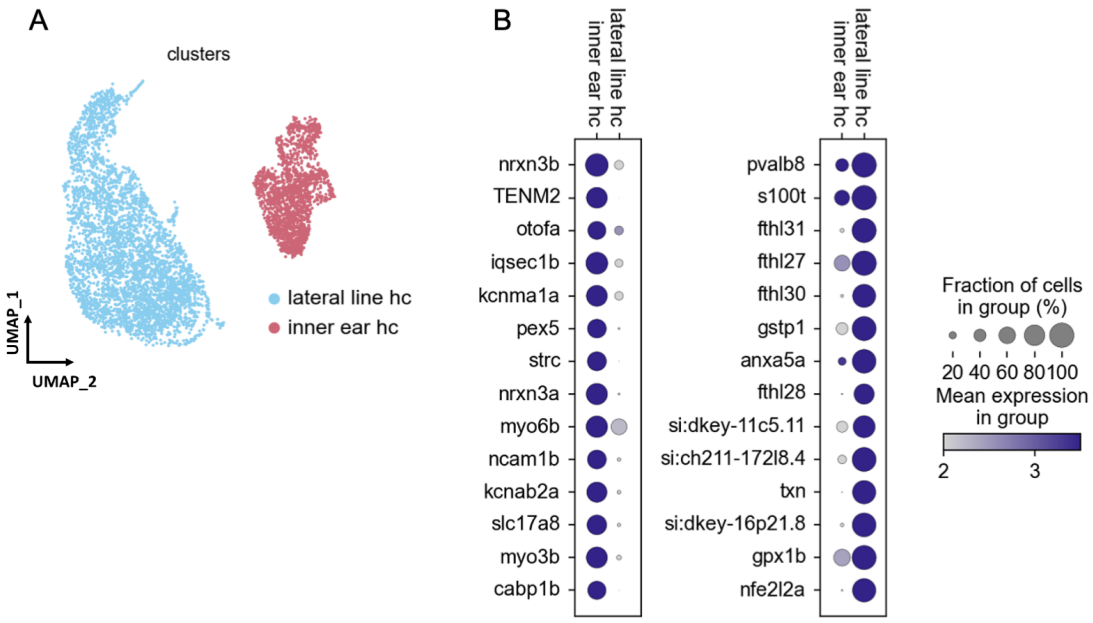

Figure 2.2.S3 Gene expression differences between lateral line and inner ear hair cells

A) UMAP of our 12 mpf hair cell dataset integrated by Scanorama with published lateral line hair cell datasets. Lateral line hair cells cluster separately from inner ear hair cells. B) Differential gene expression analysis identifies novel marker genes specific to either lateral line or inner ear hair cells.

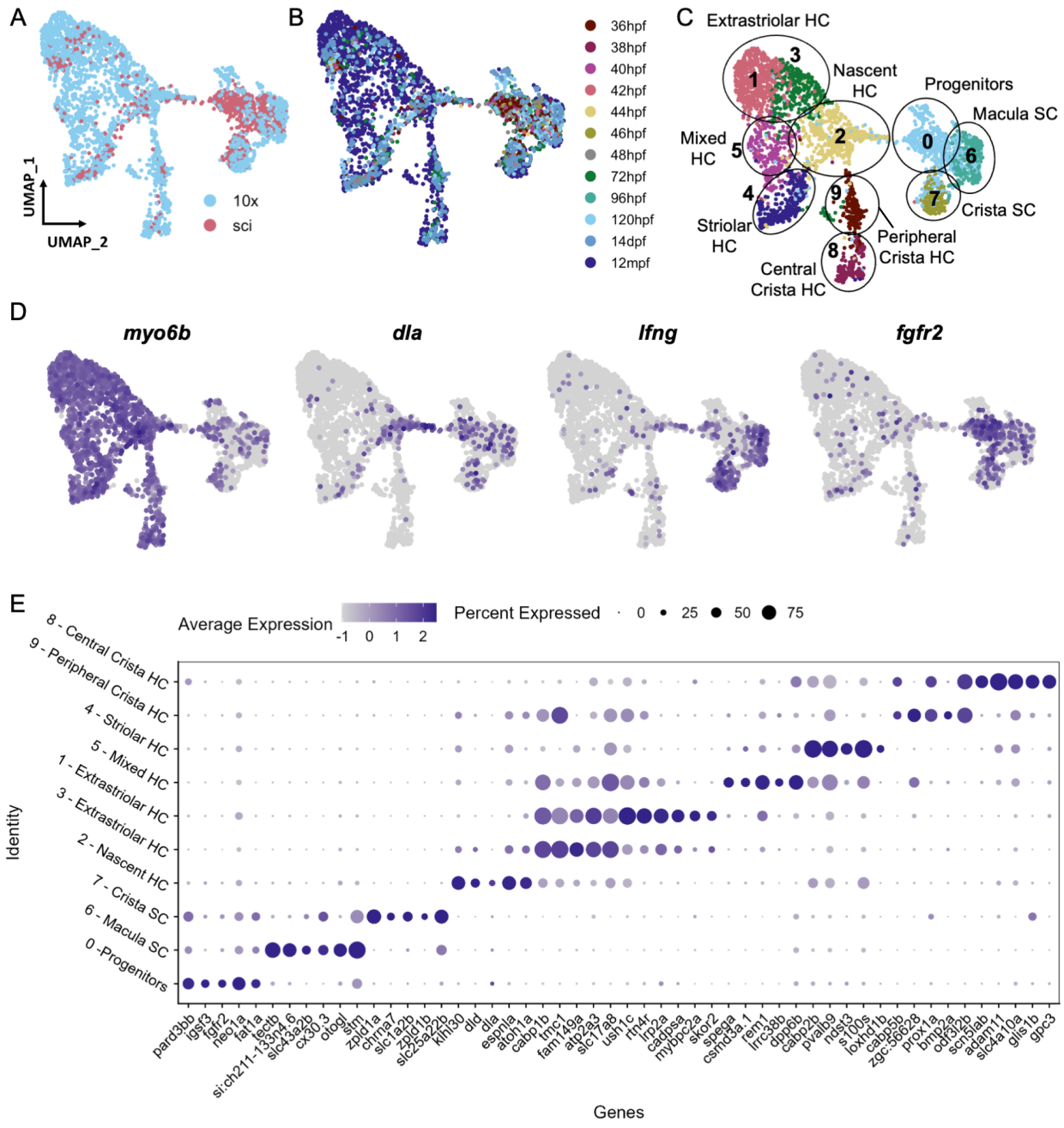

Figure 2.3 Cell subtypes in the zebrafish inner ear end organs

A-D) Integration and analysis of single-cell RNAseq data generated by sci-Seq (sci) or 10x Chromium sequencing (10x) for inner ear hair cells and supporting cells from embryonic (sci), larval (sci,10x), and adult (10x) stages. UMAP projection of cells are grouped by A) dataset of origin and B) timepoint. C) Unsupervised clustering divides cells into 10 clusters that were grouped into 9 cell subtypes. D) Feature plots showing hair cell marker *myo6b*, nascent hair cell marker *dla*, supporting cell marker *lfng*, and

putative progenitor marker *fgfr2* expression in the integrated dataset. E) Differentially expressed genes across the 10 cell clusters.

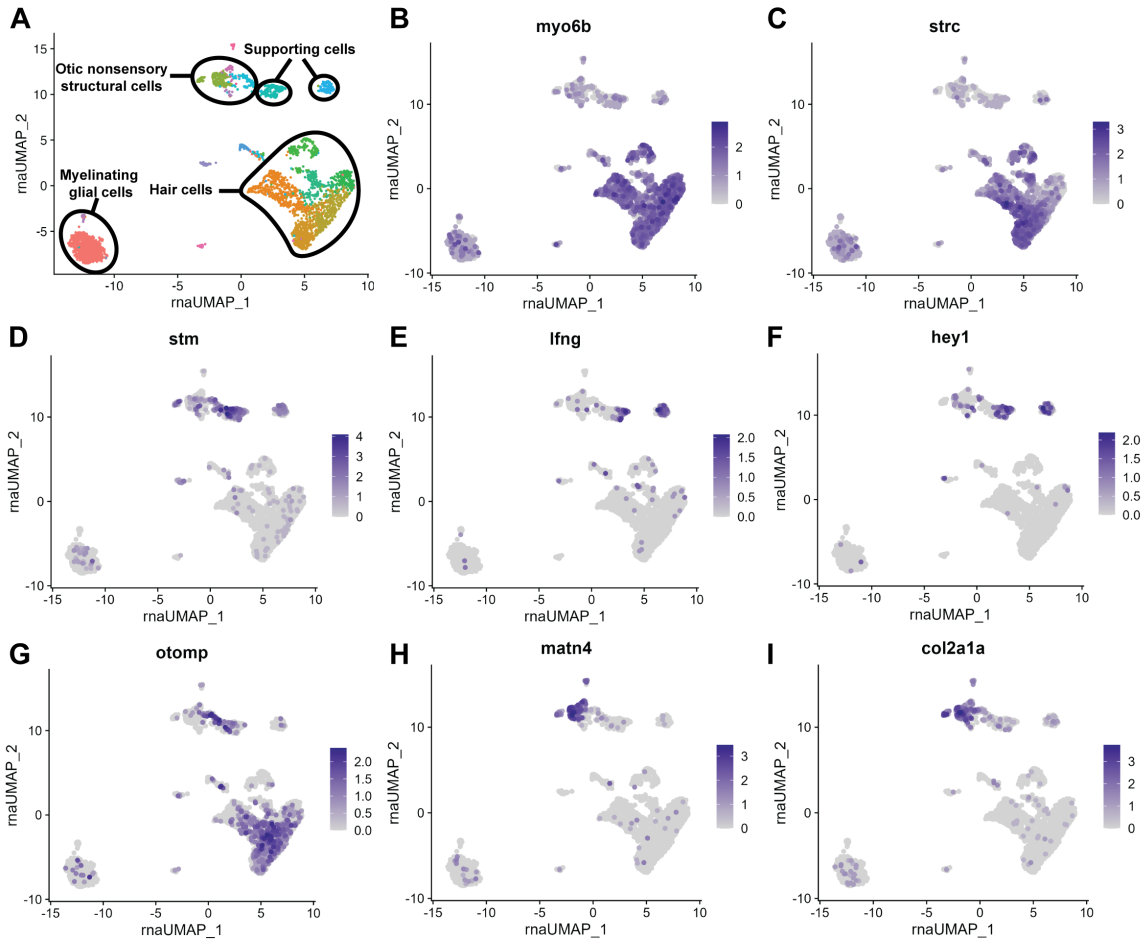

Figure 2.3.S1 scRNA-seq of 12 mpf zebrafish inner ear captures sensory hair cells and supporting cells as well as non-sensory supporting cells

A) Clustering of 12 mpf dataset to illustrate cell types in the adult zebrafish inner ear. B-I) Feature plots of 12 mpf zebrafish scRNA-seq dataset alone showing expression of hair cell markers B) *myo6b* and C) *strc*, pan-supporting cell marker D) *stm*, sensory supporting cell markers E) *lfng* and F) *hey1*, and pan-otic marker G) *otomp*, and non-sensory supporting cell markers H) *matn4* and I) *col2a1a*.

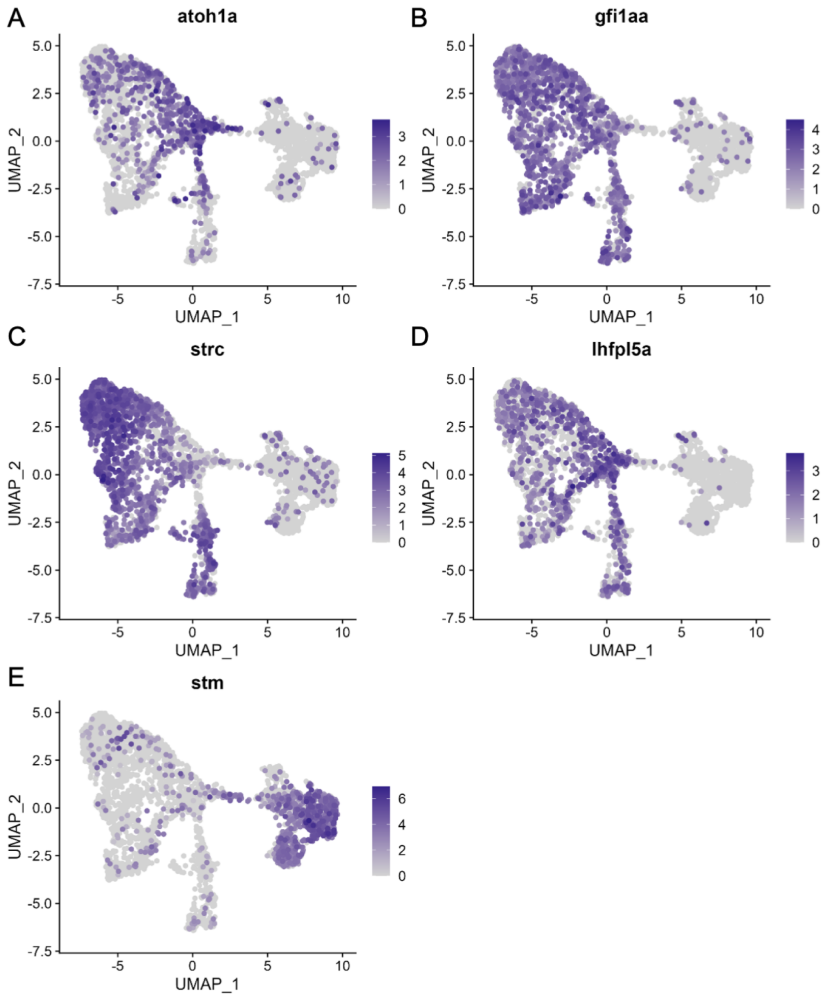

Figure 2.3.S2 Hair cell and supporting cell marker expression in the integrated scRNA-seq dataset

Feature plots of integrated zebrafish scRNA-seq datasets showing expression of nascent hair cell marker A) *atoh1a,* inner ear hair cell markers B) *strc,* C) *gfi1aa*, and D) *lhfpl5a*, and pan-supporting cell marker E) *stm*.

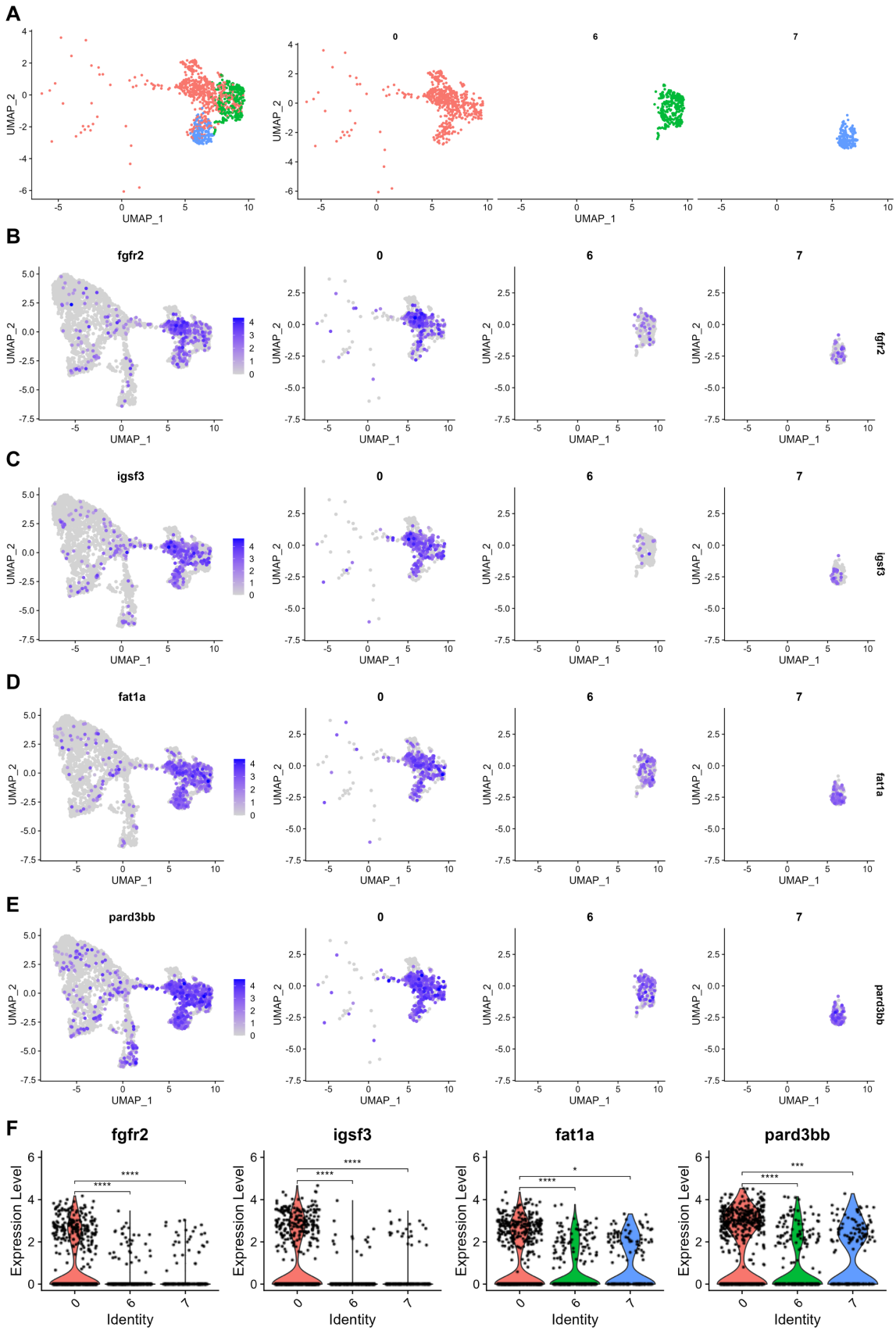
A
0
6
7
UMAP_1
UMAP_2
B
fgfr2
C
igsf3
D
fat1a
E
pard3bb
F
fgfr2
igsf3
fat1a
pard3bb
Expression Level
Identity
****
*
***

Figure 2.3.S3 Putative progenitor marker expression in individual progenitor and supporting cell clusters

A) Combined and individual UMAP projections of putative bipotent progenitor cluster (cluster 0), macular supporting cell cluster (cluster 6), and cristae supporting cell cluster (cluster 7) from the integrated zebrafish inner ear dataset. B-E) Feature plots show expression of putative progenitor genes in the integrated dataset, as well as in individual clusters of 0, 6, and 7. F) Violin plots showing differential gene expression of *fgfr2*, *igsf3*, *fat1a*, and *pard3bb* among clusters 0, 6, and 7. Wilcoxon rank sum test, *: p <= 0.05, ***: p <= 1e-3, ****: p <= 1e-4.

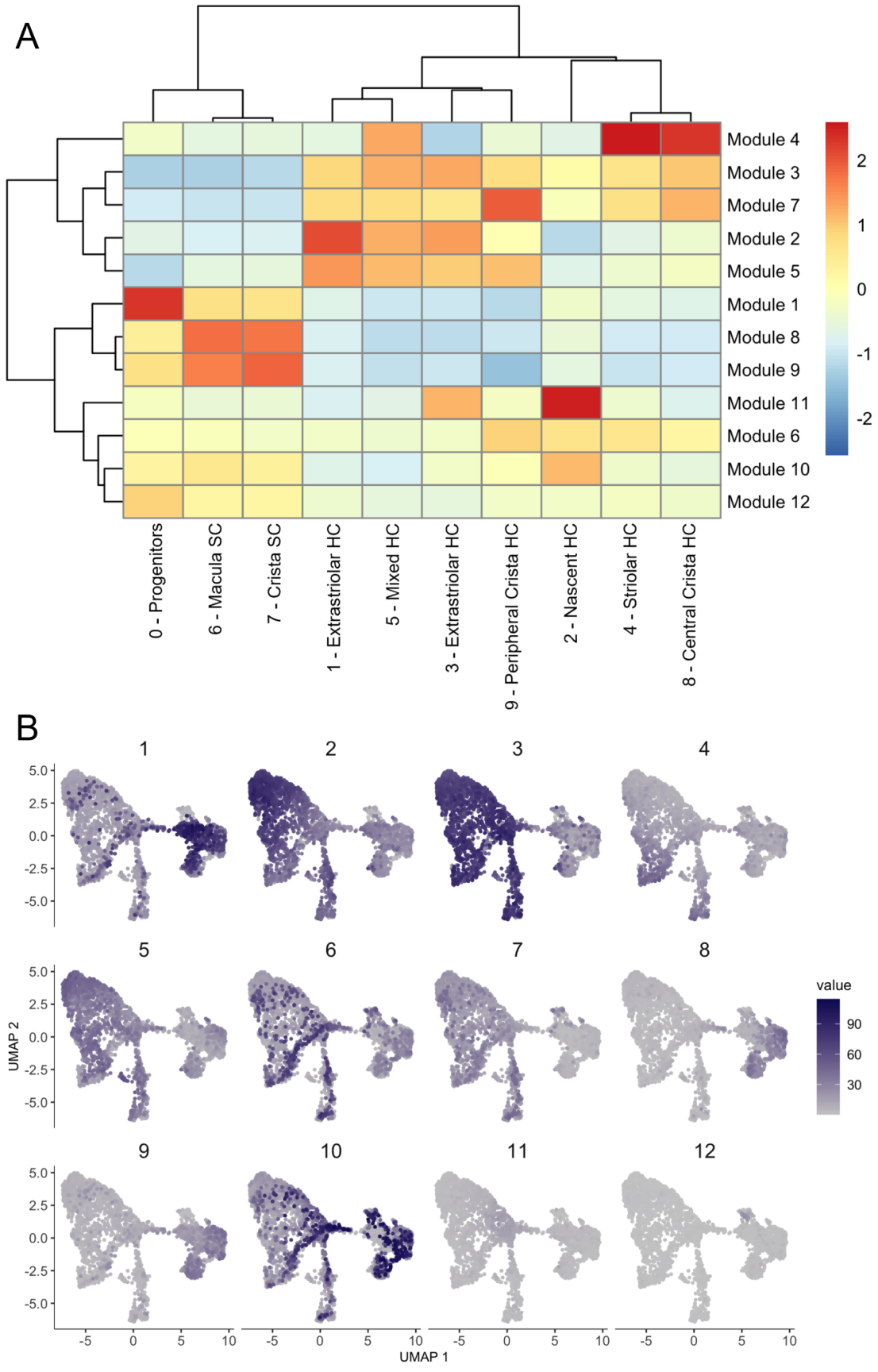
A
Module 4
Module 3
Module 7
Module 2
Module 5
Module 1
Module 8
Module 9
Module 11
Module 6
Module 10
Module 12
2
1
0
-1
-2
0 - Progenitors
6 - Macula SC
7 - Crista SC
1 - Extrastriolar HC
5 - Mixed HC
3 - Extrastriolar HC
9 - Peripheral Crista HC
2 - Nascent HC
4 - Striolar HC
8 - Central Crista HC
B
1
2
3
4
5
6
7
8
9
10
11
12
UMAP 2
UMAP 1
value
90
60
30

Figure 2.3.S4 Gene modules for integrated inner ear sensory patch dataset

Gene modules calculated in Monocle 3 for the integrated inner ear sensory patch dataset displayed as A) a heatmap of module gene enrichment by cluster where red indicates higher enrichment and blue indicates de-enrichment and B) module expression across the UMAP for the dataset. Module genes with statistical values are listed in Supplementary File 5.

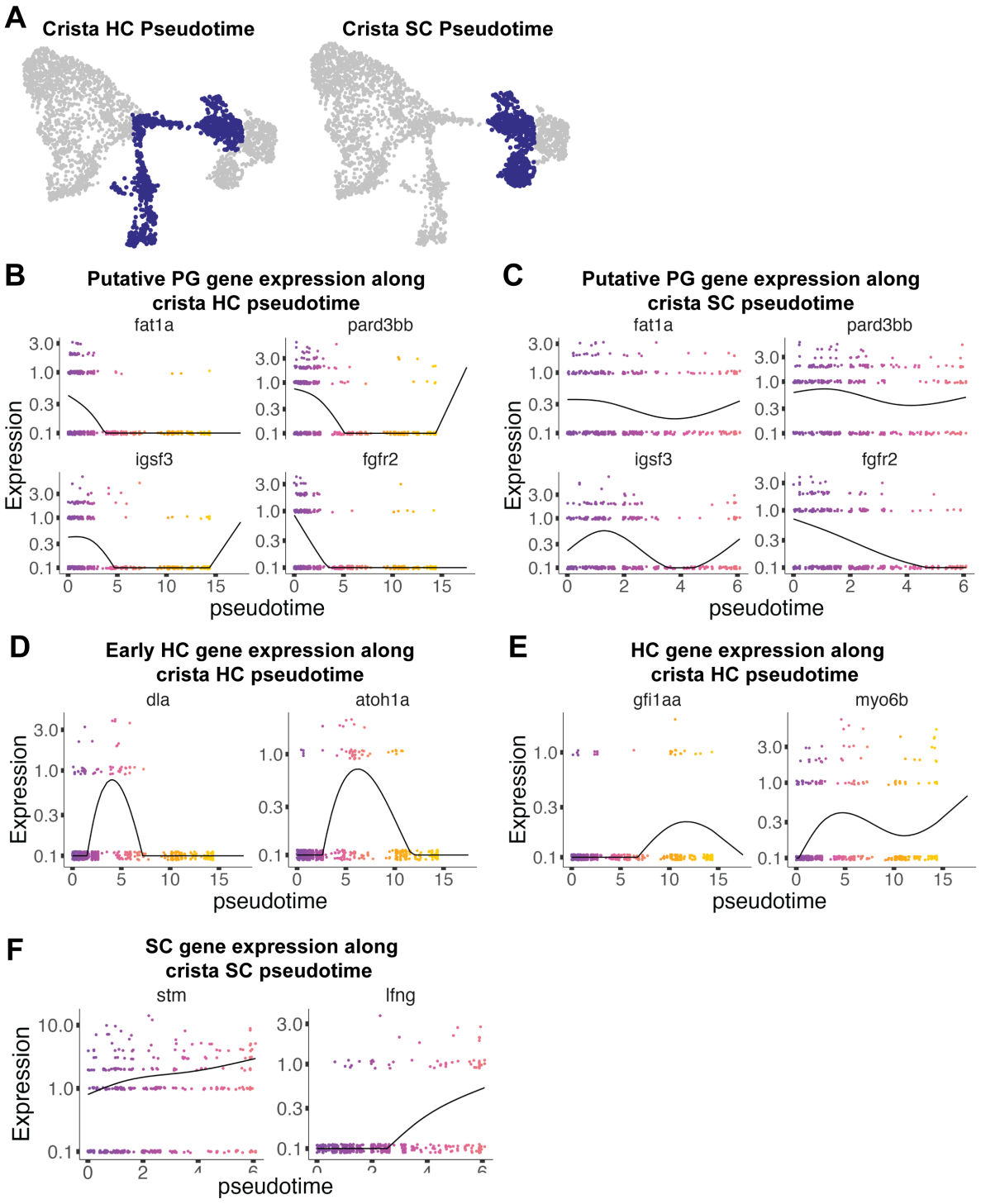

Figure 2.4 Pseudotime analysis reveals developmental trajectories in the zebrafish inner ear

A,B) Pseudotime analysis of macular cells showing simulated developmental trajectories of a putative bipotent progenitor population into hair cell and supporting cell clusters. C,D) Changes in putative

progenitor markers along C) hair cell and D) supporting cell trajectories. *fat1a* and *pard3bb* only decrease along the hair cell trajectory, while *fgfr2* and *igsf3* decrease along both hair cell and supporting cell trajectories. E) Transient expression of early hair cell genes *dla* and *atoh1a* along hair cell trajectories. F) Increases in gene expression levels of *gfi1aa* and *myo6b* along hair cell trajectories. G) Increases in *stm* and *lfng* along supporting cell trajectories.

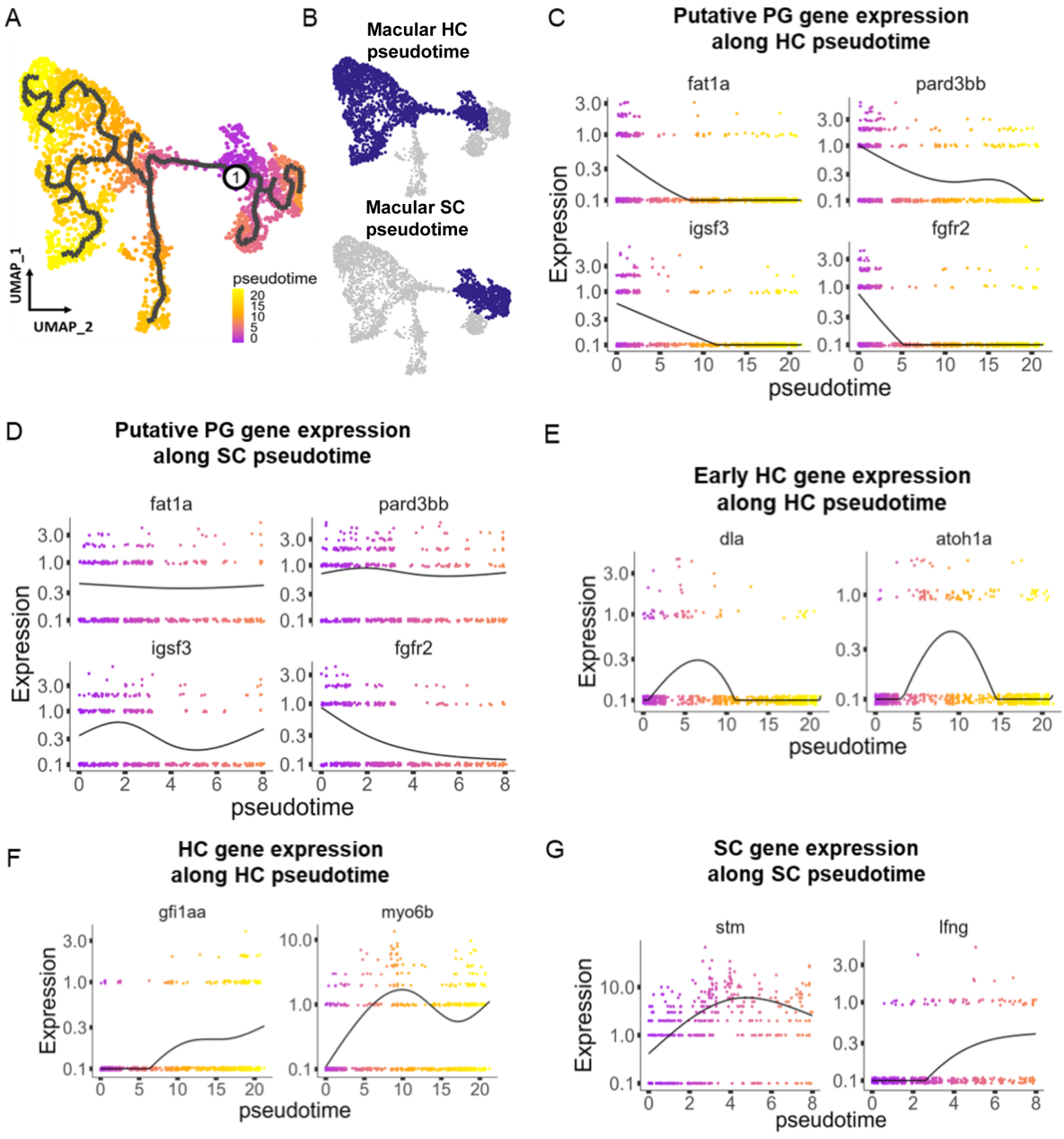

Figure 2.4.S1 Pseudotime analysis of cristae hair and supporting cells in the zebrafish inner ear

A) Pseudotime analysis showing simulated developmental trajectories of a putative bipotent progenitor population into both cristae hair and supporting cell clusters. B,C) Changes in putative progenitor markers along B) hair cell and C) supporting cell trajectories. *fat1a* and *pard3bb* only decrease along the hair cell trajectory, while *fgfr2* and *igsf3* decrease along both hair cell and supporting cell trajectories. D) Transient expression of early hair cell genes *dla* and *atoh1a* along hair cell trajectories. E) Increases in gene

expression levels of *gfi1aa* and *myo6b* along hair cell trajectories. F) Increases in *stm* and *lfng* along supporting cell trajectories.

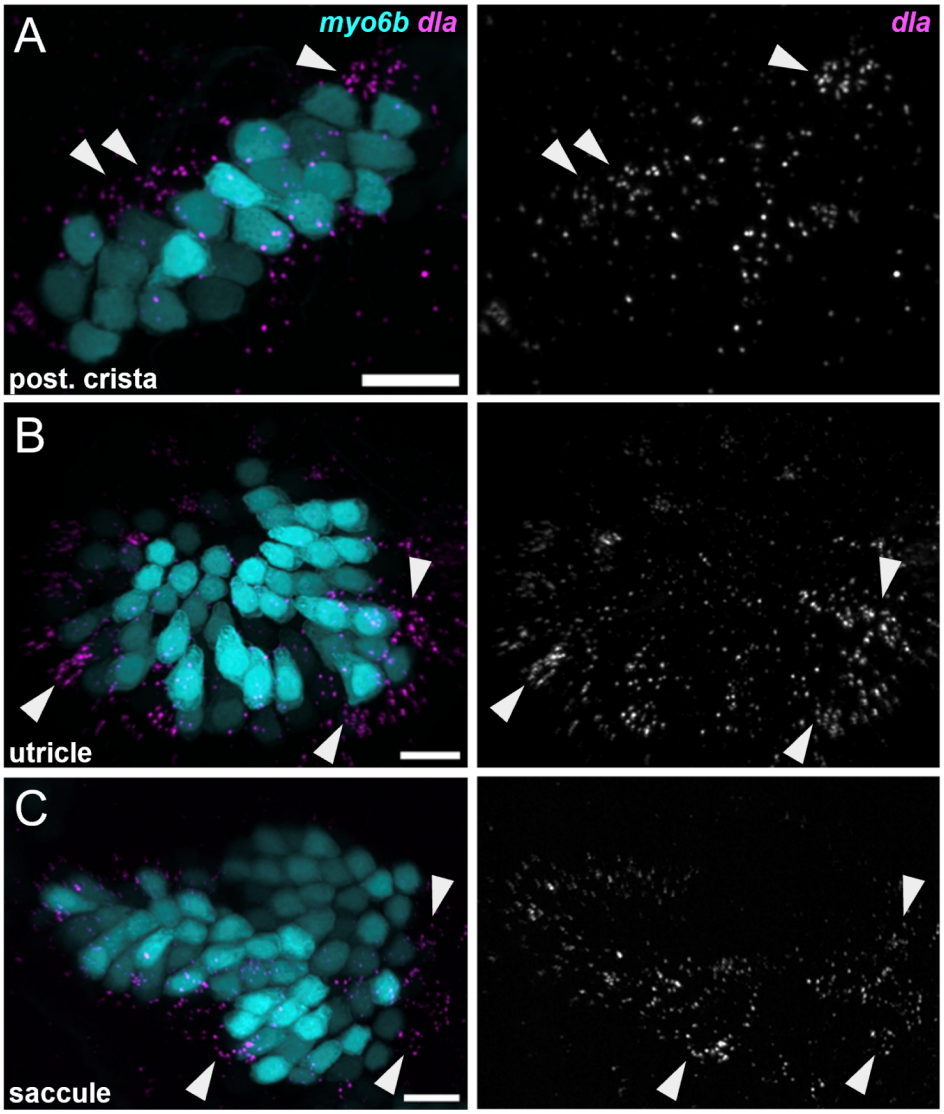

Figure 2.4.S2 *dla* labels putative hair cell progenitors in the cristae and maculae

HCR in situ hybridization of 5 dpf zebrafish. Maximum intensity projections of A) posterior crista (lateral view), B) utricle (dorsal view), and C) saccule (lateral view) showing *dla* expression in a subset of support cells (arrowheads) peripheral to *myo6b*+ hair cells. Scale bars = 10 μm.

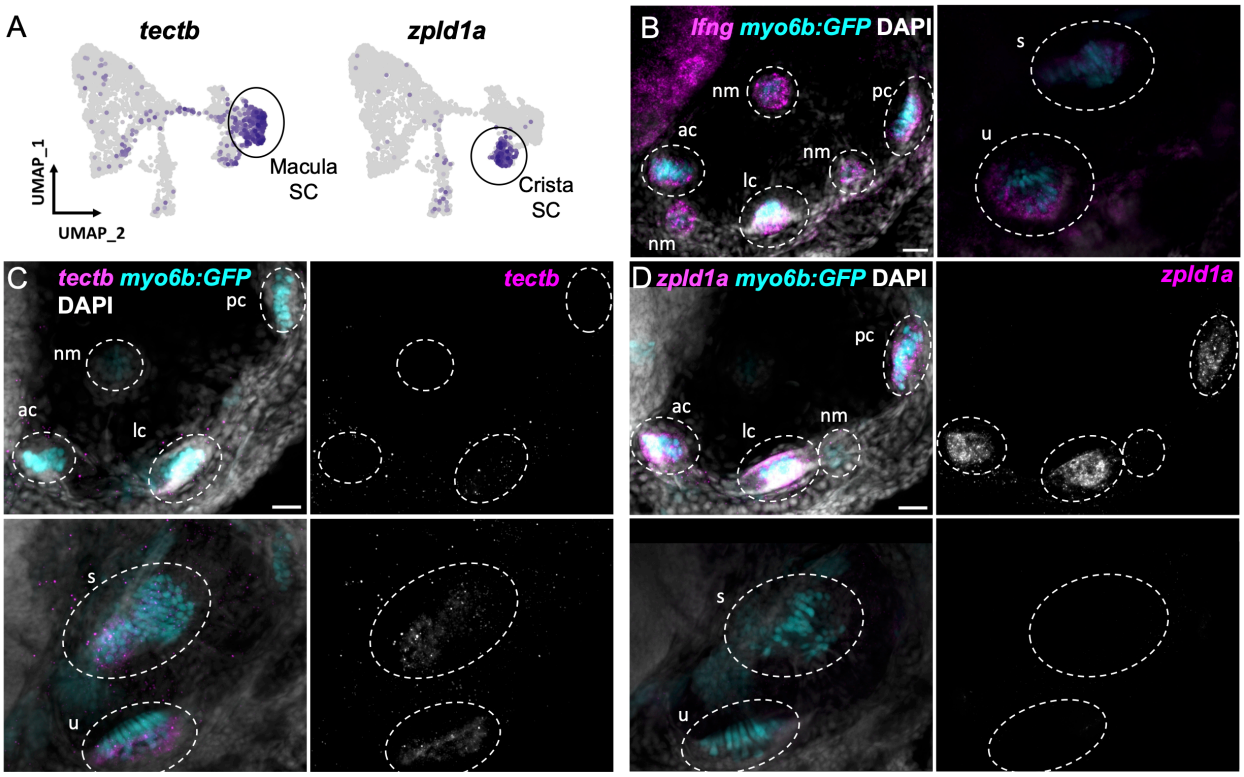

Figure 2.5 Distinct markers separate macula and crista supporting cells

A) Feature plots showing expression of macula supporting cell marker *tectb* and crista supporting cell marker *zpld1a*. B-D) HCR in situ hybridization in myo6b:GFP transgenic animals. Each set of images shown represents a projection of one z-stack split into cristae (lateral) and macula (medial) slices. Lateral line neuromasts positioned over the ear are visible in lateral slices. Expression pattern for B) the pan-supporting cell marker *lfng*, C) macula-specific marker *tectb*, and D) crista-specific marker *zpld1a* in 5 dpf myo6b:GFP fish. Each set of images shown represents a projection of one z-stack split into cristae (lateral) and macula (medial) slices. ac: anterior crista, lc: lateral crista, nm: neuromast, pc: posterior crista, u: utricle, s: saccule. Scale bars = 20 μm.

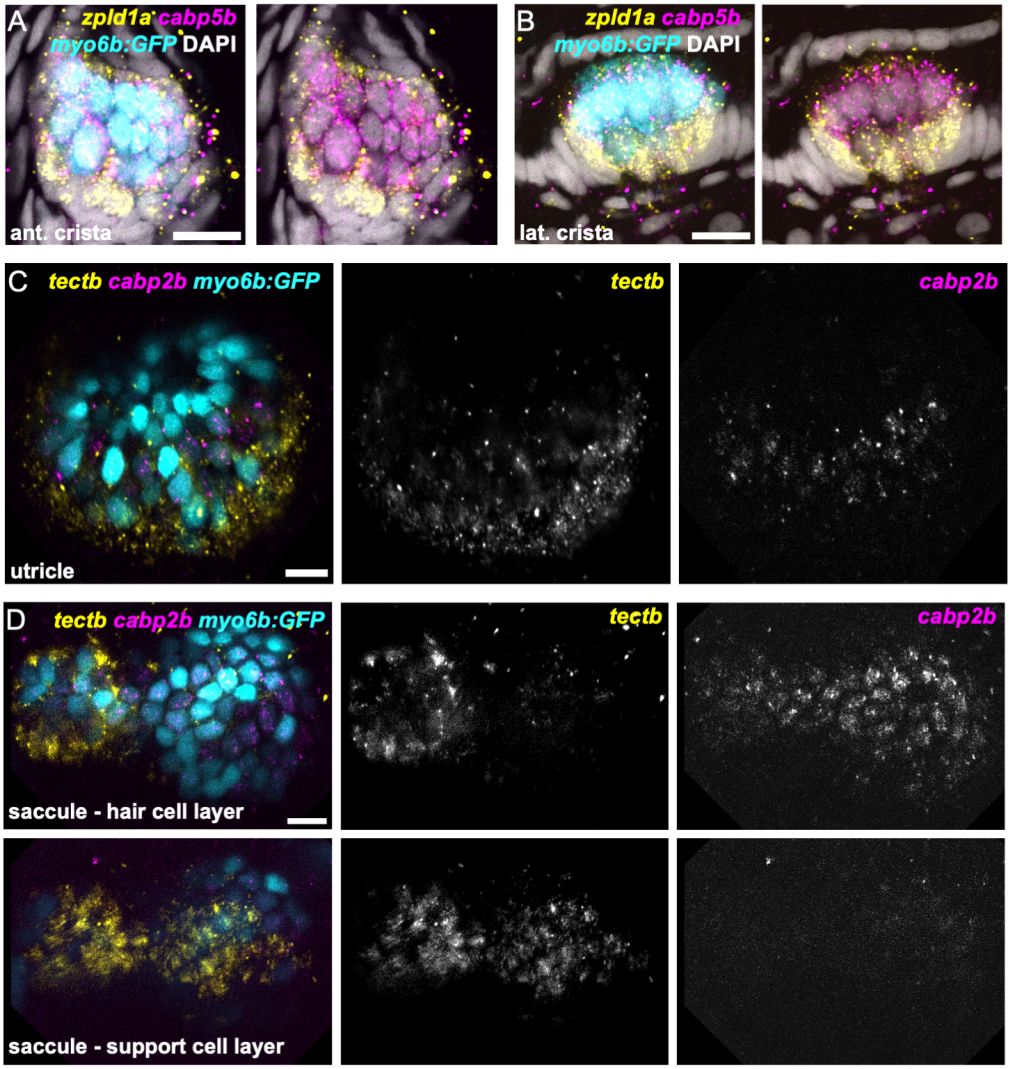

Figure 2.5.S1 *zpld1a* and *tectb* are primarily expressed in supporting cells

HCR in situ hybridization of 5 dpf myo6b:GFP zebrafish. A-B) Confocal slices through A) anterior crista and B) lateral crista (lateral view) show localization of *cabp5b* in hair cells and *zpld1a* in supporting cells. C) Slice through utricle (dorsal view) shows *cabp2b* expression in hair cells and *tectb* expression primarily in the surrounding supporting cells. D) Slices through saccule (lateral view) at the level of hair cell bodies (top row) and supporting cell bodies (bottom row). *cabp2b* is primarily expressed in hair cells and *tectb* is primarily expressed in supporting cells. Scale bars = 10 μm.

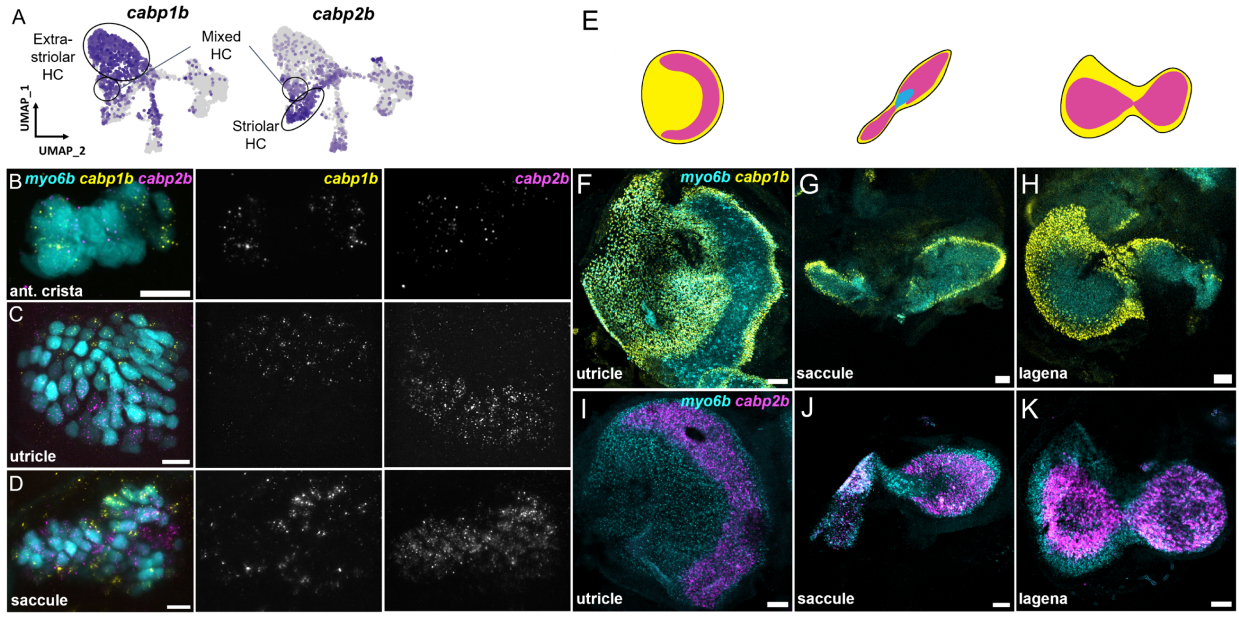

Figure 2.6 *cabp1b*+ and *cabp2b*+ label hair cells in distinct regions of sensory end organs

A) Feature plots showing differential expression of *cabp1b* and *cabp2b* among crista and macula hair cells. B-D) HCR in situ projections of individual sensory patches from 5 dpf myo6:GFP fish showing differential spatial expression patterns of *cabp1b* and *cabp2b*. B) *cabp1b* is expressed at the ends of the cristae, while *cabp2b* is expressed centrally. Anterior crista is shown. C) In the utricle, *cabp1b* is expressed medially and *cabp2b* is expressed laterally. D) In the saccule, *cabp1b* is expressed in peripheral cells at the dorsal and ventral edges of the organ. *cabp2b* is expressed centrally. Scale bars for HCR images = 10 μm. E) Cartoon illustrations of the zebrafish utricle, saccule, and lagena, and the expression patterns of *cabp1b* (yellow) and *cabp2b* (magenta) within each sensory patch. F-H) Whole mount RNAScope confocal images of adult inner ear organs showing peripheral expression pattern of *cabp1b* (n = 3) in the adult zebrafish F) utricle, G) saccule, and H) lagena. I-K) Whole mount RNAScope confocal images showing central expression pattern of *cabp2b* (n = 4) in the adult zebrafish I) utricle, J) saccule, and K) lagena. Scale bars for RNAScope images = 25 μm.

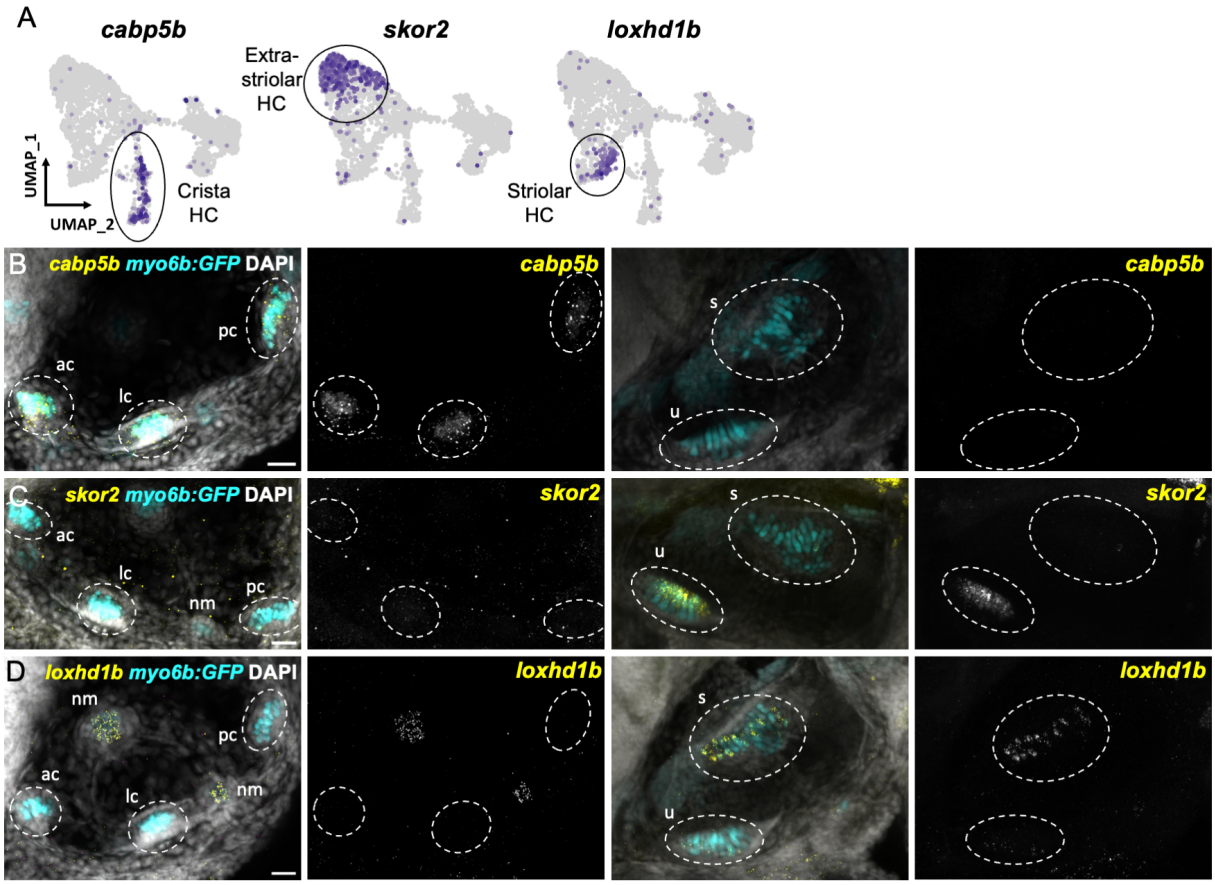

Figure 2.7 Distinct markers separate macula and crista hair cells

A) Feature plots showing marker genes enriched in organ-specific subsets of inner ear hair cells: *cabp5b*, *skor2*, and *loxhd1b* . B-D) HCR in situs in 5 dpf myo6b:GFP fish show expression of B) *cabp5b* in crista but not macula hair cells, C) *skor2* in the utricle only, and D) *loxhd1b* in the saccule, as well as lateral line neuromast hair cells. Each set of images represents an orthogonal projection of one z-stack split into cristae (lateral) and macular (medial) slices. ac: anterior crista, lc: lateral crista, nm: neuromast, pc: posterior crista, s: saccule, u: utricle. Scale bar = 20 μm.

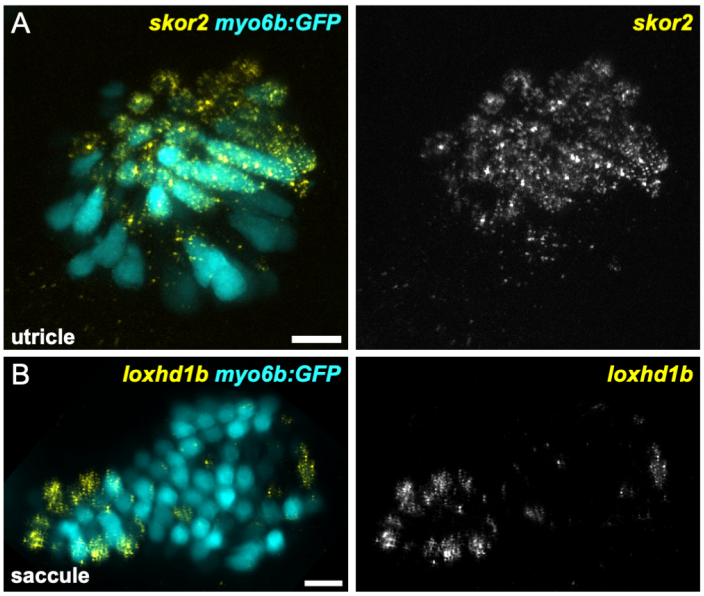

Figure 2.7.S1 *skor2* and *loxhd1b* label subsets of hair cells in utricle or saccule

HCR in situ hybridization of 5 dpf zebrafish. A) Maximum intensity projection of utricle (dorsal view) showing *skor2* expression in medially located hair cells. B) Maximum intensity projection of saccule (lateral view) showing *loxhd1b* expression in a peripheral subset of hair cells. Scale bars = 10 μm.

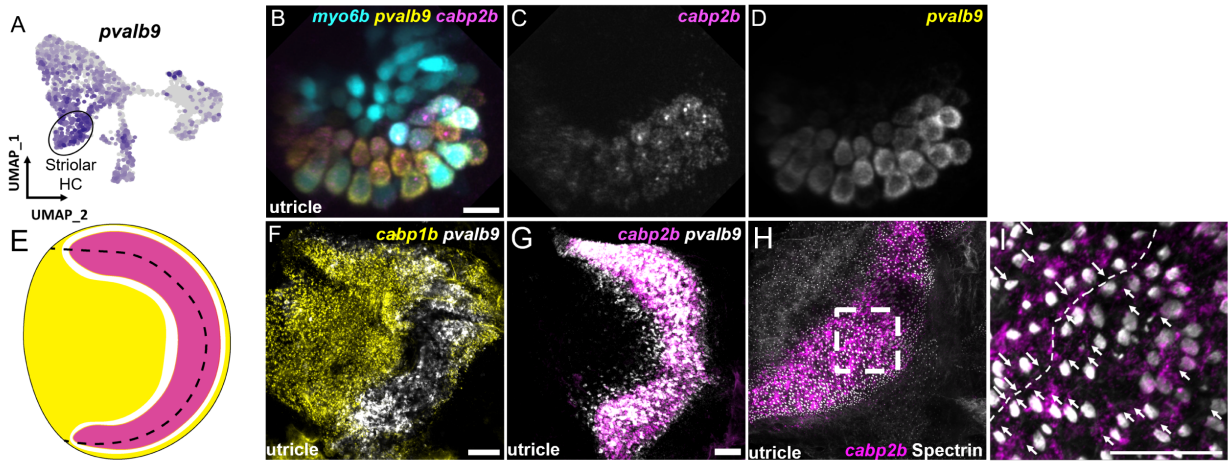

Figure 2.8. Zebrafish *cabp2b*+ domain shares features with the mouse striolar region

A) Feature plot shows enrichment for the striola marker *pvalb9* in *cabp2b*-expressing striolar cells. B-D) HCR in situs in 5 dpf myo6b:GFP fish shows *pvalb9* and *cabp2b* co-expression in the utricle. Scale bar = 10 µm. E) Cartoon illustration of overlapping expression of *pvalb9* (white) and *cabp2b* (magenta) that coincides with the line of hair cell polarity reversal. F,G) Whole-mount RNAScope confocal images of adult zebrafish utricles showing expression of *pvalb9* relative to F) *cabp1b* (n = 3) and G) *cabp2b* (n = 4). Scale bar = 25 µm. H,I) Whole-mount RNAScope RNA and protein co-detection assay showing co-localization of *cabp2b* expression (RNA) and the hair cell line of polarity reversal indicated by Spectrin (protein) staining (n = 3). Scale bar = 25 µm. Arrows denote hair cell polarity and dotted line outlines line of polarity reversal.

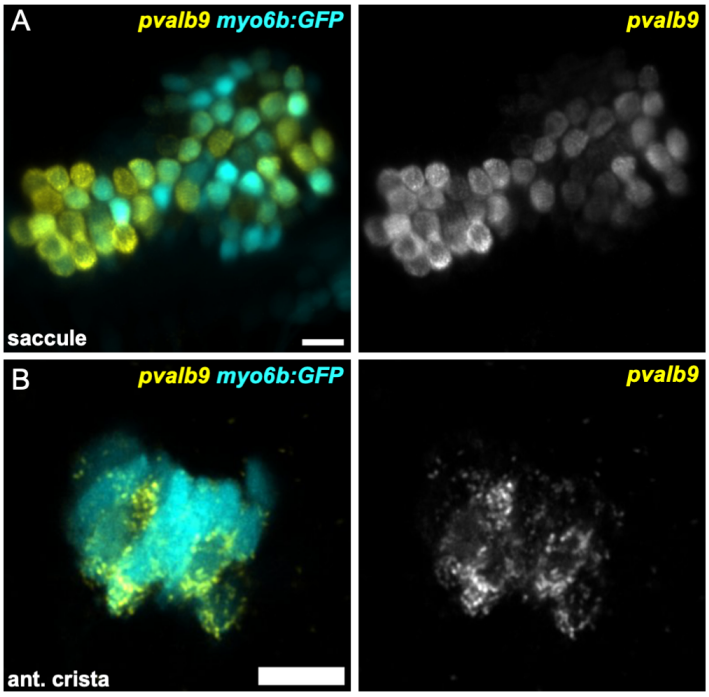

Figure 2.8.S1 Striola marker *pvalb9* is expressed in all inner ear sensory end organs

HCR in situ hybridization of 5 dpf zebrafish. A) Maximum intensity projection of saccule (lateral view) shows *pvalb9* expression in centrally located hair cells. B) Slice through the anterior crista shows *pvalb9* expression in a subset of crista hair cells. Scale bars = 10 μm.

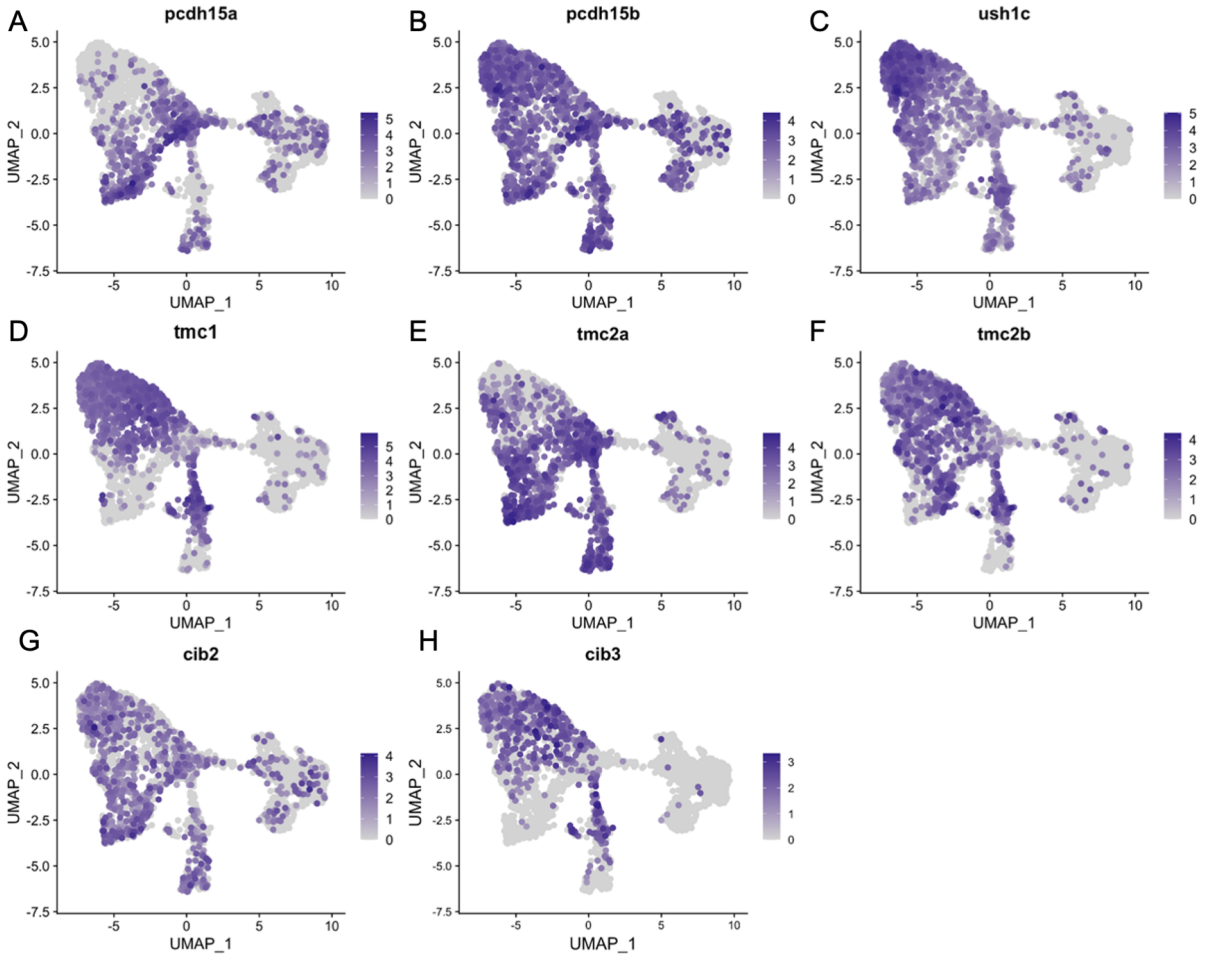

Figure 2.8.S2 Inner ear hair cell subtypes differentially express mechanosensory apparatus genes

Feature plots for mechanosensory transduction genes from the integrated zebrafish scRNA-seq dataset of Figure 3.

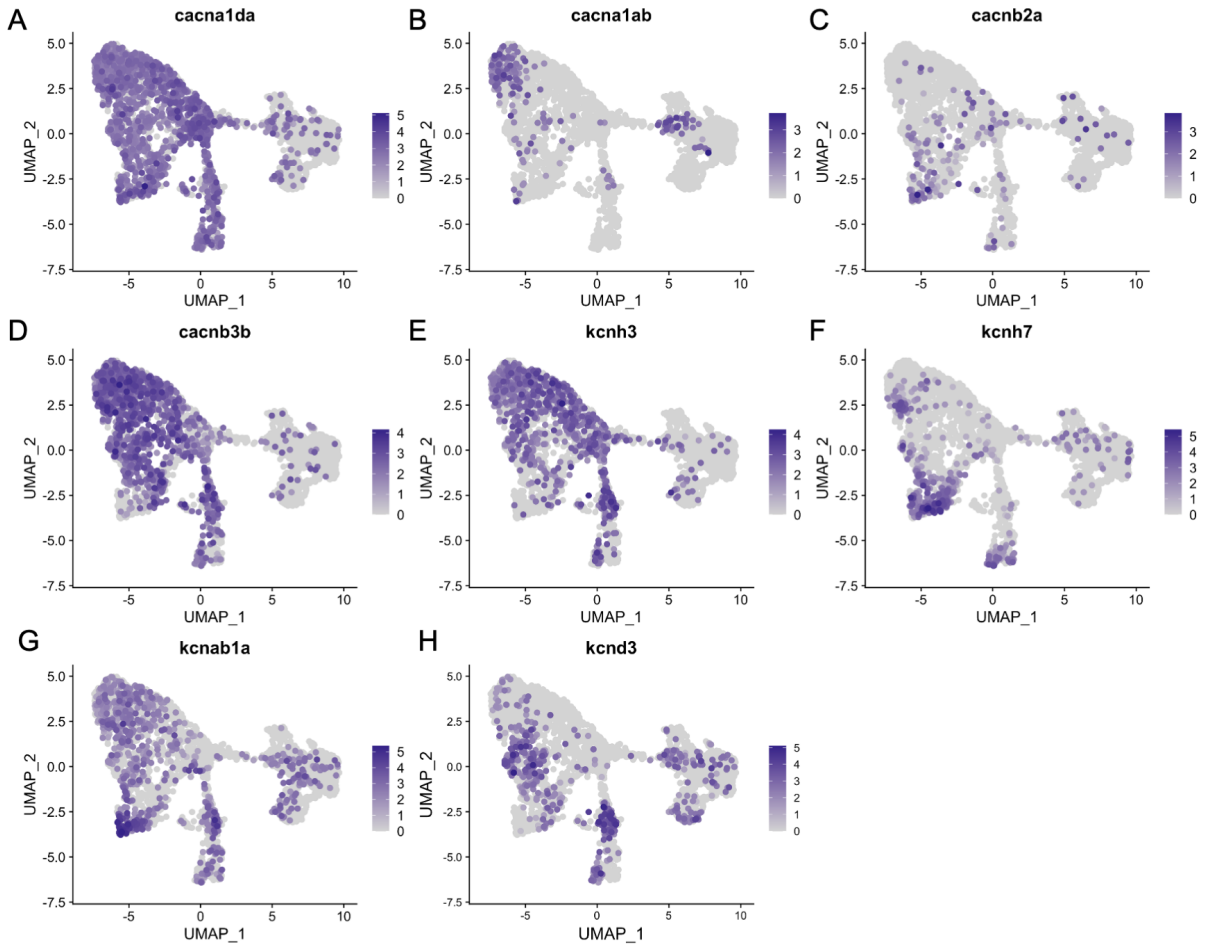

Figure 2.8.S3 Inner ear hair cell subtypes differentially express voltage-gated calcium and potassium channel genes

Feature plots for ion channel genes from the integrated zebrafish scRNA-seq dataset of Figure 3.

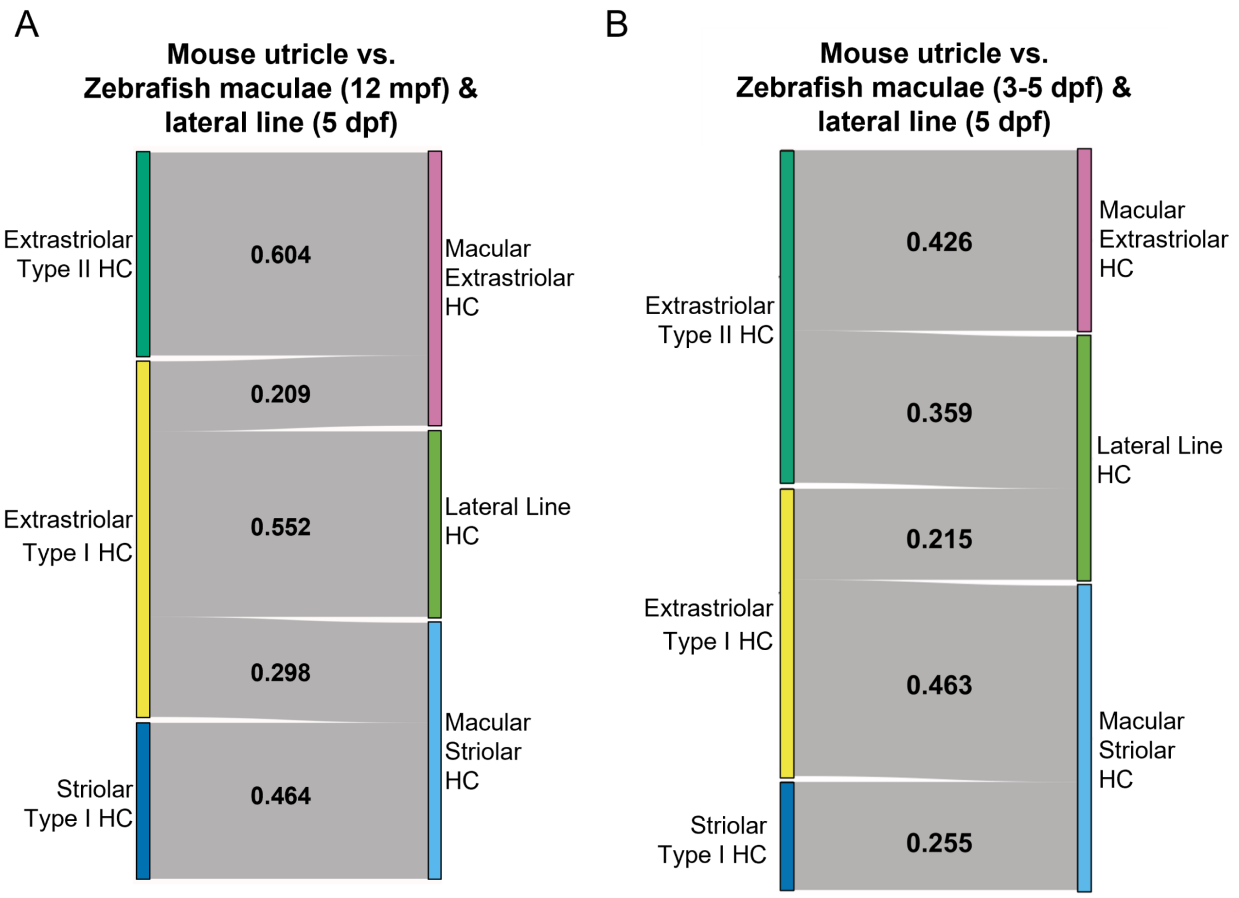

Figure 2.9 SAMap analysis reveals conserved gene expression patterns between mouse and zebrafish hair cell types

A-B) Sankey plot showing the SAMap mapping scores (0-1) that indicate transcriptome relatedness between A) mouse utricular and zebrafish macular single-cell clusters and B) mouse and zebrafish cristae single-cell clusters. A mapping score of 0 indicates no evolutionary correlation in transcriptome while a mapping score of 1 indicates perfect correlation. Correlations below 0.15 were not plotted.

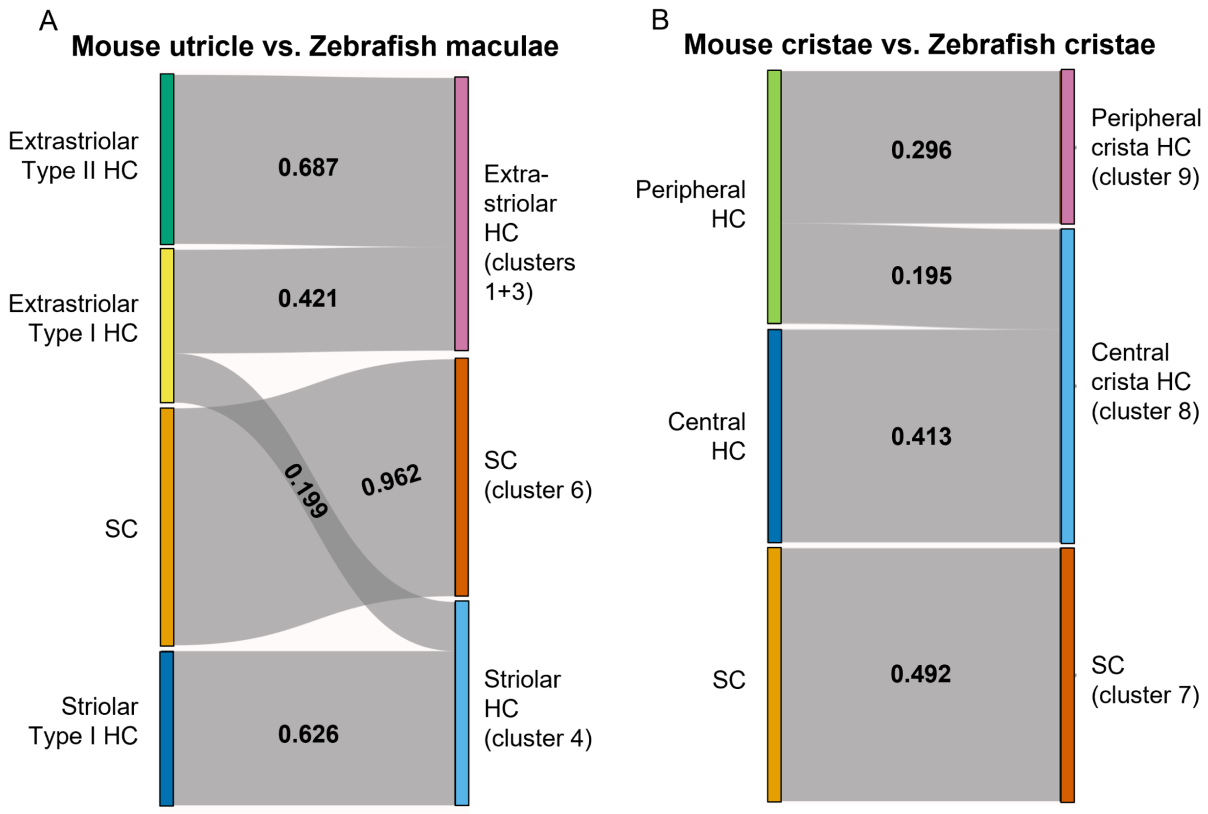

Figure 2.9.S1 SAMap analysis of mouse utricle versus zebrafish macular and lateral line cells

A-B) Sankey plot showing the SAMap mapping scores (0-1) that indicate transcriptome relatedness between mouse utricular and integrated zebrafish macular and lateral line single-cell clusters. A) Zebrafish 12 mpf macular HCs integrated with 5 dpf lateral line HCs. B) Zebrafish 3-5 dpf macular HCs integrated with 5 dpf lateral line HCs. A mapping score of 0 indicates no evolutionary correlation in transcriptome, and a mapping score of 1 indicates perfect correlation. Correlations below 0.2 were not plotted.

CHAPTER 3: TRANSDIFFERENTIATION IS UNCOUPLED FROM PROGENITOR POOL EXPANSION DURING HAIR CELL REGENERATION IN THE ZEBRAFISH INNER EAR

The contents of this chapter have been submitted to *Development* for publication with the following authors:

Marielle O. Beaulieu: Conceptualization, Methodology, Validation, Investigation, Writing - original draft, Writing – review and editing, Visualization, Funding acquisition

Eric D. Thomas: Methodology

David W. Raible: Conceptualization, Methodology, Writing – review and editing, Supervision, Funding acquisition

3.1 Abstract

Death of mechanosensory hair cells in the inner ear is a common cause of auditory and vestibular impairment in mammals, which have a limited ability to regrow these cells after damage. In contrast, non-mammalian vertebrates including zebrafish can robustly regenerate hair cells following severe organ damage. The zebrafish inner ear provides an understudied model system for understanding hair cell regeneration in organs that are highly conserved with their mammalian counterparts. Here we quantitatively examine hair cell addition during growth and regeneration of the larval zebrafish inner ear. We used a genetically encoded ablation method to induce hair cell death and observed gradual regeneration with correct spatial patterning over two weeks following ablation. Supporting cells, which surround and are a source of new hair cells, divide in response to hair cell ablation, expanding the possible progenitor pool. In parallel, nascent hair cells arise from direct transdifferentiation of progenitor pool cells uncoupled from progenitor division. These findings reveal a previously unrecognized mechanism of hair cell regeneration with implications for how hair cells may be encouraged to regenerate in the mammalian ear.

3.2 Introduction

The sensory organs of the inner ear that detect sound and head position are highly conserved across the vertebrate kingdom. The potential to regenerate these organs, however, is not as widespread. Hair cells, the mechanosensory cells of the inner ear, are particularly fragile and are vulnerable to death caused by exposure to ototoxic drugs, injury, and age-related degeneration. While mammals can regenerate hair cells at perinatal stages (Burns et al., 2012a; Mellado Lagarde et al., 2014; White et al., 2006), this ability declines rapidly after birth (Burns et al., 2012b; Cox et al., 2014; Maass et al., 2015). By adulthood, regeneration is limited in mammalian vestibular organs (Bucks et al., 2017; Forge et al., 1993; Golub et al., 2012; Kawamoto et al., 2009) and completely lost in the auditory system (Oesterle et al., 2008). As a result, hair cell death can lead to permanent auditory and vestibular deficits in humans. In contrast, many other vertebrates, including fish, amphibians, and birds, can regenerate functional hair cells throughout life (Avallone et al., 2008; Baird et al., 1996; Corwin and Cotanche, 1988; Cruz et al., 2015, 1987; Harris et al., 2003; Jimenez et al., 2021; Jones and Corwin, 1996; Lombarte et al., 1993; Ryals and Rubel, 1988; Smith et al., 2006; Taylor and Forge, 2005; Weisleder and Rubel, 1992).

Zebrafish are well-known for their regenerative potential and are commonly used to study hair cell development, death, and regeneration (reviewed in Pickett and Raible, 2019; Sheets et al., 2021). In addition to inner ear hair cells, fish and amphibians have analogous hair cells in an external sensory system called the lateral line, which is used to detect changes in water flow for behaviors such as schooling and predator evasion. Much of our current understanding of zebrafish hair cell function and regeneration comes from studies of the lateral line, while zebrafish inner ear hair cells have been relatively understudied. The zebrafish inner ear remains a promising model system for studying hair cell regeneration due to its high level of conservation with the inner ear of mammals and the extensive genetic and imaging tools available for zebrafish.

Zebrafish share several conserved inner ear organs with other vertebrates: three cristae, which sense angular rotation of the head within the semicircular canals, and two otolith organs, or maculae: the utricle and saccule (Fig. 3.1). In mammals, the utricle and saccule sense gravity and linear acceleration while an additional structure, the cochlea, is highly specialized for hearing. Zebrafish do not have a

cochlea; instead, auditory function is distributed across the macular organs, with the saccule likely playing an outsized role (Breitzler et al., 2020; Schuck and Smith, 2009). Only the utricle is indispensable for vestibular function (Riley and Moorman, 2000), but both macular organs have some capacity to respond to both auditory and vestibular stimuli (Favre-Bulle et al., 2020; Popper and Fay, 1993; Yao et al., 2016).

Within specific vestibular sensory organs, hair cells can be divided into subtypes based on differences in morphology, physiology, innervation, and gene expression. Mammalian and avian vestibular organs have type I hair cells, which are flask-shaped and innervated by afferent neurons that form calyces around hair cell bodies, and type II hair cells, which have shorter bodies with long foot-like basal projections that are innervated by bouton synapse-forming afferents (Burns and Stone, 2017; Eatock and Songer, 2011). The maculae can be divided into a central striolar region and more peripheral extrastriolar regions. Zebrafish have striolar and extrastriolar hair cells analogous to those of other vertebrates (Chang et al., 1992; Jiang et al., 2017; Liu et al., 2022; Platt, 1993; Shi et al., 2023; Tanimoto et al., 2022), but they do not have the equivalent morphological and innervation dimorphism of type I/II hair cells. The cristae are also organized into central and peripheral zones with molecularly distinct hair cells (Bang et al., 2001; Haddon and Lewis, 1996; Shi et al., 2023; Zhu et al., 2021).

Hair cells are surrounded by and interspersed with supporting cells that perform many critical roles during the life and death of hair cells (Wan et al., 2013), including acting as hair cell precursors (Corwin and Cotanche, 1988; Lin et al., 2011; Lopez-Schier and Hudspeth, 2006; Millimaki et al., 2010; Weisleder et al., 1995). The mechanism by which hair cells are regenerated differs by model system, with a critical point of difference being whether precursors divide before giving rise to new hair cells. In the lateral line, nascent hair cells are added in pairs as a result of symmetric division and differentiation of supporting cells (Lopez-Schier and Hudspeth, 2006; Mackenzie and Raible, 2012; Romero-Carvajal et al., 2015; Wibowo et al., 2011). When regeneration is observed in mature mammalian vestibular organs, hair cells are added by direct transdifferentiation of supporting cells (Golub et al., 2012). A dual mechanism has been observed in the auditory organ of birds, whereby hair cells are regenerated in an initial wave of transdifferentiation followed by a later wave of asymmetric proliferation (Roberson et al., 2004, 1996). Previous studies have demonstrated hair cell regeneration in the zebrafish inner ear (Jimenez et al., 2021; Millimaki et al., 2010; Schuck and Smith, 2009), with evidence for both proliferative replacement

and transdifferentiation, but definitive experiments are lacking. The transdifferentiation hypothesis is supported by recent single cell and nucleus RNA-seq data, which suggest that the inner ear does not have a clear mitotically cycling supporting cell population as is seen in the lateral line (Baek et al., 2022; Lush et al., 2019) and instead show a substantial transition state population during regeneration which shares gene expression aspects of both hair cells and supporting cells (Jimenez et al., 2022).

Here, we describe a mechanism of hair cell regeneration in the zebrafish inner ear in which supporting cell proliferation in response to hair cell death is not directly coupled with the differentiation of regenerating hair cells. First, we used transgenic zebrafish lines to determine the timecourse of hair cell addition during larval zebrafish development. We found that hair cells are added at a linear rate corresponding to fish growth and that few hair cells are removed due to hair cell turnover during this time. Both hair cell subtypes of the cristae are added at equivalent rates, with some cells converting from peripheral to central subtype over time, resulting in maintenance of organ patterning. When crista hair cells are ablated, hair cell numbers recovered relatively slowly over the course of two weeks, and central-type hair cells are produced at an increased rate, and proper organ patterning is ultimately recovered. We provide evidence that most regenerating hair cells are formed by transdifferentiation. We find that ablation causes an initial burst of supporting cell division, but new hair cells are not differentially derived from this dividing population. Rather, hair cell numbers recover during regeneration due to a transient increase in progenitor pool size.

3.3 Results

Zebrafish inner ear sensory patches grow constantly during the larval stage

Sensory patches in the fish inner ear add new hair cells continuously throughout the animal's life (Bang et al., 2001; Corwin, 1983, 1981; Higgs et al., 2003, 2002). To distinguish hair cell regeneration from addition during growth, we first quantified the rate of hair cell addition under homeostatic conditions. We examined the larval stage, during which the inner ear organs become functional and remain superficial enough for imaging in intact fish. Variation in environmental factors greatly affect fish growth: standard length (SL), a measurement from the snout tip to the caudal peduncle, becomes a better indicator of developmental stage than time after 5 days post-fertilization (dpf) (Parichy et al., 2009). The

larval stage begins at 72 hours post-fertilization and continues until 30-45 dpf when the fish are 11 mm SL. The utricle is formed and functional by 4 dpf (Mo et al., 2010; Riley and Moorman, 2000), and contains both striolar and extrastriolar type hair cells. The cristae do not become functional until later on when the larvae are 8 mm SL, around 30 dpf (Beck et al., 2004), when the semicircular canals are large enough to allow for adequate fluid flow to stimulate hair cells. The cristae, however, are formed by 5 dpf and contain both central and peripheral hair cell subtypes (Bang et al., 2001; Haddon and Lewis, 1996; Shi et al., 2023; Zhu et al., 2021).

To determine the baseline rate of hair cell addition in the zebrafish inner ear, we used a *Tg(myo6b:nls-Eos)* (Cruz et al., 2015) transgenic zebrafish, which expresses the photoconvertible protein Eos in hair cell nuclei. In both cristae and utricle, hair cells were added at a steady rate (Fig. 3.2A-C). In anterior and lateral cristae, hair cells were added at a rate of 19.14 ± 1.33 per mm SL and 20.30 ± 1.26 per mm SL, respectively, with no significant difference between these rates (Fig. 3.2D). In the utricle, hair cells were added at a rate of 49.96 ± 4.3 per mm SL (Fig. 3.2E). Among the cristae, the lateral crista is the earliest to form and is slightly larger than the anterior and posterior cristae at the beginning of the larval stage. This size discrepancy is maintained over time, while the anterior and posterior cristae remain similar in size (Figs 3.2D, 3.S1). Due to its similarity in size to the anterior crista and depth in larger fish, the posterior crista was not a focus of subsequent experiments. These results indicate that hair cells are added at a consistent rate in each of the sensory organs as larvae grow.

Little hair cell turnover occurs in the developing inner ear organs

Hair cells regularly turn over in the adult zebrafish lateral line, with a half-life of approximately one week (Cruz et al., 2015). Studies from birds and mice suggest that the rate of turnover varies across species (Bucks et al., 2017; Goodyear et al., 1999; Jørgensen and Mathiesen, 1988; Kil et al., 1997). To determine the rate of turnover in the zebrafish inner ear, we again used the *Tg(myo6b:nls-Eos)* line. Eos exhibits an irreversible green to red photoconversion upon exposure to UV light. Larval fish were placed under UV light for 10 minutes at 8 dpf (SL 4.0 – 4.5) and fixed and imaged either immediately after photoconversion (Fig. 3.3A, D, G) or following one week of growth (Fig. 3.3B, E, H). Hair cells that are added post-photoconversion can be identified by the absence of photoconverted Eos in their nuclei, while

older cells retain the converted Eos signal. The anterior crista, lateral crista, and utricle showed no significant decrease in photoconverted hair cell nuclei over the course of one week (Fig. 3.3C, F, I). This experiment was repeated for the subsequent week of growth, from 14 to 21 dpf, with again no discernable decrease in photoconverted hair cell number (Fig. 3.S2). Together, these results indicate that little to no hair cell turnover occurs in the zebrafish inner ear organs during larval stages.

Two hair cell subtypes are added consistently during growth

We wanted to understand how the makeup of sensory organs changes as new hair cells are added. By the larval stage, central and peripheral subtypes exist in the cristae, and striolar and extrastriolar cells are present in the maculae (Qian et al., 2022; Shi et al., 2023; Smith et al., 2023, 2020; Tanimoto et al., 2011). We previously identified marker genes for hair cell subtypes that can be used in Hybridization Chain Reaction Fluorescence in situ Hybridization (HCR-FISH)(Choi et al., 2016; Shi et al., 2023). Here, we used probes against *cabp1b* to label peripheral cells in the cristae. We photoconverted *Tg(myo6b:nls-Eos)* fish at 8 dpf and fixed fish at three subsequent timepoints for imaging: 2 days post-photoconversion (dpp), 7 dpp, and 14 dpp. HCR-FISH was then performed with *cabp1b* probes to distinguish subtypes of “new” (cyan) from “old” (magenta + cyan) hair cells (Fig 3.4A-C). During this period there is a substantial increase in the number of new hair cells with little change in old hair cells (Fig 3.4D). Based on the spatial pattern of hair cell addition occurring around the perimeter, we hypothesized that peripheral subtype hair cells would make up the majority of new hair cells. In fact, although *cabp1b*+ new hair cells were common at the peripheral poles of the crista, an almost equal percentage of new central-type *cabp1b*- hair cells were added. This even split of new central and peripheral hair cells was consistent at each timepoint examined (Fig 3.4A-C, E), indicating that both subtypes are added at relatively constant rates. When examining the identity of old hair cells, we observed an increase in the fraction of central to peripheral-type cells over time (Fig. 3.4A-C, E). This suggests that some hair cells convert from peripheral identity to central identity as sensory patches grow larger, resulting in a consistent overall ratio of central to peripheral cells.

Crista hair cells are regenerated in the week following ablation

Unlike in the lateral line, hair cells in the inner ear are protected from ototoxic drugs administered through the water, which are unable to diffuse into the ear. To overcome this limitation, we designed a *Tg(myo6b:TrpV1-mClover)* transgenic line where the mammalian TRPV1 channel is expressed in target cells (Chen et al., 2016). When exposed to its ligand capsaicin, opening of the mammalian TRPV1 channel results in cell death by cation influx. Endogenous zebrafish Trpv1 is unresponsive to capsaicin, like other non-mammalian forms (Gau et al., 2013). Expressing mammalian TRPV1 under a hair cell specific promoter and exposing the fish to capsaicin results in quick and effective hair cell death in the cristae. We crossed the Tg(myo6b:TrpV1-mClover) line to the Tg(myo6b:nls-Eos) to better visualize hair cell nuclei. Larvae were treated with 10 μM capsaicin for one hour at 8 dpf, immediately after which hair cell debris was observed across all three cristae (Fig. 3.5A-B). By 3 hours post-treatment this debris had been largely cleared (Fig. 3.5C). Though this method is highly efficient at killing crista hair cells, hair cell death was inconsistent in the lateral line and was undetectable in the macular organs, likely as a result of different expression levels due to the genetic landscape associated with the location of transgene insertion. Therefore, we focused our subsequent regeneration experiments on the crista. Dose response curves were performed at 5 dpf to determine the appropriate concentration of capsaicin for complete hair cell ablation (Fig. 3.5D) and found that a 10 μM exposure was sufficient. In all subsequent experiments, larvae were treated with 10 μM capsaicin in system water for one hour. Regeneration experiments were performed in sibling Tg(myo6b:nls-Eos) fish in a nac/roy background with and without Tg(myo6b:TrpV1-mClover). Due to the relative brightness of Eos, larvae could not be screened for mClover expression under a fluorescent dissecting microscope, even after photoconversion. Instead, fish were screened for dying hair cells immediately following capsaicin treatment; those with dying crista hair cells became the ablated group and those without dying hair cells formed the control group.

To compare hair cell addition following ablation to growth, hair cells were photoconverted and in some fish ablated at 8 dpf, and then fixed at subsequent timepoints to count hair cell nuclei (Fig. 3.6A). In ablated anterior cristae, the number of new hair cells increased significantly compared to controls over the course of two weeks post-treatment (Fig. 3.6B-C). Correspondingly, total hair cell number was decreased after capsaicin treatment in ablated fish but slowly recovered to control levels by 14 days post-ablation (dpa) (Fig. 3.6D). Similar results were obtained for the lateral crista (Fig. 3.S3). No body length

difference was observed at any timepoint between control and ablated fish, suggesting that crista hair cell ablation does not affect overall growth rates (Fig. 3.S4). The increased rate of hair cell addition and eventual recovery of hair cell numbers in ablated crista suggest that a regenerative response occurs alongside hair cell addition due to organ growth.

Hair cell identity is maintained during regeneration

We next determined whether hair cells regenerated with appropriate spatial identity. We again used HCR probes against *cabp1b* to distinguish peripheral from central type regenerated hair cells. At 2 days post-ablation, newly added *cabp1b*+ and *cabp1b*- hair cells were present in control and ablated conditions (Fig. 3.7A). In regenerating crista, the percentage of new hair cells of the *cabp1b*+ peripheral type was significantly decreased compared to controls (Fig. 3.7B). This suggests that the proportion of newly added central-type cells increases in the aftermath of hair cell ablation. To confirm this, we repeated this experiment using HCR probes for *scn5lab*, a marker of central crista hair cells (Fig. 3.S5A). As expected, the proportion of new *scn5lab*+ central-type cells was significantly increased compared to controls (Fig. 3.S5B, C). To determine whether organ patterning returned to that of homeostatic conditions following ablation, we probed for *cabp1b* in 14 dpa fish (Fig. 3.7C). At this timepoint, when total crista hair cell number in ablated fish had returned to control levels, the overall ratio of central to peripheral hair cells with their regular spatial patterning was also restored (Fig. 3.7D). Together, these data suggest that a memory of organ patterning and corresponding hair cell identities are maintained in cristae even after extensive hair cell loss.

Hair cells regenerate primarily by transdifferentiation

To determine whether proliferative mechanisms are used to regenerate hair cells in the zebrafish inner ear, we applied EdU, a thymidine analog that incorporates into the DNA of dividing cells, resulting in labeled daughter nuclei (Salic and Mitchison, 2008). We performed 24-hour EdU pulses in regenerating fish for 0-1 dpa, from 3-4 dpa, and from 6-7 dpa (Fig. 3.8A). Photoconversion was performed just prior to EdU treatment to identify hair cells added during the EdU pulse. At 1 dpa, EdU labeled hair cells in both control and ablated conditions were rare, less than 1% (Table 1), suggesting that the vast majority of hair

cells added immediately post-ablation do not arise from recently dividing progenitors. Due to the rarity of EdU labeled hair cells in individual cristae, cell counts for the anterior and lateral cristae were combined for these analyses. In both conditions, in cases where rare EdU+ hair cells were observed, they were found paired with an EdU+ supporting cell (Fig. 3.S6), suggesting that a low level of asymmetric division may occur. There was no change at either 4 or 7 dpa, with EdU-labeled hair cells still rare (Table 1), indicating that a later wave of proliferative hair cell regeneration did not occur. We conclude that transdifferentiation is the predominant mechanism by which hair cells are added to regenerating cristae.

Hair cell ablation leads to temporary expansion of a supporting cell progenitor pool

In contrast to hair cells, EdU-labeled supporting cells were common at 1 dpa, and significantly more EdU-labeled supporting cells were present compared to controls (Fig. 3.8B-C). However, there was no significant difference in the number of EdU-labeled supporting cells between control and ablated fish at the 4 or 7 dpa timepoints. These results demonstrate that there is an initial wave of supporting cell proliferation in response to hair cell damage that is not sustained at later periods.

To determine whether supporting cells that divide in response to hair cell ablation ultimately become hair cells, we repeated the regeneration experiment with an EdU pulse during the first 24 hours of regeneration and collected fish at 1, 4 or 7 dpa (Fig. 3.9A). Again, we observed a significant increase in EdU labeled supporting cells 1 dpa compared to controls (Fig 3.S8), and rare labeled hair cells in both control and ablated conditions (Table 1). EdU-labeled hair cells were increasingly common at the 4 and 7 dpa timepoints in both control and ablated fish (Fig. 3.9B, C, Table 1). By 7 dpa, significantly more EdU-labeled hair cells were present in ablated crista (Fig. 3.9B, C), corresponding to the increase in supporting cells labeled at 1 dpa. The total number of new hair cells also significantly increased in ablated compared to control fish (Fig. 3.9D). When viewed as a percentage of all new hair cells, the fraction of EdU+ hair cells is not significantly different between ablated and control conditions at any timepoint (Fig. 3.9E). Therefore, supporting cells that divided in response to hair cell ablation are not more likely to differentiate into hair cells. These results suggest that in the wake of hair cell ablation, supporting cells proliferate to increase the progenitor pool, but that this proliferative response is uncoupled to the rate of hair cell differentiation.

3.4 Discussion

We describe a steady increase in hair cell number during the growth of inner ear sensory patches during the larval phase of zebrafish development, an approximately month-long period after embryogenesis is complete. We used photoconvertible nuclear-localized Eos to distinguish pre-existing hair cells from newly added hair cells. We found that central and peripheral hair cell subtypes were added at the edges of the organ in a stereotyped pattern based on their location. We document a phenotypic switch of some older hair cells from peripheral to central subtype, resulting in conservation of spatial patterning and an overall ratio that slightly favors central-type hair cells. We also found that the number of photoconverted cells in cristae and utricle did not significantly decrease over time, suggesting that there is little hair cell turnover during larval stages.

We provide several lines of evidence that the addition of crista hair cells after damage is more than simply recovery by continued growth. We demonstrate, using photoconversion to parse the timing of differentiation, that new hair cells are added at a faster rate after hair cell ablation than during growth. We also found that compared to growth there was an increase in new hair cells of the central subtype, and as a result the organ regenerates the appropriate ratio of subtypes for correct spatial patterning. Finally, there is an increase in supporting cell proliferation in response to hair cell ablation, eventually resulting in more EdU labeled hair cells than under control conditions. If proliferation and hair cell differentiation were directly coupled, we would expect to see a disproportionate number of dividing support cells become new hair cells. The lack of difference between the fraction of EdU labeled new hair cells in control and ablated conditions indicates that the supporting cells dividing in response to ablation are not more likely than others to differentiate into new hair cells. Indeed, our experiments suggest that during growth, supporting cells convert to hair cells using mechanisms temporally uncoupled from cell division, and regenerating hair cells are added through a similar process of transdifferentiation. We hypothesize that the primary regenerative response to damage is to increase the pool of supporting cells available for differentiation into hair cells, employing the same conversion mechanisms used in normal growth to add new hair cells. Of particular note, the transient increase in supporting cell proliferation occurs before hair cell

replacement, suggesting that the cue for this event is the damage or loss of hair cells rather than depletion of supporting cells through transdifferentiation.

While our current work examines hair cell regeneration in the larval zebrafish cristae over the first month of development, our findings are consistent with previous studies examining regeneration in the zebrafish maculae. Lineage tracing in the embryonic utricle following laser ablation of hair cells provides evidence that supporting cells directly transdifferentiate into nascent hair cells (Millimaki et al., 2010). In the adult saccule, noise damage induces a burst support cell of proliferation that occurs 1-3 days post sound exposure with regenerated hair cell bundles formed in the most damaged area of the organ over approximately 10 days (Schuck and Smith, 2009), a timeline that is consistent with our findings in the cristae. Single-cell RNA-sequencing data from regenerating maculae of adult zebrafish point to the emergence of a transition-state population with qualities of both hair and supporting cells, which could potentially represent actively transdifferentiating cells (Jimenez et al., 2022). Together these studies support a model where damage induces hair cell regeneration through transdifferentiation and expansion of supporting cells through proliferation.

Our findings in the zebrafish inner ear are markedly different from the mechanism of regeneration observed in the zebrafish lateral line system. Following hair cell ablation by ototoxic drug exposure, neuromasts show significant hair cell replacement after 24h and regenerate a full complement of hair cells in just 72 hours (Ma et al., 2008), compared to a gradual replacement of hair cells that we observe in the cristae over the course of two weeks. Lateral line hair cells are regenerated in pairs by symmetrically dividing precursors (Lopez-Schier and Hudspeth, 2006; Mackenzie and Raible, 2012; Romero-Carvajal et al., 2015; Wibowo et al., 2011), while we find those in the cristae are overwhelmingly added by transdifferentiation. The rare examples of EdU-labeled hair cells we observed in the cristae were adjacent to labeled supporting cells, suggesting asymmetric division of precursors. We speculate these differences may reflect the need in the lateral line system to restore the integrity of organs exposed to the environment on the surface of the fish, while regeneration in the inner ear occurs on top of extensive growth and is needed to restore appropriate spatial patterning rather than organ integrity.

Comparison of growth and regeneration in the inner ear of zebrafish to that in birds reveals both similarities and differences. Regeneration of hair cells in avian auditory and vestibular systems occurs by

both transdifferentiation and proliferative replacement. In the regenerating avian utricle, there is evidence that hair cells are replaced both by asymmetric divisions and by transdifferentiation (Scheibinger et al., 2022; Stone et al., 1999). When hair cells are regenerated in the auditory organ, the basilar papilla (BP), they are initially added by wave of transdifferentiation that lasts for several days before a second phase of proliferative hair cell regeneration begins (Roberson et al., 2004, 1996). To determine whether there is a similar late wave of proliferation in the zebrafish cristae we administered pulses of EdU at timepoints several days after ablation but did not observe any increase in EdU-labeled hair or supporting cells compared to controls. Thus, in the zebrafish larval cristae there appears to be a single mechanism of transdifferentiation for hair cell replacement. In the mature avian vestibule, there is significant hair cell turnover with hair cells having an estimated half-life of about 20-30 days as they are removed and replaced via asymmetric division (Goodyear et al., 1999; Jørgensen and Mathiesen, 1988; Kil et al., 1997; Weisleder and Rubel, 1992). We have observed no evidence for turnover in the zebrafish cristae during larval stages but cannot rule out rare events or turnover at later stages. In the few cases where we observed hair cells labeled by EdU, they were accompanied by with neighboring Edu-labeled supporting cell, suggesting that a small amount of asymmetric division may also occur in the zebrafish inner ear.

Our findings show remarkable similarities to processes that occur in the mammalian vestibular system (Burns et al., 2012a; Wang et al., 2015). When damage is induced in the utricle of neonatal mice, new hair cells are initially generated by transdifferentiation of supporting cells, with an accompanying wave of supporting cell proliferation detected by EdU incorporation. In the following weeks a fraction of these EdU-labeled cells become new hair cells. However, the regenerative response is greatly diminished after the first week postpartum. These regenerative events parallel processes that occur during the normal postnatal growth of the mouse utricle, where approximately half of hair cells are added over the three weeks after birth from supporting cells that last divided before birth (Burns et al., 2012b). In adult mice, limited regeneration occurs by transdifferentiation of supporting cells with no detected proliferative response for their replacement, and as a consequence an overall reduction in supporting cell numbers is observed (Golub et al., 2012). Hair cell turnover, while detectable in the adult mouse utricle, is rare and not associated with supporting cell proliferation (Bucks et al., 2017). Taken together these studies support

the idea that there is uncoupled potential for both proliferative and transdifferentiation responses in the mouse utricle that wane over time.

Our study establishes the zebrafish inner ear as a model for hair cell regeneration that parallels processes that are functional for a limited period in mammals. A major difference between mammals and zebrafish is that they lose their ability to regenerate in response to damage (Burns et al., 2012a; Cox et al., 2014) even in response to exogenous factors such as altering Notch signaling or inducing Atoh1 expression (Lin et al., 2011; Liu et al., 2012; Maass et al., 2015). Whether mammals lose their ability to regenerate due to epigenetic changes affecting chromatin accessibility (Tao et al., 2021), alterations in cell cycle regulation (White et al., 2006), changes in tissue architecture (Burns and Corwin, 2014; Collado et al., 2011) or a combination with other unknown factors remains an area of active study.

Zebrafish have a remarkable ability to regenerate many organs, including the heart, liver, kidney, fin, retina, and central nervous system (reviewed in Marques et al., 2019), some of which show similarities to the inner ear regeneration mechanism we describe here. In the zebrafish olfactory bulb, death of sensory neurons by chemical exposure results in proliferation of the precursor pool during the first 24 hours following neuron death (Ma et al., 2018). Transdifferentiation has been observed during regeneration of other zebrafish organ systems, particularly in response to severe organ damage. After major damage to the liver, biliary epithelial cells proliferate and transdifferentiate into regenerated hepatocytes (Choi et al., 2014). In the zebrafish pancreas, upon ablation of insulin-responsive β-cells, some α-cells transdifferentiate into β-cells while others respond by proliferating, presumably to replace converting α-cells (Ye et al., 2015). Other organs do not exhibit transdifferentiation but rely on a resident population of multipotent cells that act in growth and regeneration. Like the in the ear and other organs, zebrafish kidneys grow throughout life in proportion to fish size(Zhou et al., 2010). Some ototoxic drugs, such as aminoglycoside antibiotics, also demonstrate nephrotoxicity. After injection of the aminoglycoside gentamicin, adult zebrafish regenerate nephrons over the course of two weeks (Diep et al., 2011). In this case, regeneration is facilitated by a resident stem cell population that acts both in adult nephrogenesis as well as regeneration (Diep et al., 2011). In the adult zebrafish central nervous system, the telencephalon contains radial glia that proliferate under homeostatic conditions (Rothenaigner et al., 2011). These same glia respond to lesion injury with proliferation and give rise to neuroblasts that migrate

to the site of injury where they differentiate into mature neurons (Kroehne et al., 2011). Our work indicates that support cells of the inner ear may represent a similar resident facultative progenitor population that can self-renew and generate hair cells during growth and regeneration. Whether inner ear support cells are comprised of subpopulations with differential potential to give rise to hair cells remains an unanswered question.

3.5 Methods

Fish maintenance

Experiments were conducted on larval zebrafish between 5dpf and approximately 45dpf (up to 11.0mm SL). Larvae were raised in E3 embryo medium (14.97 mM NaCl, 500 mM KCL, 42 mM Na2HPO4, 150 mM KH2PO4, 1 mM CaCl2 dihydrate, 1 mM MgSO4, 0.714 mM NaHCO3, pH 7.2) at 28.5°C and placed on the nursery system at 5dpf. All transgenic fish lines were crossed into a nac/roy background (Lister et al., 1999; Ren et al., 2002; White et al., 2008) to facilitate inner ear imaging. During experiments, larval fish were returned to the nursery system between treatment and collection timepoints, except during EdU incubation or when collected immediately after treatment. Zebrafish experiments and husbandry followed standard protocols in accordance with University of Washington Institutional Animal Care and Use Committee guidelines.

Photoconversion

Larvae were transferred to a 60 x 15mm petri dish and placed in a freezer box lined with aluminum foil. An iLumen 8 UV flashlight (procured from Amazon) was affixed in the freezer box lid and positioned over the dish. Larvae were exposed to UV light for 10 min before being returned to standard 100 x 15mm petri dishes to await experimentation.

TrpV1 hair cell ablation

Capsaicin (Sigma-Aldrich, #M2028) was resuspended in DMSO and stored at -20°C until use. Dose-response curves were performed on *Tg(myo6b:TrpV1-mClover)* in both *AB and Nac/Roy backgrounds. There were no apparent differences in response to capsaicin treatment between fish of the two

backgrounds. 10 μM capsaicin was determined to be an appropriate dose to effectively ablate cristae hair cells when treated for 1 hour at 28.5°C. The brightness of Eos in the *Tg(myo6b:nls-Eos)* line prevents normal fluorescent dissecting scope screening for *Tg(myo6b:TrpV1-mClover)*, even after Eos has been photoconverted. 8dpf *Tg(myo6b:nls-Eos)* siblings with and without *Tg(myo6b:TrpV1-mClover)* were treated with 10 μM capsaicin for one hour at 28.5°C. Larvae were washed 3 x 5 minutes in system water. Larvae were then screened for dying hair cells to indicate the presence (ablated) or absence (control) of TrpV1-mClover. Ablated and control fish were separately returned to the nursery system to await collection.

EdU treatment and visualization

Larvae were incubated in 500μM F-ara-EdU (Sigma, #T511293) for 24 hours at 28.5°C. Click-iT protocol was modified from Salic and Mitchison, 2008. Briefly, larvae were fixed in 4% paraformaldehyde at 4°C for 18-48 hours, depending on their size, then washed with PBS containing 0.1% Tween20 for 3 x 10 minutes. Larvae were permeabilized in 0.5% TritonX-100 in PBS for 30 minutes and washed 3 x 10 minutes with PBS alone. Reaction solution was prepared fresh each time: 2 mM CuSO4, 10 mM Alexa Fluor 647 azide, and 20 mM sodium ascorbate in PBS. Fish were incubated in reaction solution for 1 hour in the dark at room temperature, washed 3 x 20 minutes with PBS, and stored in the dark at 4°C until imaging.

HCR FISH

Hybridization chain reaction in situ hybridizations (Molecular Instruments, HCR v3.0) were performed as directed for whole-mount zebrafish embryos and larvae (Choi et al., 2018, 2016). Briefly, larvae were fixed in 4% PFA at 4°C for 18-48 hours. Larvae were washed with PBS and transferred to MeOH to be stored at -20°C until use. Larvae were rehydrated using a gradation of MeOH and PBST washes, treated with proteinase K for 25 minutes and post-fixed with 4% PFA for 20 minutes at room temperature. For the detection phase, larvae were pre-hybridized with a probe hybridization buffer for 30 minutes at 37 °C, then incubated with probes overnight at 37°C. Larvae were washed with 5X SSCT to remove excess probes. For the amplification stage, larvae were pre-incubated with an amplification buffer for 30 minutes

at room temperature and incubated with hairpins overnight in the dark at room temperature. Excess hair pins were removed by washing with 5X SSCT. Larvae were transferred to storage buffer and kept in the dark at 4°C until imaging.

Fixation and imaging preparation

Larvae were fixed in 4% paraformaldehyde at 4°C for 18-48 hours, depending on their size. Larvae were washed 3 x 15 mins in PBS containing 0.1% Tween20 and transferred to storage buffer (PBS containing 0.2% Triton, 1% DMSO, 0.02% sodium azide, and 0.2% BSA). Samples were stored for no more than 3 weeks at 4°C before imaging. Fixed fish were mounted by first drawing a thin ring of vacuum grease on the underside of a coverslip. One or more specimens were placed on their side in the center of the ring along with 1-2 drops of PBS or other storage solution. A second coverslip was placed on top and gently pushed down at the sides to create a seal around the samples to prevent evaporation and drifting while imaging. Coverslip “sandwiches” were overlayed on a flat ruler under a dissecting microscope, and standard length for each fish was measured, estimating to the nearest 0.25mm. Hair cells in the cristae and utricle were counted in fixed, intact fish as much as possible. When larval fish grew beyond approximately 8 mm, it became necessary to dissect the ear in order to image and perform accurate hair cell counts.

Imaging

Images for development, turnover, and regeneration timeline experiments were captured on a Zeiss LSM-880 with Airyscan 1.0 functionality. Z-stacks of inner ear organs were taken using a 20X/0.8 air objective at intervals of 0.32 µm. Development, turnover, regeneration timeline, EdU, and HCR experimental images were captured using a Zeiss LSM-980 with Airyscan 2.0. Z-stacks of inner ear organs were taken using a 25X/0.8 water objective at intervals of 0.58 µm. Z-stacks of whole ears were taken using a 10X/0.45 air objective at intervals of 1.32 µm. All Airyscan processing was performed at standard strength using Zen Blue software (Zeiss, www.zeiss.com). Image processing and data analysis were performed using Fiji (Schindelin et al., 2012).

Statistical analysis

Power analyses were performed in G*Power (Faul et al., 2007) using preliminary data to determine sample sizes. All other statistical analyses were performed in GraphPad Prism version 10.1.0 (GraphPad Software, Boston, Massachusetts USA, www.graphpad.com).

Data availability

All data available upon request to corresponding author.

Competing interests

No competing interests declared.

Funding

This work was supported by the National Institutes of Health T32GM007270, T32DC005361, and F31DC020898 to M.O.B.; R21DC015110 and R21DC019948 from the National Institute on Deafness and Other Communication Disorders (NIDCD) of the National Institutes of Health, Hearing Health Foundation, Hamilton and Mildred Kellogg Trust, and the Whitcraft Family Gift to D.W.R.

3.6 Acknowledgements

We would like to thank David White, Jessica Knight, George Sanders DVM, and the rest of the University of Washington zebrafish facility for fish care. We thank Tor Linbo and Brenna N. Linton for assistance with breeding and screening of fish.

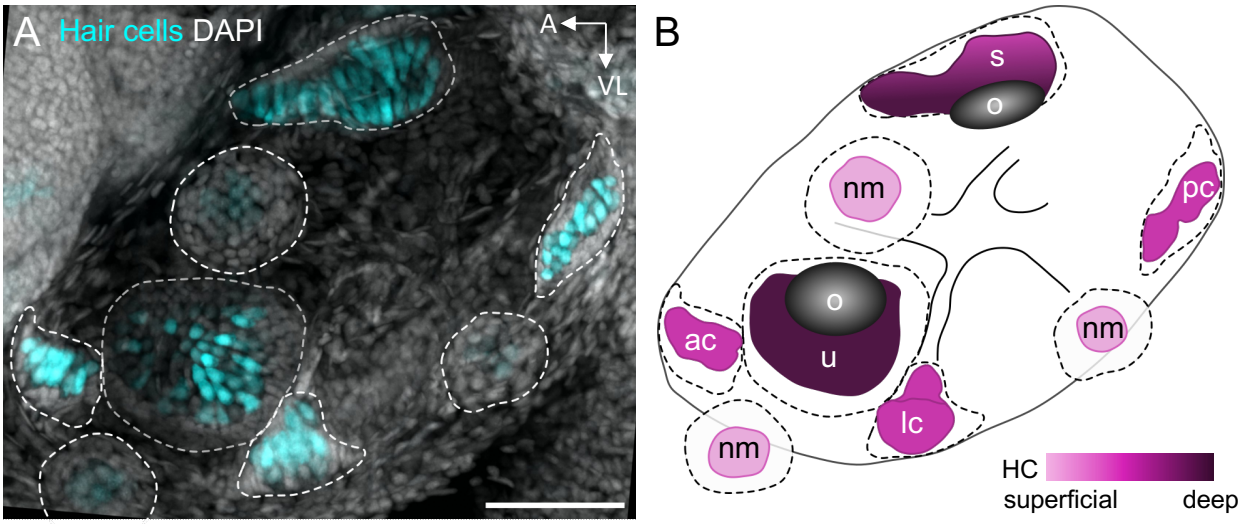

Figure 3.1 Inner ear organs of the larval zebrafish

A) Maximum intensity projection image of *Tg(myo6b:GFP)* 5dpf larval zebrafish ear. GFP-labeled hair cells are shown in cyan and DAPI-labeled nuclei are shown in grey. Dotted outlines delineate neuromast and inner ear organ boundaries. Scale bar = 50 μm. B) Diagram of 5dpf larval zebrafish ear. Color gradient indicates depth of organs where lighter colors indicate more superficial structures and darker colors indicate deeper structures. Dotted outlines delineate neuromast and inner ear organ boundaries, while color-filled areas indicate location of hair cells. ac = anterior crista, lc = lateral crista, nm = neuromast, o = otolith, pc = posterior crista, s = saccule, u = utricle.

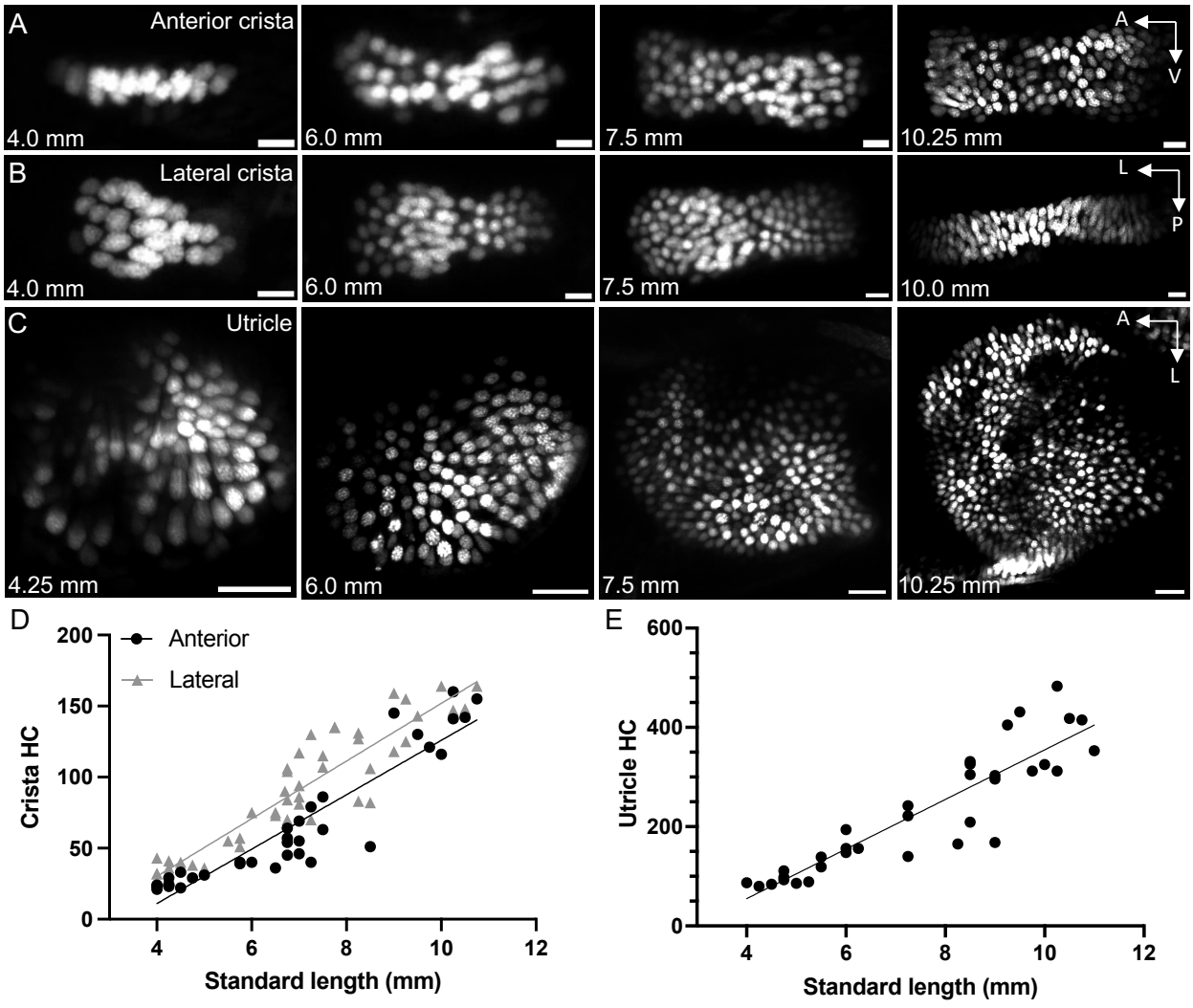

Figure 3.2 Addition of hair cells during larval zebrafish growth

A) Maximum intensity projections of *Tg(myo6b:NLS-Eos)* anterior crista hair cells at standard lengths 4.0 mm, 6.0 mm, 7.5 mm, and 10.25 mm. Scale bar = 10μm. B) Maximum intensity projections of lateral crista hair cells at standard lengths 4.0 mm, 6.0 mm, 7.5 mm, and 10.0 mm. Scale bar = 10μm. C) Maximum intensity projections of utricle hair cells at standard lengths 4.25 mm, 6.0 mm, 7.5 mm, and 10.25 mm. Scale bar = 20μm. D) Quantification of hair cell number in the anterior and lateral cristae across the larval stage of development. Anterior crista data points are represented by black circles (n = 35), while the lateral crista is represented by grey triangles (n = 47). Each data point represents one ear from one fish. Anterior crista slope = 19.14 ± 1.33 HC per mm SL, R^2 = 0.862. Lateral crista slope = 20.30 ± 1.26 HC per mm SL, R^2 = 0.853. Simple linear regression indicates no significant difference between

these two slopes (p = 0.529). E) Quantification of utricle hair cell number across the larval stage (n = 34). Linear regression of utricle hair cell number slope = 49.96 ± 4.28 HC per mm SL, R^2 = 0.812.

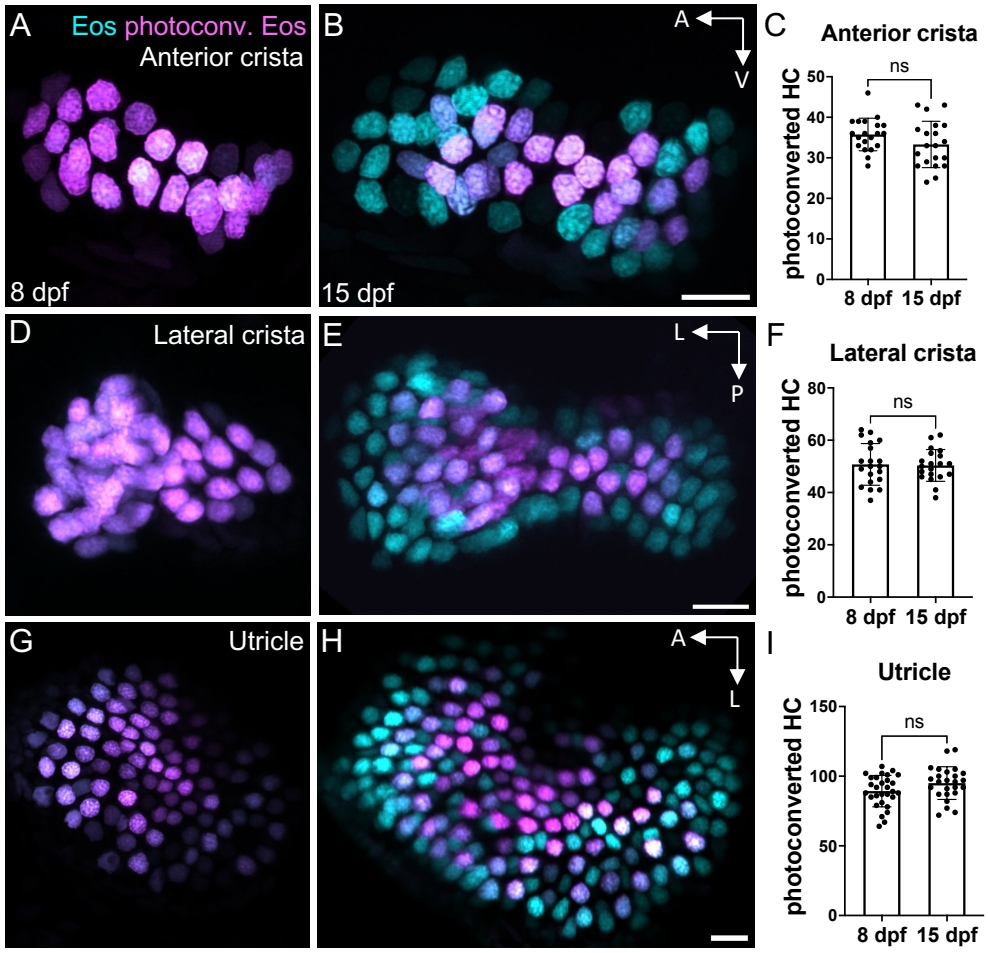

Figure 3.3 Little hair cell turnover occurs in the larval zebrafish ear

A-B) Representative maximum intensity projection images of *Tg(myo6b:NLS-Eos)* anterior cristae A) immediately post-photoconversion at 8 days post-fertilization (dpf) or B) one week post-photoconversion at 15 dpf. HC that were photoconverted retain photoconverted (magenta) Eos signal while new HC have unconverted (cyan) Eos only. C) Quantification of anterior crista photoconverted hair cells at 8 and 15 dpf (n = 20 at 8 dpf, 20 at 15 dpf). D-F) Analogous results for the lateral crista (n = 20, 20) and G-I) for the utricle (n = 29, 25). Unpaired t tests indicate no significant difference between the number of photoconverted hair cells at these two timepoints (ant crista p = 0.125, lat crista p = 0.859, utricle p = 0.071). Scale bars = 10 μm. All data is presented as mean ± s.d.

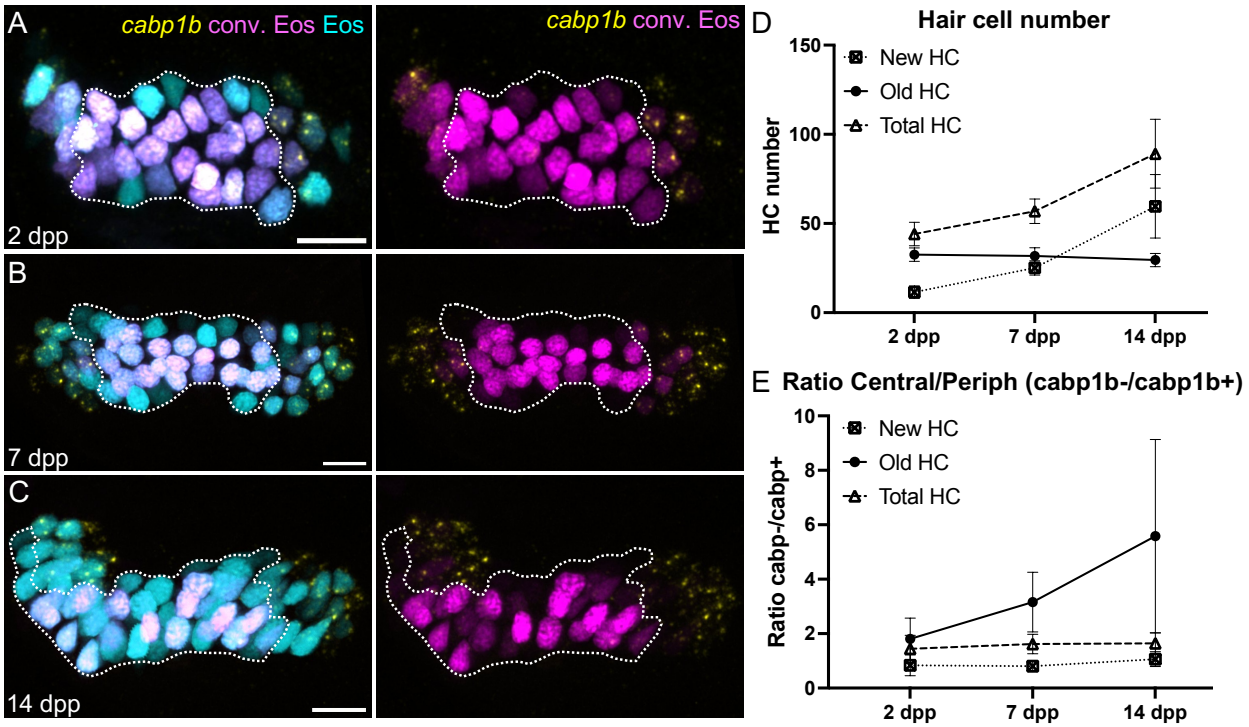

Figure 3.4 Identification of inner ear hair cell subtypes during larval growth

A-C) Maximum intensity projection images of HCR-FISH probing for *cabp1b* expression in *Tg(myo6b:NLS-Eos)* anterior cristae at A) 2 days post-photoconversion (dpp) (10 dpf, n = 14); B) 7 days dpp (15 dpf, n = 12); and C) 14 dpp (22 dpf, n = 8). Old HC retain photoconverted (magenta) Eos signal while new HC have unconverted (cyan) Eos only. Peripheral-type hair cells are labeled by the *cabp1b* HCR probe (yellow). Dotted outline delineates central, *cabp1b*- region of the sensory patch. Scale bars = 10 µm. D) Increase in hair cell numbers over the course of the experiment. E) ratio of central (*cabp1*-) to peripheral (*cabp1b*+) hair cells over time. The increased ratio for old cells suggests phenotypic conversion from peripheral to central hair cell typeover time. All data is presented as mean ± s.d.

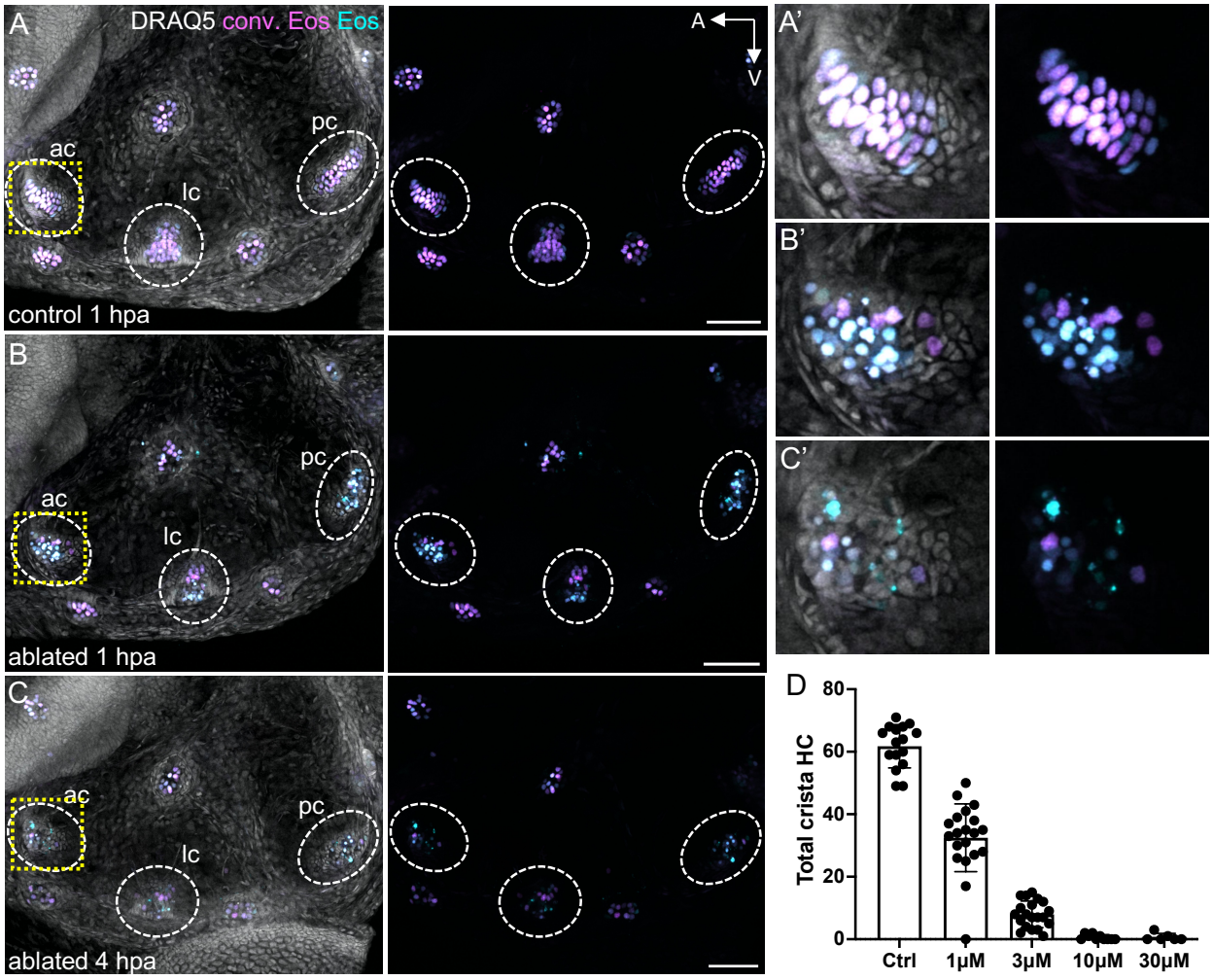

Figure 3.5 Trpv1-capsaicin hair cell ablation

A) Maximum intensity projection of a photoconverted 8dpf *Tg(myo6b:NLS-Eos)* larval inner ear one hour after capsaicin treatment. B) Maximum intensity projection of a sibling *Tg(myo6b:NLS-Eos);Tg(myo6b:TrpV1-mClover)* inner ear one hour after capsaicin treatment or C) four hours after capsaicin treatment. Images show photoconverted (magenta) and unconverted (cyan) Eos signal with and without DRAQ5-labeled nuclei. Dashed oval regions indicate anterior, lateral, and posterior cristae. Dashed yellow box indicates magnified anterior cristae region shown in A'-C'. D) Dose-response curve for hair cells following one hour of treatment with capsaicin at different concentrations. Control treatment represents DMSO alone. Each data point represents the number of hair cells in combined anterior, lateral, and posterior crista of one fish ear (n = 6-20). All data is presented as mean ± s.d.

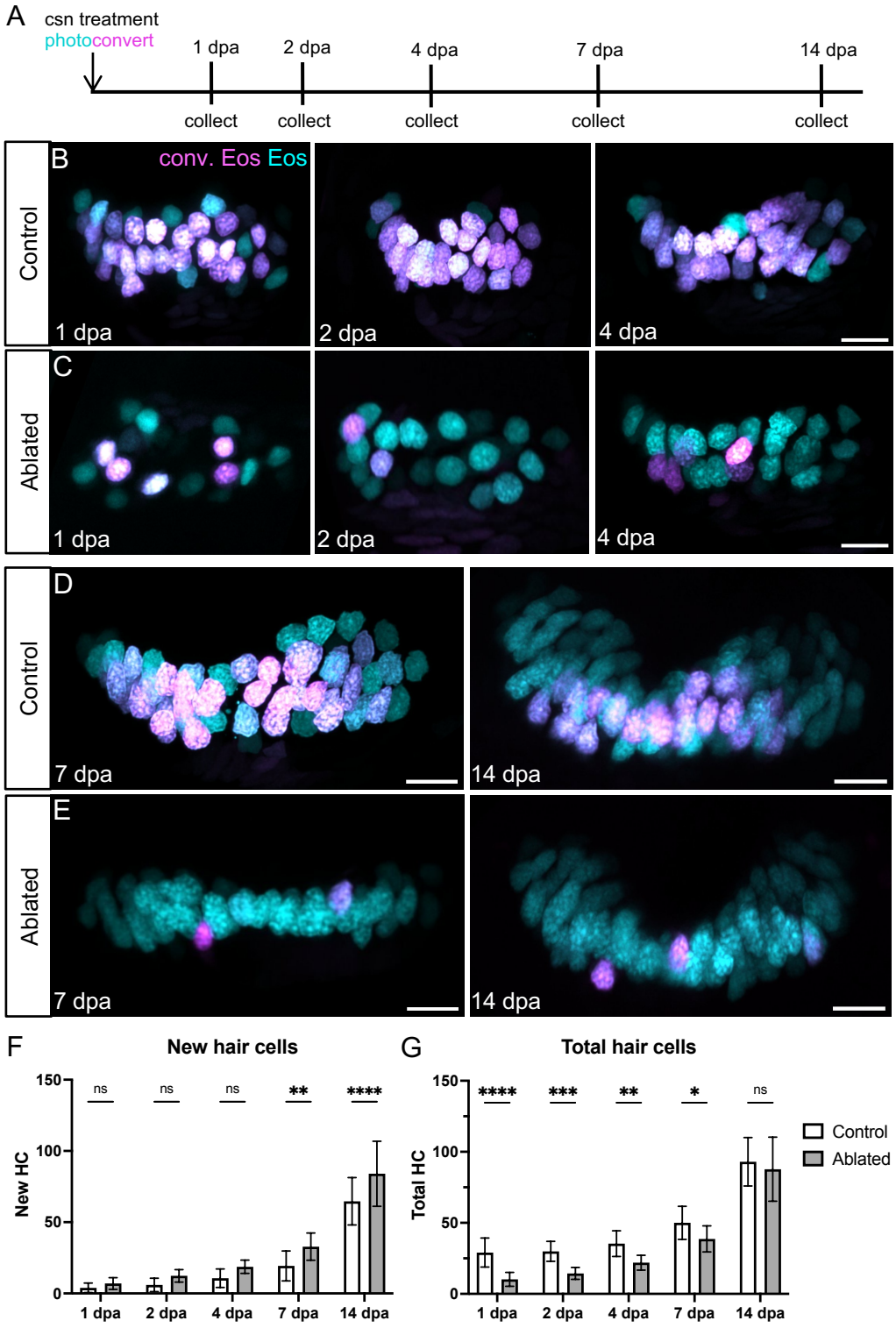

Figure 3.6 Anterior crista hair cells regenerate during the two weeks following ablation

A) *Tg(myo6b:NLS-Eos)* sibling larvae with or without *Tg(myo6b:TrpV1-mClover)* were photoconverted and treated with capsaicin to ablate hair cells at 8dpf. Larvae were collected at five timepoints over the following two weeks: 1 (n = 22 control, 25 ablated), 2 (n = 13, 20), 4 (n = 19, 18), 7 (n = 16, 13), or 14 (n = 18, 15) days-post ablation. B) Representative maximum intensity projections of anterior crista in control and ablated fish at five timepoints following treatment. Nuclei of cells that survived capsaicin treatment contain photoconverted Eos (magenta). Hair cells newly added after capsaicin treatment have nuclei with only unconverted Eos (cyan). Scale bars = 10 μm. C) Quantification of new (cyan-only) hair cells in ablated and control anterior crista. Two-way ANOVA variation across condition $p < 0.0001$; Šídák's multiple comparisons post-hoc test for 7 dpa adjusted p-value = 0.0021, 14 dpa adjusted p-value < 0.0001. D) Quantification of total hair cells in ablated and control anterior crista. Two-way ANOVA variation across condition $p < 0.0001$; Šídák's multiple comparisons post-hoc test for 1 dpa adjusted p-value < 0.0001, 2 dpa adjusted p-value = 0.0006, 4 dpa adjusted p-value = 0.0015, 7 dpa adjusted p-value = 0.0342. All data is presented as mean ± s.d.

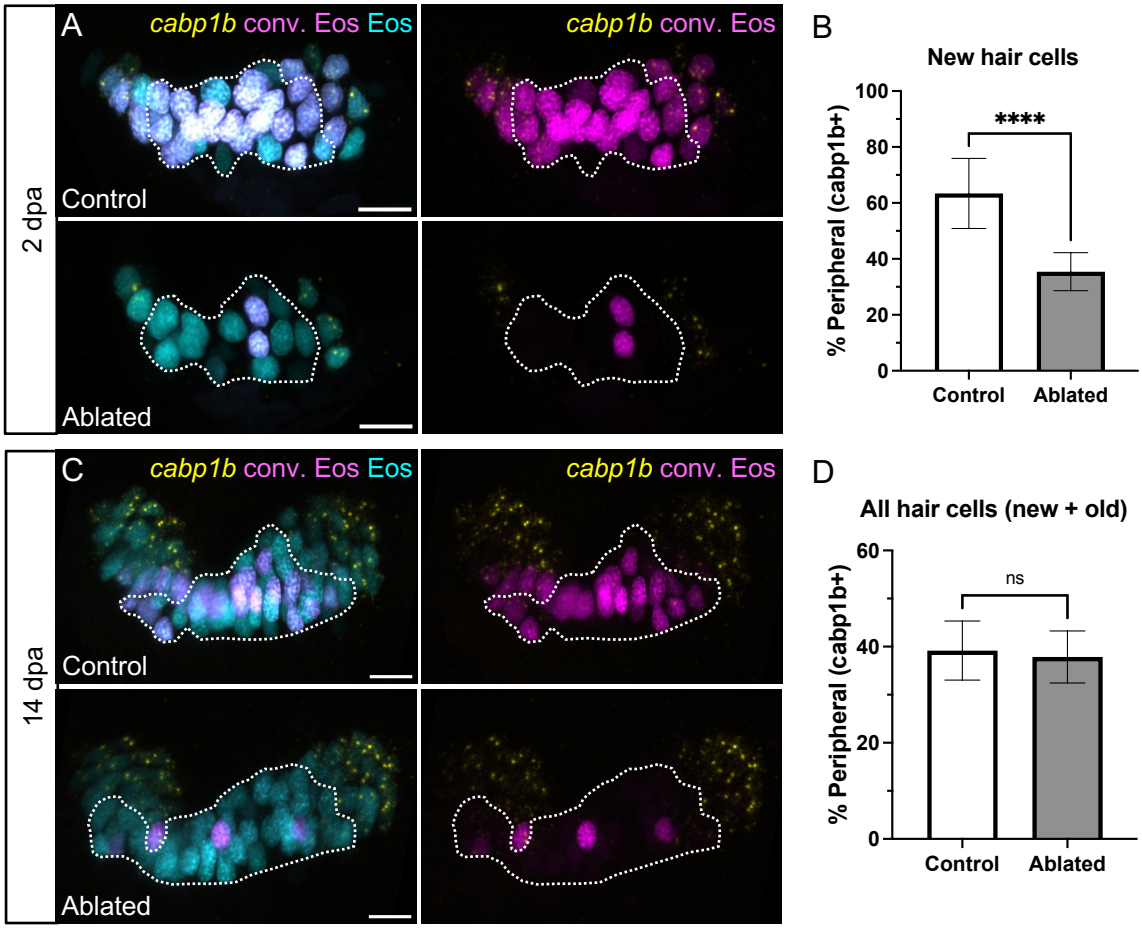

Figure 3.7 Hair cell central-peripheral patterning is restored following ablation

A) Representative maximum intensity projections of anterior crista in control and ablated fish at 2 dpa with *cabp1b* HCR-FISH. Photoconverted Eos (magenta) and *cabp1b* (yellow) channels are shown with and without unconverted Eos (cyan). Dotted outline delineates central, *cabp1b*- region of the sensory patch. B) Quantification of *cabp1b*+ new hair cells, shown as a percentage of all new (cyan-only) hair cells in control (n = 18) and ablated (n = 16) anterior cristae. Unpaired t test $p < 0.0001$. C-D) Analogous data to A-B for crista at 14 dpa (n = 18 control, 15 ablated). Unpaired t test $p = 0.5226$. Scale bars = 10 μm. All data is presented as mean ± s.d.

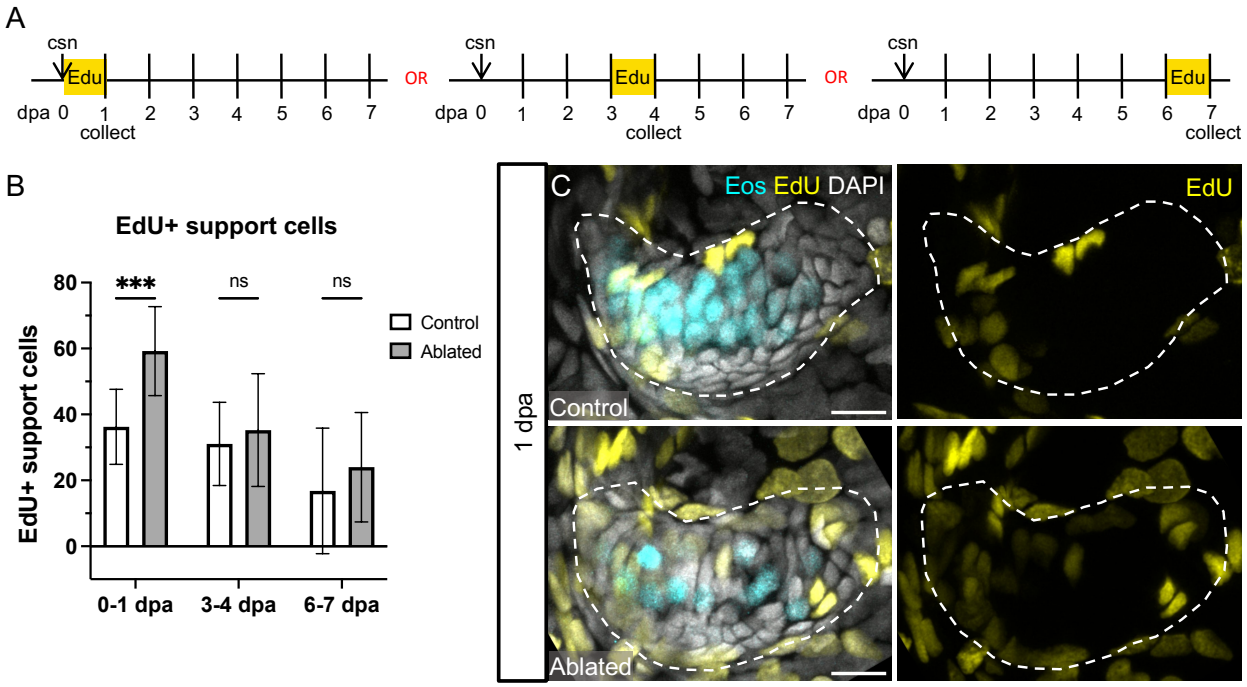

Figure 3.8 Support cells proliferate in response to hair cell ablation

A) Larvae were incubated in EdU for 24 hours immediately after hair cell ablation, at 3 dpa, or at 6 dpa and collected at the end of the 24-hour incubation. B) Quantification of EdU-labeled support cells in the anterior and lateral cristae combined in control and ablated fish incubated in EdU from 0-1 dpa (n = 13 control, 14 ablated), 3-4 dpa (n = 19, 12), or 6-7 dpa (n = 9, 7). Two-way ANOVA is significant across condition p = 0.0021, Šídák's multiple comparisons post-hoc test 0-1 dpa adjusted p-value = 0.0004. All data is presented as mean ± s.d. C) Representative maximum intensity projections of anterior crista in control and ablated fish incubated with EdU from 0-1 dpa with Eos-labeled hair cells in cyan and EdU-labeled nuclei in yellow.

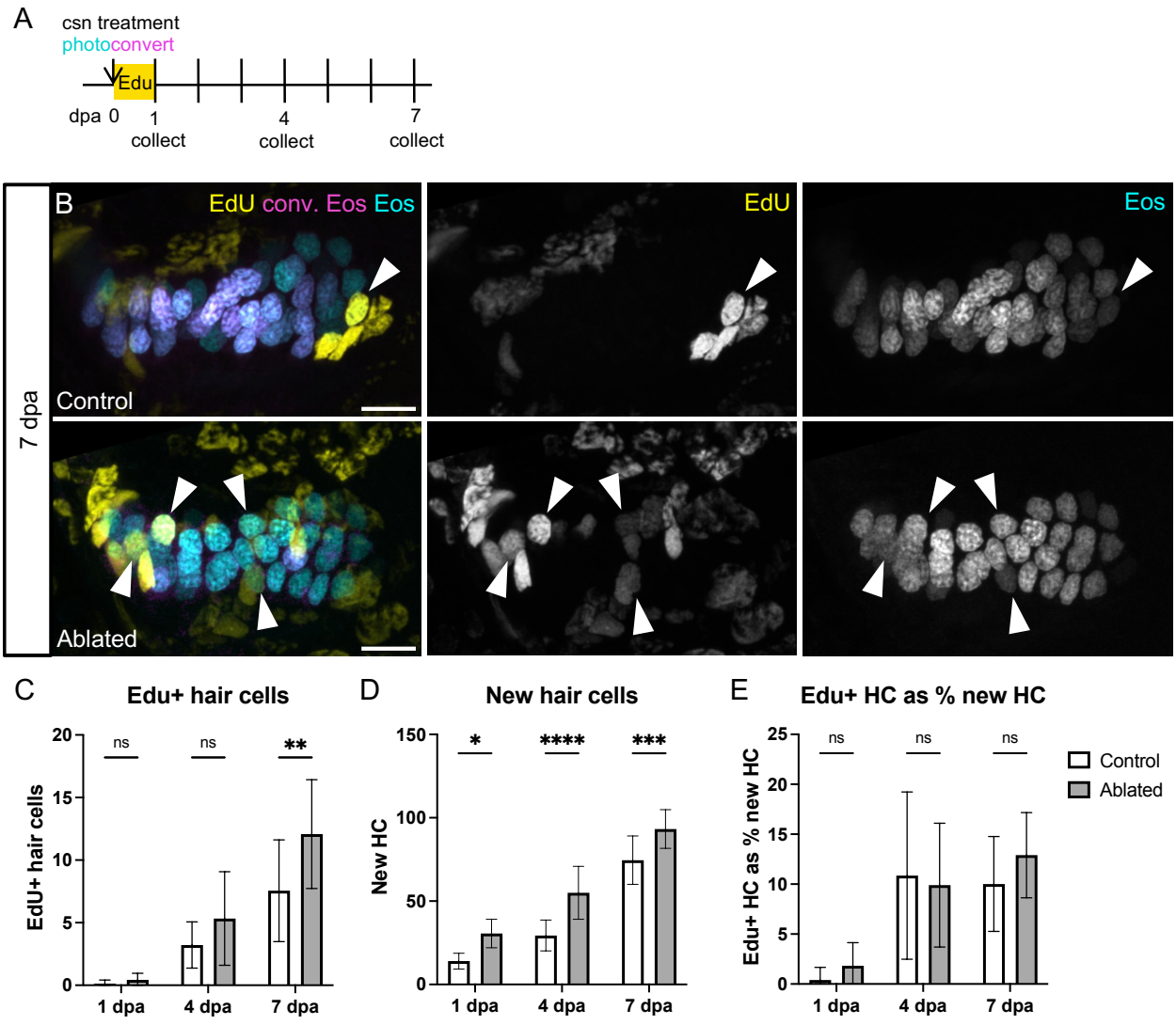

Figure 3.9 EdU-labeling of hair cells over the week following ablation

A) Larvae were incubated in EdU for 24 hours after photoconversion and hair cell ablation and collected either at the end of the incubation (1 dpa; n = 10 control, 7 ablated) or at 4 (n = 14, 8) or 7 (n = 9, 13) dpa. B) Representative maximum intensity projections of anterior crista in control and ablated fish at 7 dpa. White arrowheads indicate hair cells added since ablation with EdU signal (yellow), unconverted Eos (cyan), and without photoconverted eos (magenta). Scale bars = 10 μm. C) Quantification of EdU+ hair cells in the combined anterior and lateral cristae at each timepoint in control and ablated fish. Two-way ANOVA is significant across condition p = 0.0050, Šídák's multiple comparisons post-hoc test 7 dpa adjusted p-value = 0.0034. D) Quantification of new (cyan-only) hair cells at each timepoint in control and

ablated fish. Two-way ANOVA is significant across condition $p < 0.0001$, Šídák's multiple comparisons post-hoc test 1 dpa adjusted p-value = 0.0123, 4 dpa adjusted p-value <0.0001, 7 dpa adjusted p-value = 0.0010. E) EdU+ hair cells as a percentage of new hair cells. Two-way ANOVA with Šídák's multiple comparisons post-hoc test is not significant across condition at any timepoint. All data is presented as mean ± s.d.

		Control				Ablated			
Fig.	Timepoint	EdU+ HC	New HC	Edu % new HC	N	EdU+ HC	New HC	Edu % new HC	N
8	0-1 dpa	0.23 (± 0.48)	-	-	13	0.36 (± 0.63)	-	-	14
	3-4 dpa	0.32 (± 0.48)	13.26 (± 5.51)	2.0 (± 3.21)	19	0.42 (± 1.16)	16.25 (± 5.33)	1.75 (± 4.86)	12
	6-7 dpa	0.33 (± 0.71)	14.78 (± 5.52)	1.80 (± 3.61)	9	0.43 (± 0.53)	17.29 (± 8.67)	2.08 (± 2.63)	7
9	1 dpa	0.10 (± 0.32)	14.0 (± 4.71)	0.40 (± 1.26)	10	0.43 (± 0.53)	30.57 (± 8.54)	1.83 (± 2.30)	7
	4 dpa	3.21 (± 1.85)	29.36 (± 9.25)	10.8 (± 8.38)	14	5.33 (± 3.74)	55.0 (± 15.88)	9.90 (± 6.20)	9
	7 dpa	7.56 (± 4.07)	74.55 (± 14.53)	10.01 (± 4.75)	9	12.08 (± 4.35)	93.23 (± 11.60)	12.90 (± 4.26)	13

Table 3.1 EdU+ hair cell averages with percent new hair cells for EdU experiments

Values shown are mean (± s.d.) for combined anterior and lateral cristae.

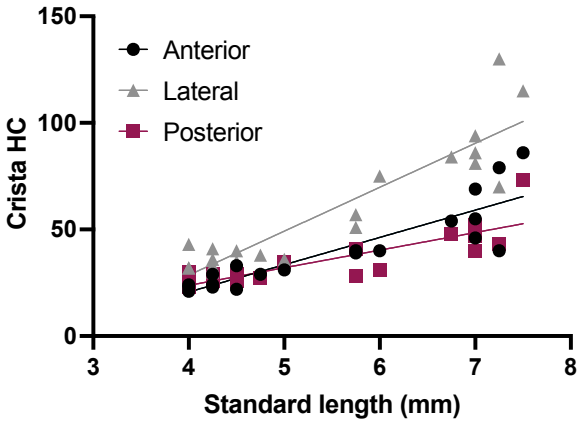

Figure 3.S1 The posterior crista is similar in size to the anterior crista

Hair cell counts from the anterior, lateral, and posterior cristae from the same set of fish. Each data point represents one ear from one fish (n = 21). Linear regression of anterior crista slope 12.8 = ± 1.59, R^2 = 0.773; lateral crista slope = 20.61 ± 2.12, R^2 = 0.832; posterior crista slope = 8.26 ± 1.21, R^2 = 0.720.

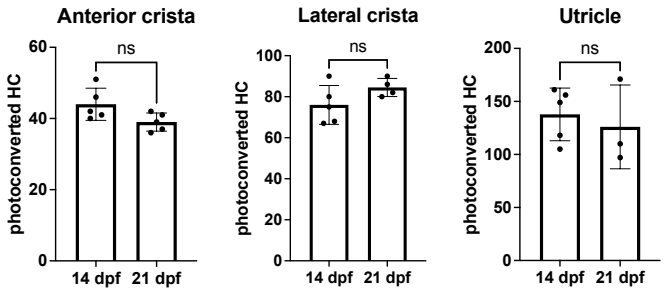

Figure 3.S2 Little hair cell turnover occurs in the third week post-fertilization

Quantification of anterior crista, lateral crista, and utricle photoconverted hair cells at 14 (n = 5 ant crista, 5 lat crista, 5 utricle) and 21 dpf (n = 5 ant crista, 4 lat crista, 3 utricle). Mann-Whitney tests indicate no significant difference between the number of photoconverted hair cells at these two timepoints (ant crista p = 0.095, lat crista p = 0.174, utricle p = 0.786). All data is presented as mean ± s.d.

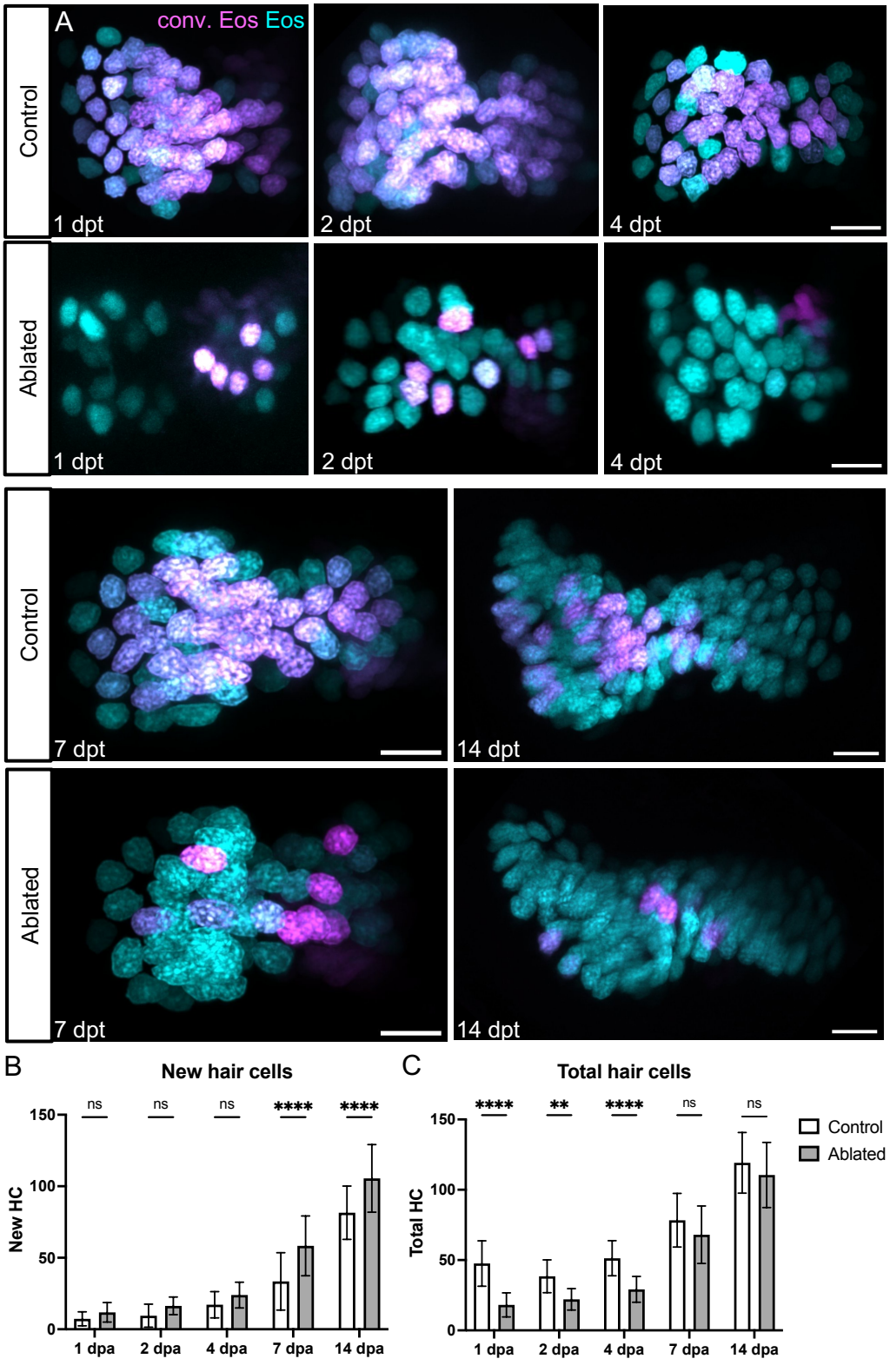

Figure 3.S3 Lateral crista hair cells regenerate during the two weeks following ablation

A) *Tg(myo6b:NLS-Eos)* sibling larvae with or without *Tg(myo6b:TrpV1-mClover)* were photoconverted and treated with capsaicin to ablate hair cells at 8dpf. Larvae were collected at five timepoints over the following two weeks: 1 (n = 22 control, 25 ablated), 2 (n = 20, 22), 4 (n = 19, 17), 7 (n = 16, 12), or 14 (n = 18, 14) days post-ablation (dpa). Representative maximum intensity projections of lateral crista in control and ablated fish at five timepoints following treatment. Nuclei of cells that survived capsaicin treatment contain photoconverted Eos (magenta). Hair cells newly added after capsaicin treatment have nuclei with only unconverted Eos (cyan). Scale bars = 10 μm. B) Quantification of new (cyan-only) hair cells in ablated and control lateral crista. Two-way ANOVA variation across condition $p < 0.0001$; Šídák's multiple comparisons post-hoc test for 7 dpa adjusted p-value < 0.0001, 14 dpa adjusted p-value < 0.0001. C) Quantification of total hair cells in ablated and control anterior crista. Two-way ANOVA variation across condition $p < 0.0001$; Šídák's multiple comparisons post-hoc test for 1 dpa adjusted p-value < 0.0001, 2 dpa adjusted p-value = 0.0051, 4 dpa adjusted p-value < 0.0001. All data is presented as mean ± s.d.

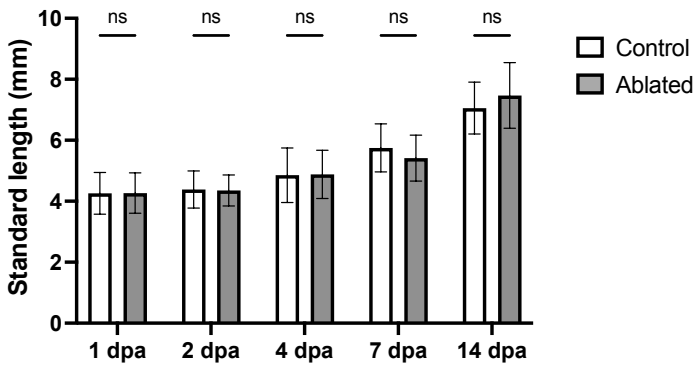

Figure 3.S4 Crista hair cell ablation does not affect larval growth

Standard length measurements across 1 (n = 23 control, 27 ablated), 2 (n = 13, 22), 4 (n = 12, 17), 7 (n = 15, 6), or 14 (n = 32, 16) dpa timepoints for ablated and control larvae. Two-way ANOVA with Šídák's multiple comparisons post-hoc test indicates no significant differences across condition at any timepoint.

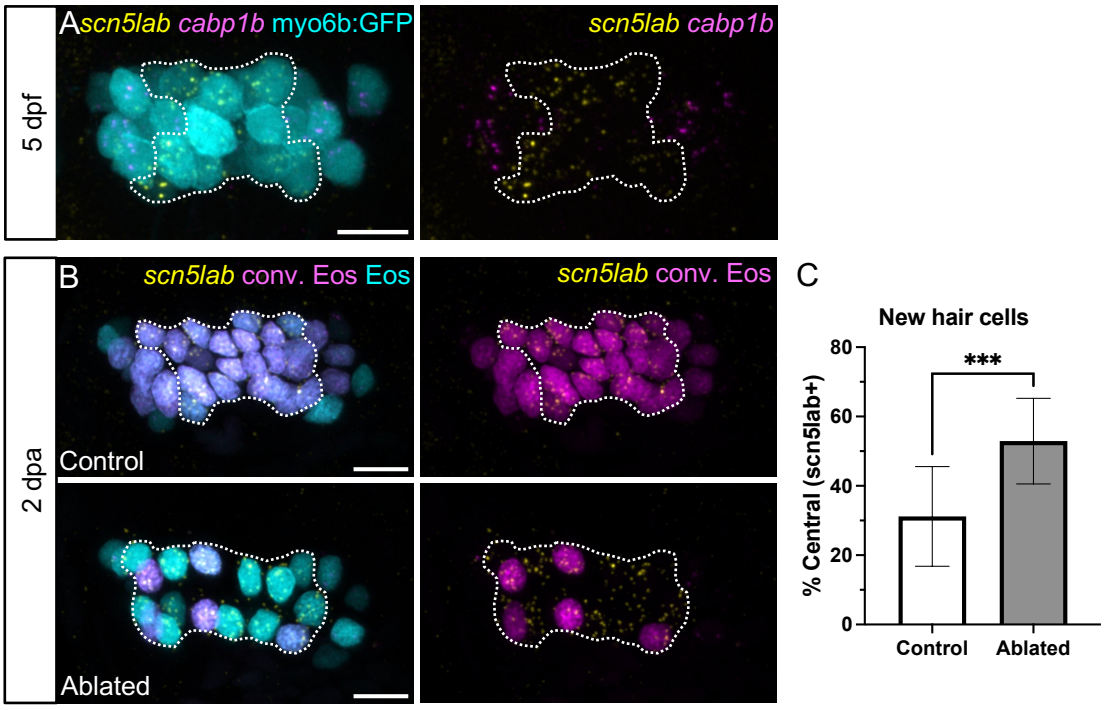

Figure 3.S5 Central-type hair cells are preferentially added following hair cell ablation

A) Representative maximum intensity projections of the anterior crista of a *Tg(myo6b:GFP)* (cyan) 5 dpf larvae treated with HCR *cabp1b* (magenta) and *scn5lab* (yellow) probes to label peripheral- and central-type hair cells, respectively. Dotted outline delineates central, *cabp1b*-;*scn5lab*+ region of the sensory patch. B) Representative maximum intensity projections of anterior crista in control and ablated fish at 2 dpa with *scn5lab* HCR-FISH. Photoconverted Eos (magenta) and *scn5lab* (yellow) channels are shown with and without unconverted Eos (cyan). Dotted outline delineates central, *scn5lab*+ region of the sensory patch. Scale bars = 10 μm C) Quantification of *scn5lab*+ new hair cells, shown as a percentage of all new (cyan-only) hair cells in control (n = 13) and ablated (n = 17) anterior cristae. Unpaired t test p = 0.0001.

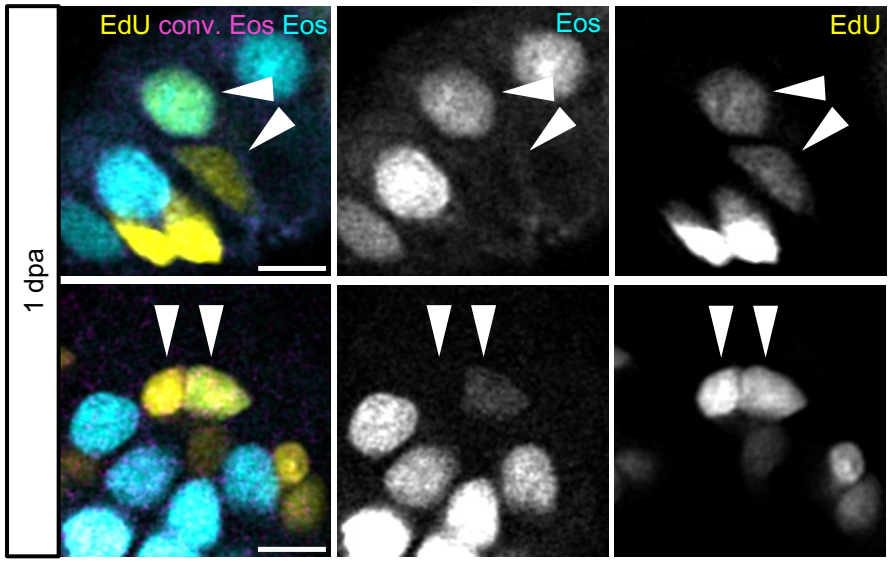

Figure 3.S6 EdU-labeled hair cell-supporting cell pairs are observed following hair cell ablation

Two examples of hair cell-supporting cell EdU+ pairs in ablated fish after 24h EdU incubation (1 dpa). Arrows indicate pairs where both cells are labeled with EdU (yellow), but only one expresses the Eos (cyan) hair cell marker. Scale bars = 5 μm

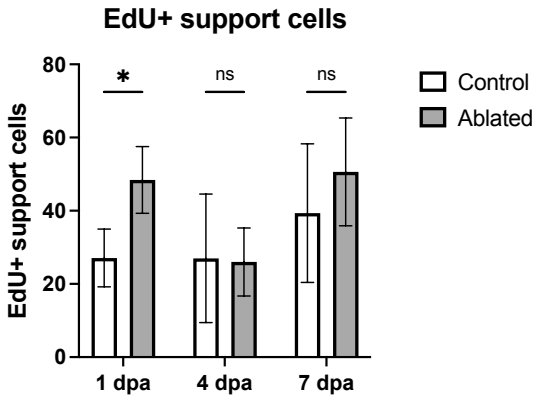

Figure 3.S7 EdU-labeling of supporting cells over the week following ablation

Larvae were incubated in EdU for 24 hours after photoconversion and hair cell ablation and collected either at the end of the incubation (1 dpa; n = 10 control, 7 ablated) or at 4 (n = 14, 8) or 7 (n = 9, 13) dpa. Quantification of EdU+ supporting cells in the combined anterior and lateral cristae at each timepoint in control and ablated fish. Two-way ANOVA is significant across condition p = 0.0069, Šídák's multiple comparisons post-hoc test 1 dpa adjusted p-value = 0.0107. All data is presented as mean ± s.d.

CHAPTER 4: CONCLUSIONS AND FUTURE DIRECTIONS

The work presented herein has substantially advanced the zebrafish inner ear as a model system for studying hair cell regeneration. Beyond characterizing regeneration of hair cells in the zebrafish ear, it has also provided clarity on the relationship of the zebrafish inner ear to other commonly studied model systems, including the zebrafish lateral line and the mammalian utricle.

In Chapter 2, I provided evidence for molecularly distinct hair and supporting cells of the zebrafish inner ear that are present from embryogenesis to adult stages. By analyzing single-cell RNA seq data, I and my co-first author Tuo Shi identified molecular markers for these distinct populations that can now be used to identify cell types in vivo. Hair and supporting cell subtypes and progenitor cells of the inner ear can be identified in tissues using the RNA FISH probes validated in this chapter. These markers and other differentially expressed genes from our dataset can be used to make transgenic zebrafish lines that label cell subtypes to facilitate experiments involving live imaging and fate mapping. In particular, transgenic lines that are specific to inner ear supporting cells are currently lacking but could be generated using highly expressed genes that we validated, such as *zpld1a* in the cristae and *tectb* in the maculae.

This chapter also presented computational comparisons of cells in the zebrafish inner ear with cells of the lateral line and, separately, those of the mammalian inner ear. The comparison of zebrafish hair cells between the lateral line and inner ear revealed that hair cells of the two systems can be distinguished in single-cell RNA seq data even at embryonic and early larval timepoints, and that lateral line hair cells are more similar in expression profile to extrastriolar hair cells in the ear. When comparing zebrafish inner ear cells to those of the mouse, we found expected parallels between the expression profiles of striolar and extrastriolar cells in the maculae and between central and peripheral cells in the cristae of the two species. Computational comparison of '-omics' data across species is a complex task and developing appropriate methods of comparing large datasets from multiple species is an active area of research. The data generated from this study adds to a growing repository of gene expression information that can be publicly mined and used in future meta-analyses.

In Chapter 3, I presented in vivo studies characterizing hair cell addition and regeneration in the larval zebrafish ear. I quantified hair cell addition over the course of the larval phase of development and determined that little hair cell turnover occurs in the ear of zebrafish larvae. I demonstrated that both

central and peripheral type hair cells are added to the periphery of the crista during development, and that fate switching likely occurs in some hair cells to maintain organ patterning as the cristae grow. The experiments this chapter provide evidence that hair cells are indeed regenerated to recover hair cell numbers following damage in the zebrafish inner ear, rather than added through additional developmental production. Hair cells are primarily regenerated by transdifferentiation, while reactive supporting cell proliferation contributes to an equivalent pool of progenitors. This two-step regeneration mechanism is remarkably different from regeneration in the lateral line, where hair cells are replaced by a hierarchy of progenitor cell proliferation. Reexamining the literature, we found that regeneration experiments from the neonatal mouse utricle are consistent with the uncoupled mechanism of regeneration we observed in the zebrafish ear (Burns et al., 2012a; Wang et al., 2015). In both animal models, support cells proliferate but regenerated hair cells show little incorporation of cell division markers, suggesting that the two steps are independent. Future fate mapping, gene expression profiling, and other experiments in zebrafish and mouse will help to determine the extent of similarity of these mechanisms.

4.1 Future directions

The results presented here, in combination with current work from others in the field, have propelled forward the zebrafish inner ear as a model system by providing tools for the zebrafish community. There are now two genetically-encoded methods of hair cell ablation – one that works well in the cristae (Chapter 3) and one that works well in the maculae (Jimenez et al., 2021). There are an increasing number of known differentially expressed genes with functional relevance (Smith et al., 2023, 2020). Single cell sequencing data from the zebrafish inner ear are also beginning to accumulate (Jimenez et al., 2021; Qian et al., 2022; Shi et al., 2023), which can be accessed publicly and reanalyzed. The zebrafish inner ear is now poised to be a highly useful model system in which to study auditory and vestibular loss and regeneration.

Validation of the crista hair cell regeneration mechanism

In Chapter 3, I presented evidence for a temporally uncoupled mechanism for hair cell regeneration in the zebrafish cristae wherein support cells proliferate and later transdifferentiate into hair

cells. It will be necessary to further validate this mechanism and whether the two steps of this mechanism are truly uncoupled. To test whether transdifferentiation can occur in the absence of support cell proliferation, mitotic inhibitors could be introduced following hair cell ablation. Transdifferentiation of hair cells in the central organ region in the presence of these inhibitors would bolster the argument that the proliferation and transdifferentiation step of the mechanism are uncoupled from each other. This approach has been used in other models to demonstrate that proliferation is not required for hair cell regeneration (Adler and Raphael, 1996; Baird et al., 1996).

An approach to validating the transdifferentiation step of the mechanism could be to perform live imaging using a transgenic line labeling hair cell precursors. sfrp1a is a predicted wnt ligand that labels a multipotent quiescent progenitor cell population in the zebrafish lateral line (Thomas and Raible, 2019). *sfrp1a* is also expressed in the zebrafish maculae and, to a lesser extent, the cristae, but currently available single cell RNA sequencing data does not have the resolution to separate *sfrp1a*-expressing otic cells as a clearly defined subtype. My preliminary experiments indicate that ablating *sfrp1a*+ cells in the inner ear prevents hair cell regeneration, suggesting either that these cells are necessary for hair cell survival or that they themselves are hair cell progenitors. Using fish with scatter-labeling of *sfrp1a:NLS-Eos*, timelapse live imaging could be performed during regeneration which could validate the transdifferentiation model proposed in Chapter 3.

Separating differentiation from transdifferentiation of hair cells in regenerating cristae is a difficult problem that could potentially be addressed using single-cell RNA sequencing. By performing single-cell RNA sequencing on developing and regenerating larval cristae using the Trpv1 hair cell ablation system, it may be possible to distinguish the signaling pathways involved in regeneration from those at work in development. There may be individual genes that act in regeneration but not development that could be probed by HCR to identify regenerating cells within the tissue. This experiment would greatly benefit from a transgenic line labeling all otic sensory patch cells, so that cell sorting could be used to concentrate cells for sequencing. RNA velocity analysis of sequencing data from developing and regenerating ears would further enhance our understanding of the cell fate changes occurring during these processes. Performing any kind of single-cell sequencing experiment in the larval ear would circumvent difficulties of working with adult tissue, such as dissociation of rigidly structured tissues.

Spatial analysis of development and regeneration

The rapid hair cell addition during sensory organ growth in the zebrafish inner ear complicates many analyses of hair cell regeneration. Being able to delineate the growing region of the organ and the region in homeostasis would be immensely helpful in distinguishing growth and regeneration. Developing an automated pipeline for analyzing cell position within a sensory organ would be one way to approach this problem. This could be achieved using a similar method to that which has been developed to segment 3D images of lateral line hair and support cells (Hewitt et al., 2024). This pipeline would require high-resolution z-stacks of cristae with fluorescently labeled cells or nuclei and a method of rotating and/or transforming the images to standardize the area of analysis. With a top-down view of a crista, it may be possible to define a likely region of homeostasis that could be projected onto regenerating crista to determine whether hair cells that appear post-ablation are in a 'regeneration zone' as compared to a 'growth zone'.

Spatial analysis of regeneration could also potentially be used to identify hair cell precursors. During regeneration, a subset of support cells divides to increase the progenitor pool. Whether there is something inherently different about these cells from other supporting cells remains unknown. In the EdU experiments in Chapter 3, we observed that support cells dividing in growing cristae appear mostly around the periphery of the organ, whereas in regeneration more support cells divide that are centrally located. Positional mapping of nucleus centroids could be used to determine whether these dividing cells are, in fact, more likely to be centrally located in regenerating cristae. It is possible that these cells make up a damage-activated subset of support cells. Unlike in the lateral line, sequencing studies have not had the resolution to identify subtypes of supporting cells within individual otic sensory patches. In the mouse utricle, a subset of supporting cells expressing *Lgr5*, a Wnt target gene, is damage-activated and able to regenerate type I and II hair cells (Wang et al., 2015). Combining transcriptional profiling with other methods such as cell position or shape analysis may provide the higher resolution needed to identify support cell subtypes. Regardless of whether support cell subtypes are identified in the inner ear, the mechanisms that allow hair cells to acquire a positionally-appropriate identity will be an interesting and important avenue of research.

Comparison of macula and crista hair cell regeneration

Finally, it will be important to determine whether the mechanism of hair cell regeneration is similar between the cristae and maculae. To perform this analysis, it would be helpful to have a method of hair cell ablation that works in both types of organs. Whether the DTR method (Jimenez et al., 2021) of zebrafish macula hair cell ablation works in the cristae and whether it works in the ear in larval fish has not yet been published. We believe the restriction of effective ablation of hair cells to the cristae in our TrpV1 ablation model could be due to the genetic landscape of the transgene insertion site. Thus, it may be possible to develop a similar line where TrpV1 is inserted into a location that allows for more robust expression in all hair cell organs, which would allow more direct comparison of the cristae and maculae. In the mouse, the utricle is the most studied vestibular organ for hair cell regeneration, and cross-species comparison would benefit from further study of the mechanism of regeneration in the zebrafish utricle.

Ultimately, untangling the mechanisms of hair cell regeneration in the zebrafish inner ear will allow us to better understand why zebrafish are masters of regeneration and mammals are not. The information gleaned from the zebrafish inner ear could provide fruitful strategies for increasing precursor proliferation in the mammalian ear, a currently absent step in the regeneration of mammalian vestibular organs.

BIBLIOGRAPHY

Adler HJ, Raphael Y. 1996. New hair cells arise from supporting cell conversion in the acoustically damaged chick inner ear. *Neurosci Lett* **205**:17–20.

Agrawal Y, Ward BK, Minor LB. 2013. Vestibular dysfunction: Prevalence, impact and need for targeted treatment. *J Vestib Res Equilib Orientat*. doi:10.3233/VES-130498

Anniko M, Nordemar H, Van De Water TR. 1979. Embryogenesis of the inner ear. I. Development and differentiation of the mammalian crista ampullaris in vivo and in vitro. *Arch oto-rhino-laryngology = Arch für Ohren-, Nasen- und Kehlkopfheilkunde*.

Atkinson PJ, Najarro EH, Sayyid ZN, Cheng AG. 2015. Sensory hair cell development and regeneration: Similarities and differences. *Dev* **142**:1561–1571. doi:10.1242/dev.114926

Atkinson PJ, Wise AK, Flynn BO, Nayagam BA, Richardson RT. 2014. Hair cell regeneration after ATOH1 gene therapy in the cochlea of profoundly deaf adult guinea pigs. *PLoS One* **9**. doi:10.1371/journal.pone.0102077

Avallone B, Fascio U, Balsamo G, Marmo F. 2008. Gentamicin ototoxicity in the saccule of the lizard Podarcis Sicula induces hair cell recovery and regeneration. *Hear Res* **235**:15–22. doi:10.1016/j.heares.2007.09.009

Baek S, Tran NTT, Diaz DC, Tsai Y-Y, Acedo JN, Lush ME, Piotrowski T. 2022. Single-cell transcriptome analysis reveals three sequential phases of gene expression during zebrafish sensory hair cell regeneration. *Dev Cell* **57**:799-819.e6. doi:10.1016/j.devcel.2022.03.001

Baeza-Loya S, Raible DW. 2023. Vestibular physiology and function in zebrafish. *Front Cell Dev Biol* **11**:1–11. doi:10.3389/fcell.2023.1172933

Baird RA, Steyger PS, Schuff NR. 1996. Mitotic and nonmitotic hair cell regeneration in the bullfrog vestibular otolith organs. *Ann N Y Acad Sci* **781**:59–70. doi:10.1111/j.1749-6632.1996.tb15693.x

Bang PI, Sewell WF, Malicki JJ. 2001. Morphology and cell type heterogeneities of the inner ear epithelia in adult and juvenile zebrafish (Danio rerio). *J Comp Neurol* **438**:173–190. doi:10.1002/cne.1308

Beck JC, Gilland E, Tank DW, Baker R. 2004. Quantifying the ontogeny of optokinetic and vestibuloocular behaviors in zebrafish, medaka, and goldfish. *J Neurophysiol* **92**:3546–3561. doi:10.1152/jn.00311.2004

Benkafadar N, Janesick A, Scheibinger M, Ling AH, Jan TA, Heller S. 2021. Transcriptomic characterization of dying hair cells in the avian cochlea. *Cell Rep* **34**:108902. doi:10.1016/j.celrep.2021.108902

Bermingham-McDonogh O, Rubel EW. 2003. Hair cell regeneration: Winging our way towards a sound future. *Curr Opin Neurobiol* **13**:119–126. doi:10.1016/S0959-4388(03)00018-7

Bever MM, Fekete DM. 2002. Atlas of the developing inner ear in zebrafish. *Dev Dyn* **223**:536–543. doi:10.1002/dvdy.10062

Bhandiwad AA, Zeddies DG, Raible DW, Rubel EW, Sisneros JA. 2013. Auditory sensitivity of larval zebrafish (Danio rerio) measured using a behavioral prepulse inhibition assay. *J Exp Biol* **216**:3504–3513. doi:10.1242/jeb.087635

Boyle R, Highstein SM, Carey JP, Xu J. 2002. Functional Recovery of Anterior Semicircular Canal Afferents following Hair Cell Regeneration in Birds. *J Assoc Res Otolaryngol* **3**:149–166. doi:10.1007/s101620020018

Breitzler L, Lau IH, Fonseca PJ, Vasconcelos RO. 2020. Noise-induced hearing loss in zebrafish: investigating structural and functional inner ear damage and recovery. *Hear Res* **391**:107952. doi:10.1016/j.heares.2020.107952

Bucks SA, Cox BC, Vlosich BA, Manning JP, Nguyen TB, Stone JS. 2017. Supporting cells remove and replace sensory receptor hair cells in a balance organ of adult mice. *Elife* **6**:e18128. doi:10.7554/elife.18128

Burns JC, Corwin JT. 2014. Responses to Cell Loss Become Restricted as the Supporting Cells in Mammalian Vestibular Organs Grow Thick Junctional Actin Bands Develop High Stability. *J Neurosci* **34**:1998 LP – 2011. doi:10.1523/JNEUROSCI.4355-13.2014

Burns JC, Cox BC, Thiede BR, Zuo J, Corwin JT. 2012a. In vivo proliferative regeneration of balance hair cells in newborn mice. *J Neurosci* **32**:6570–7. doi:10.1523/jneurosci.6274-11.2012

Burns JC, On D, Baker W, Collado MS, Corwin JT. 2012b. Over half the hair cells in the mouse utricle first appear after birth, with significant numbers originating from early postnatal mitotic production in peripheral and striolar growth zones. *JARO - J Assoc Res Otolaryngol* **13**:609–627. doi:10.1007/s10162-012-0337-0

Burns JC, Stone JS. 2017. Development and regeneration of vestibular hair cells in mammals. *Semin Cell Dev Biol* **65**:96–105. doi:10.1016/j.semcdb.2016.11.001

Cao J, Spielmann M, Qiu X, Huang X, Ibrahim DM, Hill AJ, Zhang F, Mundlos S, Christiansen L, Steemers FJ, Trapnell C, Shendure J. 2019. The single-cell transcriptional landscape of mammalian organogenesis. *Nature*. doi:10.1038/s41586-019-0969-x

Chang JSY, Popper AN, Saidel WM. 1992. Heterogeneity of sensory hair cells in a fish ear. *J Comp Neurol* **324**:621–640. doi:https://doi.org/10.1002/cne.903240413

Chatterjee P, Padmanarayana M, Abdullah N, Holman CL, LaDu J, Tanguay RL, Johnson CP. 2015. Otoferlin Deficiency in Zebrafish Results in Defects in Balance and Hearing: Rescue of the Balance and Hearing Phenotype with Full-Length and Truncated Forms of Mouse Otoferlin. *Mol Cell Biol* **35**:1043–1054. doi:10.1128/MCB.01439-14

Chen S, Chiu CN, McArthur KL, Fetcho JR, Prober DA. 2016. TRP channel mediated neuronal activation and ablation in freely behaving zebrafish. *Nat Methods* **13**:147–50. doi:10.1038/nmeth.3691

Choi HMT, Calvert CR, Husain N, Huss D, Barsi JC, Deverman BE, Hunter RC, Kato M, Lee SM, Abelin ACT, Rosenthal AZ, Akbari OS, Li Y, Hay BA, Sternberg PW, Patterson PH, Davidson EH, Mazmanian SK, Prober DA, Van De Rijn M, Leadbetter JR, Newman DK, Readhead C, Bronner ME, Wold B, Lansford R, Sauka-Spengler T, Fraser SE, Pierce NA. 2016. Mapping a multiplexed zoo of mRNA expression. *Dev* **143**:3632–3637. doi:10.1242/dev.140137

Choi HMT, Schwarzkopf M, Fornace ME, Acharya A, Artavanis G, Stegmaier J, Cunha A, Pierce NA. 2018. Third-generation in situ hybridization chain reaction: multiplexed, quantitative, sensitive, versatile, robust. *Development* **145**:dev165753. doi:10.1242/dev.165753

Choi TY, Ninov N, Stainier DYR, Shin D. 2014. Extensive conversion of hepatic biliary epithelial cells to hepatocytes after near total loss of hepatocytes in zebrafish. *Gastroenterology* **146**:776–788. doi:10.1053/j.gastro.2013.10.019

Coffin AB, Dale E, Molano O, Pederson A, Costa EK, Chen J. 2024. Age-related changes in the zebrafish and killifish inner ear and lateral line. *Sci Rep* **14**:1–19. doi:10.1038/s41598-024-57182-z

Collaborators GBD 2019 USAHL, Haile LM, Orji AU, Reavis KM, Briant PS, Lucas KM, Alahdab F, Bärnighausen TW, Bell AW, Cao C, Dai X, Hay SI, Heidari G, Karaye IM, Miller TR, Mokdad AH,

Mostafavi E, Natto ZS, Pawar S, Rana J, Seylani A, Singh JA, Wei J, Yang L, Ong KL, Steinmetz JD. 2024. Hearing Loss Prevalence, Years Lived With Disability, and Hearing Aid Use in the United States From 1990 to 2019: Findings From the Global Burden of Disease Study. *Ear Hear* **45**.

Collado MS, Thiede BR, Baker W, Askew C, Igbani LM, Corwin JT. 2011. The Postnatal Accumulation of Junctional E-Cadherin Is Inversely Correlated with the Capacity for Supporting Cells to Convert Directly into Sensory Hair Cells in Mammalian Balance Organs. *J Neurosci* **31**:11855–11866. doi:10.1523/jneurosci.2525-11.2011

Corwin J. 1983. Postembryonic growth of the macula neglecta auditory detector in the ray, Raja clavata: continual increases in hair cell number, neural convergence, and physiological sensitivity. *J Comp Neurol* **217**:345–356. doi:10.1002/cne.902170309

Corwin J. 1981. Postembryonic production and aging of inner ear hair cells in sharks. *J Comp Neurol* **201**:541–533. doi:10.1002/cne.902010406

Corwin JT, Cotanche DA. 1988. Regeneration of Sensory Hair Cells After Acoustic Trauma. *Science (80-)* **240**:1772–1774. doi:10.1126/science.3381100

Cotanche D. 1987. Regeneration of the tectorial membrane in the chick cochlea following severe acoustic trauma. *Hear Res* **30**:197–206.

Cox BC, Chai R, Lenoir A, Liu Z, Zhang LL, Nguyen DH, Chalasani K, Steigelman KA, Fang J, Cheng AG, Zuo J. 2014. Spontaneous hair cell regeneration in the neonatal mouse cochlea in vivo. *Dev* **141**:816–29. doi:10.1242/dev.103036

Cruz IA, Kappedal R, Mackenzie SM, Hailey DW, Hoffman TL, Schilling TF, Raible DW. 2015. Robust regeneration of adult zebrafish lateral line hair cells reflects continued precursor pool maintenance. *Dev Biol* **402**:229–238. doi:10.1016/j.ydbio.2015.03.019

Cruz RM, Lambert PR, Rubel EW. 1987. Light microscopic evidence of hair cell regeneration after gentamicin toxicity in chick cochlea. *Arch Otolaryngol Neck Surg* **113**:1058–1062. doi:10.1001/archotol.1987.01860100036017

Cui G, Meyer AC, Calin-Jageman I, Neef J, Haeseeler F, Moser T, Lee A. 2007. Ca2+-binding proteins tune Ca2+-feedback to Cav1.3 channels in mouse auditory hair cells. *J Physiol* **585**:791–803. doi:10.1113/jphysiol.2007.142307

Cunningham LL, Tucci DL. 2017. Hearing Loss in Adults. *N Engl J Med* **377**:2465–2473. doi:10.1056/NEJMra1616601

Curthoys IS. 2017. The new vestibular stimuli: sound and vibration—anatomical, physiological and clinical evidence. *Exp Brain Res* **235**:957–972. doi:10.1007/s00221-017-4874-y

Daudet N, Żak M. 2020. Notch Signalling: The Multitask Manager of Inner Ear Development and Regeneration BT - Notch Signaling in Embryology and Cancer: Notch Signaling in Embryology In: Reichrath J, Reichrath S, editors. Cham: Springer International Publishing. pp. 129–157. doi:10.1007/978-3-030-34436-8_8

Dernedde J, Weise C, Müller E-C, Hagiwara A, Bachmann S, Suzuki M, Reutter W, Tauber R, Scherer H. 2014. Cupulin Is a Zona Pellucida-Like Domain Protein and Major Component of the Cupula from the Inner Ear. *PLoS One* **9**:e111917.

Desai SS, Ali H, Lysakowski A. 2005a. Comparative Morphology of Rodent Vestibular Periphery. II. Cristae Ampullares. *J Neurophysiol* **93**:267–280. doi:10.1152/jn.00747.2003

Desai SS, Zeh C, Lysakowski A. 2005b. Comparative morphology of rodent vestibular periphery. I. Saccular and utricular maculae. *J Neurophysiol* **93**:251–266. doi:10.1152/jn.00746.2003

Di Donato V, Auer TO, Duroure K, Del Bene F. 2013. Characterization of the Calcium Binding Protein Family in Zebrafish. *PLoS One* **8**:e53299.

Dickman JD, Lim I. 2004. Posture, Head Stability, and Orientation Recovery During Vestibular Regeneration In Pigeons. *J Assoc Res Otolaryngol* **5**:323–336. doi:10.1007/s10162-004-4047-0

Diep CQ, Ma D, Deo RC, Holm TM, Naylor RW, Arora N, Wingert RA, Bollig F, Djordjevic G, Lichman B, Zhu H, Ikenaga T, Ono F, Englert C, Cowan CA, Hukriede NA, Handin RI, Davidson AJ. 2011. Identification of adult nephron progenitors capable of kidney regeneration in zebrafish. *Nature* **470**:95–101. doi:10.1038/nature09669

Down M, Power M, Smith SI, Ralston K, Spanevello M, Burns GF, Boyd AW. 2005. Cloning and expression of the large zebrafish protocadherin gene, Fat. *Gene Expr Patterns* **5**:483–490. doi:https://doi.org/10.1016/j.modgep.2004.12.005

Eatock RA, Songer JE. 2011. Vestibular hair cells and afferents: Two channels for head motion signals. *Annu Rev Neurosci* **34**:501–534. doi:10.1146/annurev-neuro-061010-113710

Erickson T, Nicolson T. 2015. Identification of sensory hair-cell transcripts by thiouracil-tagging in zebrafish. *BMC Genomics* **16**:1–10. doi:10.1186/s12864-015-2072-5

Erickson T, Pacentine I V., Venuto A, Clemens R, Nicolson T. 2020. The lhfpl5 Ohnologs lhfpl5a and lhfpl5b Are Required for Mechanotransduction in Distinct Populations of Sensory Hair Cells in Zebrafish. *Front Mol Neurosci* **12**:1–14. doi:10.3389/fnmol.2019.00320

Ernest S. 2000. Mariner is defective in myosin VIIA: a zebrafish model for human hereditary deafness. *Hum Mol Genet*. doi:10.1093/hmg/9.14.2189

Faul F, Erdfelder E, Lang A-G, Buchner A. 2007. G*Power 3: A flexible statistical power analysis program for the social, behavioral, and biomedical sciences. *Behav Res Methods* **39**:175–191. doi:10.3758/BF03193146

Favre-Bulle IA, Taylor MA, Marquez-Legorreta E, Vanwalleghem G, Poulsen RE, Rubinsztein-Dunlop H, Scott EK. 2020. Sound generation in zebrafish with Bio-Opto-Acoustics. *Nat Commun* **11**:1–8. doi:10.1038/s41467-020-19982-5

Feng Y, Xu Q. 2010. Pivotal role of hmx2 and hmx3 in zebrafish inner ear and lateral line development. *Dev Biol* **339**:507–518. doi:https://doi.org/10.1016/j.ydbio.2009.12.028

Fernandez C, Goldberg JM. 1976. Physiology of peripheral neurons innervating otolith organs of the squirrel monkey. II. Directional selectivity and force response relations. *J Neurophysiol* **39**:985–995. doi:10.1152/jn.1976.39.5.985

Forge A, Li L, Corwin JT, Nevill G. 1993. Ultrastructural evidence for hair cell regeneration in the mammalian inner ear. *Science (80-)* **259**:1616–9. doi:10.1126/science.8456284

Gacek RR. 2009. Fusion as an evolutionary principle of the vertebrate labyrinth. *Ann Otol Rhinol Laryngol* **118**:845–851. doi:10.1177/000348940911801204

Gau P, Poon J, Ufret-Vincenty C, Snelson CD, Gordon SE, Raible DW, Dhaka A. 2013. The Zebrafish Ortholog of TRPV1 Is Required for Heat-Induced Locomotion. *J Neurosci* **33**:5249 LP – 5260. doi:10.1523/JNEUROSCI.5403-12.2013

Girod DA, Duckert LG, Rubel EW. 1989. Possible precursors of regenerated hair cells in the avian cochlea following acoustic trauma. *Hear Res* **42**:175–194. doi:10.1016/0378-5955(89)90143-3

Golub JS, Tong L, Ngyuen TB, Hume CR, Palmiter RD, Rubel EW, Stone JS. 2012. Hair cell replacement

in adult mouse utricles after targeted ablation of hair cells with diphtheria toxin. *J Neurosci* **32**:15093–105. doi:10.1523/JNEUROSCI.1709-12.2012

Goode CT, Carey JP, Fuchs AF, Rubel EW. 1999. Recovery of the Vestibulocolic Reflex After Aminoglycoside Ototoxicity in Domestic Chickens. *J Neurophysiol* **81**:1025–1035. doi:10.1152/jn.1999.81.3.1025

Goodyear RJ, Gates R, Lukashkin AN, Richardson GP. 1999. Hair-cell numbers continue to increase in the utricular macula of the early posthatch chick. *J Neurocytol* **28**:851–861. doi:10.1023/A:1007070121751

Goodyear RJ, Lu X, Deans MR, Richardson GP. 2017. A tectorin-based matrix and planar cell polarity genes are required for normal collagen-fibril orientation in the developing tectorial membrane. *Development* **144**:3978–3989. doi:10.1242/dev.151696

Haas P, Gilmour D. 2006. Chemokine Signaling Mediates Self-Organizing Tissue Migration in the Zebrafish Lateral Line. *Dev Cell* **10**:673–680. doi:https://doi.org/10.1016/j.devcel.2006.02.019

Haddon C, Lewis J. 1996. Early ear development in the embryo of the zebrafish, Danio rerio. *J Comp Neurol* **365**:113–128. doi:10.1002/(SICI)1096-9861(19960129)365:1<113::AID-CNE9>3.0.CO;2-6

Haden M, Einarsson R, Yazejian B. 2013. Patch clamp recordings of hair cells isolated from zebrafish auditory and vestibular end organs. *Neuroscience* **248**:79–87. doi:https://doi.org/10.1016/j.neuroscience.2013.05.062

Hailey DW, Esterberg R, Linbo TH, Rubel EW, Raible DW. 2017. Fluorescent aminoglycosides reveal intracellular trafficking routes in mechanosensory hair cells. *J Clin Invest* **127**:472–486. doi:10.1172/JCI85052

Harris J, Cheng A, Cunningham L, MacDonald G, Raible D, Rubel E. 2003. Neomycin-induced hair cell death and rapid regeneration in the lateral line of zebrafish (Danio rerio). *J Assoc Res Otolaryngol* **4**:219–234. doi:10.1007/S10162-002-3022-X

Hewitt MN, Cruz IA, Raible DW. 2024. Spherical harmonics analysis reveals cell shape-fate relationships in zebrafish lateral line neuromasts. *Development* **151**:dev202251. doi:10.1242/dev.202251

Hie B, Bryson B, Berger B. 2019. Efficient integration of heterogeneous single-cell transcriptomes using Scanorama. *Nat Biotechnol* **37**:685–691. doi:10.1038/s41587-019-0113-3

Higgs DM, Rollo AK, Souza MJ, Popper AN. 2003. Development of form and function in peripheral auditory structures of the zebrafish (Danio rerio) . *J Acoust Soc Am* **113**:1145–1154. doi:10.1121/1.1536185

Higgs DM, Souza MJ, Wilkins HR, Presson JC, Popper AN. 2002. Age- and size-related changes in the inner ear and hearing ability of the adult zebrafish (Danio rerio). *JARO - J Assoc Res Otolaryngol* **3**:174–184. doi:10.1007/s101620020035

Hoffman LF, Choy KR, Sultemeier DR, Simmons DD. 2018. Oncomodulin Expression Reveals New Insights into the Cellular Organization of the Murine Utricle Striola. *J Assoc Res Otolaryngol* **19**:33–51. doi:10.1007/s10162-017-0652-6

Holt JR, Stauffer EA, Abraham D, Géléoc GSG. 2007. Dominant-Negative Inhibition of M-Like Potassium Conductances in Hair Cells of the Mouse Inner Ear. *J Neurosci* **27**:8940 LP – 8951. doi:10.1523/JNEUROSCI.2085-07.2007

Jan TA, Eltawil Y, Ling AH, Chen L, Ellwanger DC, Heller S, Cheng AG. 2021. Spatiotemporal dynamics of inner ear sensory and non-sensory cells revealed by single-cell transcriptomics. *Cell Rep* **36**:109358. doi:10.1016/j.celrep.2021.109358

Janesick AS, Heller S. 2019. Stem cells and the bird cochlea—where is everybody? *Cold Spring Harb Perspect Med* **9**. doi:10.1101/cshperspect.a033183

Jen HI, Hill MC, Tao L, Sheng K, Cao W, Zhang H, Yu H V., Llamas J, Zong C, Martin JF, Segil N, Groves AK. 2019. Transcriptomic and epigenetic regulation of hair cell regeneration in the mouse utricle and its potentiation by Atoh1. *Elife* **8**. doi:10.7554/eLife.44328

Jiang T, Kindt K, Wu DK. 2017. Transcription factor emx2 controls stereociliary bundle orientation of sensory hair cells. *Elife* **6**:e23661. doi:10.7554/eLife.23661

Jimenez E, Slevin CC, Colón-Cruz L, Burgess SM. 2021. Vestibular and Auditory Hair Cell Regeneration Following Targeted Ablation of Hair Cells With Diphtheria Toxin in Zebrafish. *Front Cell Neurosci* **15**:721950. doi:10.3389/fncel.2021.721950

Jimenez E, Slevin CC, Song W, Chen Z, Frederickson SC, Gildea D, Wu W, Elkahloun AG, Ovcharenko I, Burgess SM. 2022. A regulatory network of Sox and Six transcription factors initiate a cell fate transformation during hearing regeneration in adult zebrafish. *Cell Genomics* **2**:100170.

doi:10.1016/j.xgen.2022.100170

Jones JE, Corwin JT. 1996. Regeneration of sensory cells after laser ablation in the lateral line system: Hair cell lineage and macrophage behavior revealed by time-lapse video microscopy. *J Neurosci* **16**:649–662. doi:10.1523/jneurosci.16-02-00649.1996

Jørgensen JM. 1991. Regeneration of lateral line and inner ear vestibular cells. *Ciba Found Symp* **160**:151–63. doi:10.1002/9780470514122.ch8

Jørgensen JM, Mathiesen C. 1988. The avian inner ear. Continuous production of hair cells in vestibular sensory organs, but not in the auditory papilla. *Naturwissenschaften* **75**:319–320. doi:10.1007/BF00367330

Kague E, Gallagher M, Burke S, Parsons M, Franz-Odendaal T, Fisher S. 2012. Skeletogenic Fate of Zebrafish Cranial and Trunk Neural Crest. *PLoS One* **7**:e47394.

Kalka M, Markiewicz N, Ptak M, Sone ED, Ożyhar A, Dobryszycki P, Wojtas M. 2019. In vivo and in vitro analysis of starmaker activity in zebrafish otolith biomineralization. *FASEB J* **33**:6877–6886. doi:https://doi.org/10.1096/fj.201802268R

Katayama A, Corwin JT. 1989. Cell production in the chicken cochlea. *J Comp Neurol* **281**:129–135. doi:https://doi.org/10.1002/cne.902810110

Kawamoto K, Izumikawa M, Beyer LA, Atkin GM, Raphael Y. 2009. Spontaneous hair cell regeneration in the mouse utricle following gentamicin ototoxicity. *Hear Res* **247**:17–26. doi:10.1016/j.heares.2008.08.010

Kharkovets T, Hardelin JP, Safieddine S, Schweizer M, El-Amraoui A, Petit C, Jentsch TJ. 2000. KCNQ4, a K+ channel mutated in a form of dominant deafness, is expressed in the inner ear and the central auditory pathway. *Proc Natl Acad Sci U S A* **97**:4333–4338. doi:10.1073/pnas.97.8.4333

Khorevin VI. 2008. The lagena (the third otolith endorgan in vertebrates). *Neurophysiology* **40**:142–159. doi:10.1007/s11062-008-9021-8

Kil J, Warchol ME, Corwin JT. 1997. Cell death, cell proliferation, and estimates of hair cell life spans in the vestibular organs of chicks. *Hear Res* **114**:117–126. doi:10.1016/S0378-5955(97)00166-4

Kinoshita M, Fujimoto C, Iwasaki S, Kashio A, Kikkawa YS, Kondo K, Okano H, Yamasoba T. 2019. Alteration of Musashi1 Intra-cellular Distribution During Regeneration Following Gentamicin-Induced

Hair Cell Loss in the Guinea Pig Crista Ampullaris . *Front Cell Neurosci* .

Kozak EL, Palit S, Miranda-Rodríguez JR, Janjic A, Böttcher A, Lickert H, Enard W, Theis FJ, López-Schier H. 2020. Epithelial Planar Bipolarity Emerges from Notch-Mediated Asymmetric Inhibition of Emx2. *Curr Biol* **30**:1142-1151.e6. doi:https://doi.org/10.1016/j.cub.2020.01.027

Kroehne V, Freudenreich D, Hans S, Kaslin J, Brand M. 2011. Regeneration of the adult zebrafish brain from neurogenic radial glia-type progenitors. *Development* **138**:4831–4841. doi:10.1242/dev.072587

Ladich F, Schulz-Mirbach T. 2016. Diversity in Fish Auditory Systems: One of the Riddles of Sensory Biology . *Front Ecol Evol* .

Lanford PJ, Popper AN. 1996. Novel afferent terminal structure in the crista ampullaris of the goldfish, Carassius auratus. *J Comp Neurol* **366**:572–579. doi:10.1002/(SICI)1096-9861(19960318)366:4<572::AID-CNE2>3.0.CO;2-1

Lapeyre P, Guilhaume A, Cazals Y. 1992. Differences in Hair Bundles Associated with Type I and Type II Vestibular Hair Cells of the Guinea Pig Saccule. *Acta Otolaryngol* **112**:635–642. doi:10.3109/00016489209137453

Lau IH, Vasconcelos RO. 2023. Noise-induced damage in the zebrafish inner ear endorgans: Evidence for higher acoustic sensitivity of saccular and lagenar hair cells. *J Exp Biol* **226**:jeb245992. doi:10.1242/jeb.245992

Lee SG, Huang M, Obholzer ND, Sun S, Li W, Petrillo M, Dai P, Zhou Y, Cotanche DA, Megason SG, Li H, Chen Z-Y. 2016. Myc and Fgf Are Required for Zebrafish Neuromast Hair Cell Regeneration. *PLoS One* **11**:e0157768.

Li A, Xue J, Peterson EH. 2008. Architecture of the mouse utricle: Macular organization and hair bundle heights. *J Neurophysiol* **99**:718–733. doi:10.1152/jn.00831.2007

Li H, Liu H, Heller S. 2003. Pluripotent stem cells from the adult mouse inner ear. *Nat Med* **9**:1293–1299. doi:10.1038/nm925

Lim DJ, Anniko M. 1985. Developmental morphology of the mouse inner ear. A scanning electron microscopic observation. *Acta oto-laryngologica*.

Lin L, Forge A. 1997. Morphological evidence for supporting cell to hair cell conversion in the mammalian utricular macula. *Int J Dev Neurosci* **15**:433–446. doi:10.1016/S0736-5748(96)00102-5

Lin V, Golub JS, Nguyen TB, Hume CR, Oesterle EC, Stone JS. 2011. Inhibition of Notch activity promotes nonmitotic regeneration of hair cells in the adult mouse utricles. *J Neurosci* **31**:15329–39. doi:10.1523/JNEUROSCI.2057-11.2011

Lindeman HH. 1969. Regional Differences in Sensitivity of the Vestibular Sensory Epithelia to Ototoxic Antibiotics. *Acta Otolaryngol* **67**:177–189. doi:10.3109/00016486909125441

Lister JA, Robertson CP, Lepage T, Johnson SL, Raible DW. 1999. nacre encodes a zebrafish microphthalmia-related protein that regulates neural-crest-derived pigment cell fate. *Development* **126**:3757–3767. doi:10.1242/dev.126.17.3757

Liu Z, Dearman JA, Cox BC, Walters BJ, Zhang L, Ayrault O, Zindy F, Gan L, Roussel MF, Zuo J. 2012. Age-Dependent In Vivo Conversion of Mouse Cochlear Pillar and Deiters Cells to Immature Hair Cells by Atoh1 Ectopic Expression. *J Neurosci* **32**:6600 LP – 6610. doi:10.1523/JNEUROSCI.0818-12.2012

Liu Z, Hildebrand DGC, Morgan JL, Jia Y, Slimmon N, Bagnall MW. 2022. Organization of the gravity-sensing system in zebrafish. *Nat Commun* **13**:5060. doi:10.1038/s41467-022-32824-w

Lombarte A, Popper AN. 1994. Quantitative analyses of postembryonic hair cell addition in the otolithic endorgans of the inner ear of the european hake, merluccius merluccius (gadiformes, teleostei). *J Comp Neurol* **345**:419–428. doi:10.1002/CNE.903450308

Lombarte A, Yan HY, Popper AN, Chang JS, Platt C. 1993. Damage and regeneration of hair cell ciliary bundles in a fish ear following treatment with gentamicin. *Hear Res* **64**:166–174. doi:10.1016/0378-5955(93)90002-I

Lopez-Schier H, Hudspeth AJ. 2006. A two-step mechanism underlies the planar polarization of regenerating sensory hair cells. *Proc Natl Acad Sci U S A* **103**:18615–20. doi:10.1073/pnas.0608536103

Lopez I, Honrubia V, Lee SC, Li G, Beykirch K. 1998. Hair cell recovery in the chinchilla crista ampullaris after gentamicin treatment: A quantitative approach. *Otolaryngol - Head Neck Surg* **119**:255–262. doi:10.1016/S0194-5998(98)70060-9

Lush ME, Diaz DC, Koenecke N, Baek S, Boldt H, St Peter MK, Gaitan-Escudero T, Romero-Carvajal A, Busch-Nentwich EM, Perera AG, Hall KE, Peak A, Haug JS, Piotrowski T. 2019. scRNA-Seq

reveals distinct stem cell populations that drive hair cell regeneration after loss of Fgf and Notch signaling. *Elife* **8**:e44431. doi:10.7554/eLife.44431

Lysakowski A, Goldberg J. 2004. Morphophysiology of the vestibular periphery In: Highstein S, Popper A, Fay R, editors. The Vestibular System. Springer-Verlag. pp. 57–152.

Ma EY, Heffern K, Cheresh J, Gallagher EP. 2018. Differential copper-induced death and regeneration of olfactory sensory neuron populations and neurobehavioral function in larval zebrafish. *Neurotoxicology* **69**:141–151. doi:10.1016/j.neuro.2018.10.002

Ma EY, Rubel EW, Raible DW. 2008. Notch signaling regulates the extent of hair cell regeneration in the zebrafish lateral line. *J Neurosci* **28**:2261–2273. doi:10.1523/JNEUROSCI.4372-07.2008

Maass JC, Gu R, Basch ML, Waldhaus J, Lopez EM, Xia A, Oghalai JS, Heller S, Groves AK. 2015. Changes in the regulation of the Notch signaling pathway are temporally correlated with regenerative failure in the mouse cochlea. *Front Cell Neurosci* **9**:110. doi:10.3389/fncel.2015.00110

Mackenzie SM, Raible DW. 2012. Proliferative regeneration of zebrafish lateral line hair cells after different ototoxic insults. *PLoS One* **7**:e47257. doi:10.1371/journal.pone.0047257

Marques IJ, Lupi E, Mercader N. 2019. Model systems for regeneration: Zebrafish. *Dev* **146**. doi:10.1242/dev.167692

Mason MM, Lee E, Westphal H, Reitman M. 1995. Expression of the Chicken β-Globin Gene Cluster in Mice: Correct Developmental Expression and Distributed Control. *Mol Cell Biol* **15**:407–414. doi:10.1128/MCB.15.1.407

Matsunaga M, Yamamoto R, Kita T, Ohnishi H, Yamamoto N, Okano T, Omori K, Nakagawa T. 2023. Stepwise fate conversion of supporting cells to sensory hair cells in the chick auditory epithelium. *iScience* **26**:106046. doi:10.1016/j.isci.2023.106046

McGraw HF, Drerup CM, Culbertson MD, Linbo T, Raible DW, Nechiporuk A V. 2011. Lef1 is required for progenitor cell identity in the zebrafish lateral line primordium. *Development* **138**:3921–3930. doi:10.1242/dev.062554

Mellado Lagarde MM, Wan G, Zhang LL, Gigliello AR, McInnis JJ, Zhang Y, Bergles D, Zuo J, Corfas G. 2014. Spontaneous regeneration of cochlear supporting cells after neonatal ablation ensures hearing in the adult mouse. *Proc Natl Acad Sci U S A* **111**:16919–16924.

doi:10.1073/pnas.1408064111

Meredith FL, Rennie KJ. 2016. Channeling your inner ear potassium: K+ channels in vestibular hair cells. *Hear Res* **338**:40–51. doi:https://doi.org/10.1016/j.heares.2016.01.015

Millimaki BB, Sweet EM, Dhason MS, Riley BB. 2007. Zebrafish atoh1 genes: Classic proneural activity in the inner ear and regulation by Fgh and Notch. *Development* **134**:295–305. doi:10.1242/dev.02734

Millimaki BB, Sweet EM, Riley BB. 2010. Sox2 is required for maintenance and regeneration, but not initial development, of hair cells in the zebrafish inner ear. *Dev Biol* **338**:262–9. doi:10.1016/j.ydbio.2009.12.011

Mo W, Chen F, Nechiporuk A, Nicolson T. 2010. Quantification of vestibular-induced eye movements in zebrafish larvae. *BMC Neurosci* **11**:110. doi:10.1186/1471-2202-11-110

Monroe JD, Rajadinakaran G, Smith ME. 2015. Sensory hair cell death and regeneration in fishes. *Front Cell Neurosci* **9**:1–18. doi:10.3389/fncel.2015.00131

Moravec WJ, Peterson EH. 2004. Differences Between Stereocilia Numbers on Type I and Type II Vestibular Hair Cells. *J Neurophysiol* **92**:3153–3160. doi:10.1152/jn.00428.2004

Mosimann C, Kaufman CK, Li P, Pugach EK, Tamplin OJ, Zon LI. 2011. Ubiquitous transgene expression and Cre-based recombination driven by the ubiquitin promoter in zebrafish. *Development* **138**:169–177. doi:10.1242/dev.059345

Musser JM, Schippers KJ, Nickel M, Mizzon G, Kohn AB, Pape C, Ronchi P, Papadopoulos N, Tarashansky AJ, Hammel JU, Wolf F, Liang C, Hernández-Plaza A, Cantalapiedra CP, Achim K, Schieber NL, Pan L, Ruperti F, Francis WR, Vargas S, Kling S, Renkert M, Polikarpov M, Bourenkov G, Feuda R, Gaspar I, Burkhardt P, Wang B, Bork P, Beck M, Schneider TR, Kreshuk A, Wörheide G, Huerta-Cepas J, Schwab Y, Moroz LL, Arendt D. 2021. Profiling cellular diversity in sponges informs animal cell type and nervous system evolution. *Science (80-)* **374**:717–723. doi:10.1126/science.abj2949

Nordemar H. 1983. Embryogenesis of the Inner Ear: Ii. The Late Differentiation of the Mammalian Crista Ampullaris in Vivo and in Vitro. *Acta Otolaryngol* **96**:1–8. doi:10.3109/00016488309132868

Obholzer N, Wolfson S, Trapani JG, Mo W, Nechiporuk A, Busch-Nentwich E, Seiler C, Sidi S, Söllner C, Duncan RN, Boehland A, Nicolson T. 2008. Vesicular Glutamate Transporter 3 Is Required for

Synaptic Transmission in Zebrafish Hair Cells. *J Neurosci* **28**:2110 LP – 2118. doi:10.1523/JNEUROSCI.5230-07.2008

Oesterle EC, Campbell S, Taylor RR, Forge A, Hume CR. 2008. Sox2 and Jagged1 expression in normal and drug-damaged adult mouse inner ear. *JARO - J Assoc Res Otolaryngol* **9**:65–89. doi:10.1007/s10162-007-0106-7

Ohta S, Ji YR, Martin D, Wu DK. 2020. Emx2 regulates hair cell rearrangement but not positional identity within neuromasts. *Elife* **9**:e60432. doi:10.7554/eLife.60432

Olt J, Johnson SL, Marcotti W. 2014. In vivo and in vitro biophysical properties of hair cells from the lateral line and inner ear of developing and adult zebrafish. *J Physiol* **592**:2041–2058. doi:https://doi.org/10.1113/jphysiol.2013.265108

Parichy DM, Elizondo MR, Mills MG, Gordon TN, Engeszer RE. 2009. Normal table of postembryonic zebrafish development: Staging by externally visible anatomy of the living fish. *Dev Dyn* **238**:2975–3015. doi:10.1002/dvdy.22113

Petko JA, Millimaki BB, Canfield VA, Riley BB, Levenson R. 2008. Otoc1: A novel otoconin-90 ortholog required for otolith mineralization in zebrafish. *Dev Neurobiol* **68**:209–222. doi:https://doi.org/10.1002/dneu.20587

Phillips BT, Storch EM, Lekven AC, Riley BB. 2004. A direct role for Fgf but not Wnt in otic placode induction. *Development* **131**:923–931. doi:10.1242/dev.00978

Picher MM, Gehrt A, Meese S, Ivanovic A, Predoehl F, Jung S, Schrauwen I, Dragonetti AG, Colombo R, Van Camp G, Strenzke N, Moser T. 2017. Ca2+-binding protein 2 inhibits Ca2+-channel inactivation in mouse inner hair cells. *Proc Natl Acad Sci* **114**:E1717–E1726. doi:10.1073/pnas.1617533114

Pickett SB, Raible DW. 2019. Water Waves to Sound Waves: Using Zebrafish to Explore Hair Cell Biology. *JARO - J Assoc Res Otolaryngol* **20**:1–19. doi:10.1007/s10162-018-00711-1

Platt C. 1993. Zebrafish inner ear sensory surfaces are similar to those in goldfish. *Hear Res* **65**:133–140. doi:10.1016/0378-5955(93)90208-I

Platt C. 1977. Hair cell distribution and orientation in goldfish otolith organs. *J Comp Neurol* **172**:283–297. doi:https://doi.org/10.1002/cne.901720207

Popper AN. 2000. Hair cell heterogeneity and ultrasonic hearing: Recent advances in understanding fish

hearing. *Philos Trans R Soc B Biol Sci* **355**:1277–1280. doi:10.1098/rstb.2000.0683

Popper AN. 1977. A scanning electron microscopic study of the sacculus and lagena in the ears of fifteen species of teleost fishes. *J Morphol* **153**:397–417. doi:10.1002/jmor.1051530306

Popper AN, Fay RR. 1993. Sound detection and processing by fish: critical review and major research questions. *Brain Behav Evol* **41**:14–38. doi:10.1159/000316111

Popper AN, Hoxter B. 1984. Growth of a fish ear: 1. Quantitative analysis of hair cell and ganglion cell proliferation. *Hear Res* **15**:133–142. doi:https://doi.org/10.1016/0378-5955(84)90044-3

Postlethwait JH. 2007. The zebrafish genome in context: ohnologs gone missing. *J Exp Zool Part B Mol Dev Evol* **308B**:563–577. doi:https://doi.org/10.1002/jez.b.21137

Poulsen RE, Scholz LA, Constantin L, Favre-Bulle I, Vanwalleghem GC, Scott EK. 2021. Broad frequency sensitivity and complex neural coding in the larval zebrafish auditory system. *Curr Biol* **31**:1977-1987.e4. doi:https://doi.org/10.1016/j.cub.2021.01.103

Qian F, Wei G, Gao Y, Wang Xin, Gong J, Guo C, Wang Xiaoning, Zhang X, Zhao J, Wang C, Xu M, Hu Y, Yin G, Kang J, Chai R, Xie G, Liu D. 2022. Single-cell RNA-sequencing of zebrafish hair cells reveals novel genes potentially involved in hearing loss. *Cell Mol Life Sci* **79**:385. doi:10.1007/s00018-022-04410-2

Ren JQ, McCarthy WR, Zhang H, Adolph AR, Li L. 2002. Behavioral visual responses of wild-type and hypopigmented zebrafish. *Vision Res* **42**:293–299. doi:https://doi.org/10.1016/S0042-6989(01)00284-X

Riley BB, Chiang MY, Farmer L, Heck R. 1999. The deltaA gene of zebrafish mediates lateral inhibition of hair cells in the inner ear and is regulated by pax2.1. *Development* **126**:5669–5678. doi:10.1242/dev.126.24.5669

Riley BB, Moorman SJ. 2000. Development of utricular otoliths, but not saccular otoliths, is necessary for vestibular function and survival in zebrafish. *J Neurobiol* **43**:329–337. doi:10.1002/1097-4695(20000615)43:4<329::AID-NEU2>3.0.CO;2-H

Roberson DF, Weisleder P, Bohrer PS, Rubel EW. 1992. Ongoing production of sensory cells in the vestibular epithelium of the chick. *Hear Res* **57**:166–74. doi:10.1016/0378-5955(92)90149-H

Roberson DW, Alosi JA, Cotanche DA. 2004. Direct transdifferentiation gives rise to the earliest new hair

cells in regenerating avian auditory epithelium. *J Neurosci Res* **78**:461–471. doi:10.1002/jnr.20271

Roberson DW, Kreig CS, Rubel EW. 1996. Light microscopic evidence that direct transdifferentiation gives rise to new hair cells in regenerating avian auditory epithelium. *Audit Neurosci* **2**:195–205.

Roberson DW, Rubel EW. 1994. Cell division in the gerbil cochlea after acoustic trauma. *Am J Otol* **15**:22–34.

Rohs P, Ebert AM, Zuba A, McFarlane S. 2013. Neuronal expression of fibroblast growth factor receptors in zebrafish. *Gene Expr Patterns* **13**:354–361. doi:https://doi.org/10.1016/j.gep.2013.06.006

Romero-Carvajal A, Navajas Acedo J, Jiang L, Kozlovskaja-Gumbriene A, Alexander R, Li H, Piotrowski T. 2015. Regeneration of Sensory Hair Cells Requires Localized Interactions between the Notch and Wnt Pathways. *Dev Cell* **34**:267–282. doi:10.1016/j.devcel.2015.05.025

Rothenaigner I, Krecsmarik M, Hayes JA, Bahn B, Lepier A, Fortin G, Götz M, Jagasia R, Bally-Cuif L. 2011. Clonal analysis by distinct viral vectors identifies bona fide neural stem cells in the adult zebrafish telencephalon and characterizes their division properties and fate. *Development* **138**:1459–1469. doi:10.1242/dev.058156

Rubel EW, Dew LA, Roberson DW, Warchol ME, Corwin JT, Forge A, Li L, Nevill G. 1995. Mammalian vestibular hair cell regeneration. *Science (80-)* **267**:701–707. doi:10.1126/science.7839150

Rubel EW, Ryals BM. 1982. Patterns of hair cell loss in chick basilar papilla after intense auditory stimulation: Exposure duration and survival time. *Acta Otolaryngol* **93**:31–41. doi:10.3109/00016488209130849

Ruben RJ. 1967. Development of the inner ear of the mouse: a radioautographic study of terminal mitoses. *Acta Otolaryngol Suppl* **220**:1–44.

Rüsch A, Lysakowski A, Eatock RA. 1998. Postnatal Development of Type I and Type II Hair Cells in the Mouse Utricle: Acquisition of Voltage-Gated Conductances and Differentiated Morphology. *J Neurosci* **18**:7487 LP – 7501. doi:10.1523/JNEUROSCI.18-18-07487.1998

Ryals BM, Rubel EW. 1988. Hair Cell Regeneration After Acoustic Trauma in Adult Coturnix Quail. *Science (80-)* **240**:1774–1776. doi:10.1126/science.3381101

Sahly I, Andermann P, Petit C. 1999. The zebrafish eya1 gene and its expression pattern during embryogenesis. *Dev Genes Evol* **209**:399–410. doi:10.1007/s004270050270

Salic A, Mitchison TJ. 2008. A chemical method for fast and sensitive detection of DNA synthesis in vivo. *Proc Natl Acad Sci U S A* **105**:2415–2420. doi:10.1073/pnas.0712168105

Sato MP, Benkafadar N, Heller S. 2024. Hair cell regeneration, reinnervation, and restoration of hearing thresholds in the avian hearing organ. *Cell Rep* **43**:113822. doi:10.1016/j.celrep.2024.113822

Saunders LM, Srivatsan SR, Duran M, Dorrity MW, Ewing B, Linbo TH, Shendure J, Raible DW, Moens CB, Kimelman D, Trapnell C. 2023. Embryo-scale reverse genetics at single-cell resolution. *Nature* **623**:782–791. doi:10.1038/s41586-023-06720-2

Sayyid ZN, Wang T, Chen L, Jones SM, Cheng AG. 2019. Atoh1 Directs Regeneration and Functional Recovery of the Mature Mouse Vestibular System. *Cell Rep* **28**:312-324.e4. doi:10.1016/j.celrep.2019.06.028

Schacht J, Talaska AE, Rybak LP. 2012. Cisplatin and Aminoglycoside Antibiotics: Hearing Loss and Its Prevention. *Anat Rec* **295**:1837–1850. doi:https://doi.org/10.1002/ar.22578

Scheibinger M, Janesick A, Benkafadar N, Ellwanger DC, Jan TA, Heller S. 2022. Cell-type identity of the avian utricle. *Cell Rep* **40**:111432. doi:10.1016/j.celrep.2022.111432

Schindelin J, Arganda-Carreras I, Frise E, Kaynig V, Longair M, Pietzsch T, Preibisch S, Rueden C, Saalfeld S, Schmid B, Tinevez JY, White DJ, Hartenstein V, Eliceiri K, Tomancak P, Cardona A. 2012. Fiji: An open-source platform for biological-image analysis. *Nat Methods* **9**:676–682. doi:10.1038/nmeth.2019

Schrauwen I, Helfmann S, Inagaki A, Predoehl F, Tabatabaiefar MA, Picher MM, Sommen M, Zazo Seco C, Oostrik J, Kremer H, Dheedene A, Claes C, Fransen E, Chaleshtori MH, Coucke P, Lee A, Moser T, Van Camp G. 2012. A Mutation in CABP2, Expressed in Cochlear Hair Cells, Causes Autosomal-Recessive Hearing Impairment. *Am J Hum Genet* **91**:636–645. doi:https://doi.org/10.1016/j.ajhg.2012.08.018

Schuck JB, Smith ME. 2009. Cell proliferation follows acoustically-induced hair cell bundle loss in the zebrafish saccule. *Hear Res* **253**:67–76. doi:10.1016/j.heares.2009.03.008

Seiler C, Finger-Baier KC, Rinner O, Makhankov Y V, Schwarz H, Neuhauss SCF, Nicolson T. 2005. Duplicated genes with split functions: independent roles of protocadherin15 orthologues in zebrafish hearing and vision. *Development* **132**:615–623. doi:10.1242/dev.01591

Sheets L, Holmgren M, Kindt KS. 2021. How Zebrafish Can Drive the Future of Genetic-based Hearing and Balance Research. *JARO - J Assoc Res Otolaryngol* **22**:215–235. doi:10.1007/s10162-021-00798-z

Sheets L, Kindt KS, Nicolson T. 2012. Presynaptic Ca_V1.3 Channels Regulate Synaptic Ribbon Size and Are Required for Synaptic Maintenance in Sensory Hair Cells. *J Neurosci* **32**:17273 LP – 17286. doi:10.1523/JNEUROSCI.3005-12.2012

Sher AE. 1971. The embryonic and postnatal development of the inner ear of the mouse. *Acta oto-laryngologica*.

Shi T, Beaulieu MO, Saunders LM, Fabian P, Trapnell C, Segil N, Crump JG, Raible DW. 2023. Single-cell transcriptomic profiling of the zebrafish inner ear reveals molecularly distinct hair cell and supporting cell subtypes. *Elife* **12**:e82978. doi:10.7554/eLife.82978

Smith ET, Pacentine I, Shipman A, Hill M, Nicolson T. 2020. Disruption of tmc1/2a/2b genes in zebrafish reveals subunit requirements in subtypes of inner ear hair cells. *J Neurosci* **40**:4457–4468. doi:10.1523/JNEUROSCI.0163-20.2020

Smith ET, Sun P, Yu SK, Raible DW, Nicolson T. 2023. Differential expression of mechanotransduction complex genes in auditory/vestibular hair cells in zebrafish . *Front Mol Neurosci* .

Smith ME, Coffin AB, Miller DL, Popper AN. 2006. Anatomical and functional recovery of the goldfish (Carassius auratus) ear following noise exposure. *J Exp Biol* **209**:4193–4202. doi:10.1242/jeb.02490

Sobkowicz HM, August BK, Slapnick SM. 1997. Cellular interactions as a response to injury in the organ of corti in culture. *Int J Dev Neurosci* **15**:463–485. doi:https://doi.org/10.1016/S0736-5748(96)00104-9

Söllner C, Burghammer M, Busch-Nentwich E, Berger J, Schwarz H, Riekel C, Nicolson T. 2003. Control of Crystal Size and Lattice Formation by Starmaker in Otolith Biomineralization. *Science (80-)* **302**:282–286. doi:10.1126/science.1088443

Söllner C, Rauch G-J, Siemens J, Geisler R, Schuster SC, Müller U, Nicolson T, Consortium the T 2000 S. 2004. Mutations in cadherin 23 affect tip links in zebrafish sensory hair cells. *Nature* **428**:955–959. doi:10.1038/nature02484

Staecker H, Praetorius M, Baker K, Brough DE. 2007. Vestibular Hair Cell Regeneration and Restoration

of Balance Function Induced by Math1 Gene Transfer. *Otol Neurotol* **28**.

Steiner AB, Kim T, Cabot V, Hudspeth AJ. 2014. Dynamic gene expression by putative hair-cell progenitors during regeneration in the zebrafish lateral line. *Proc Natl Acad Sci U S A* **111**. doi:10.1073/pnas.1318692111

Stone JS, Choi YS, Woolley SMN, Yamashita H, Rubel EW. 1999. Progenitor cell cycling during hair cell regeneration in the vestibular and auditory epithelia of the chick. *J Neurocytol* **28**:863–876. doi:10.1023/a:1007022205821

Stone JS, Cotanche DA. 2007. Hair cell regeneration in the avian auditory epithelium. *Int J Dev Biol* **51**:633–647. doi:10.1387/ijdb.072408js

Stone JS, Pujol R, Nguyen TB, Cox BC. 2021. The transcription factor sox2 is required to maintain the cell type-specific properties and innervation of type II vestibular hair cells in adult mice. *J Neurosci* **41**:6217–6233. doi:10.1523/JNEUROSCI.1831-20.2021

Stooke-Vaughan GA, Obholzer ND, Baxendale S, Megason SG, Whitfield TT. 2015. Otolith tethering in the zebrafish otic vesicle requires otogelin and α-Tectorin. *Dev* **142**:1137–1145. doi:10.1242/dev.116632

Tanaka K, Smith CA. 1978. Structure of the chicken's inner ear: SEM and TEM study. *Am J Anat* **153**:251–271. doi:https://doi.org/10.1002/aja.1001530206

Tanimoto M, Ota Y, Inoue M, Oda Y. 2011. Origin of inner ear hair cells: Morphological and functional differentiation from ciliary cells into hair cells in zebrafish inner ear. *J Neurosci* **31**:3784–3794. doi:10.1523/JNEUROSCI.5554-10.2011

Tanimoto M, Watakabe I, Higashijima S. 2022. Tiltable objective microscope visualizes selectivity for head motion direction and dynamics in zebrafish vestibular system. *Nat Commun* **13**:7622. doi:10.1038/s41467-022-35190-9

Tao L, Yu H V, Llamas J, Trecek T, Wang X, Stojanova Z, Groves AK, Segil N. 2021. Enhancer decommissioning imposes an epigenetic barrier to sensory hair cell regeneration. *Dev Cell* **56**:2471-2485.e5. doi:10.1016/j.devcel.2021.07.003

Tarashansky AJ, Xue Y, Li P, Quake SR, Wang B. 2019. Self-assembling manifolds in single-cell RNA sequencing data. *Elife* **8**. doi:10.7554/elife.48994

Taylor RR, Forge A. 2005. Hair cell regeneration in sensory epithelia from the inner ear of a urodele amphibian. *J Comp Neurol* **484**:105–120. doi:10.1002/cne.20450

Taylor RR, Jagger DJ, Saeed SR, Axon P, Donnelly N, Tysome J, Moffatt D, Irving R, Monksfield P, Coulson C, Freeman SR, Lloyd SK, Forge A. 2015. Characterizing human vestibular sensory epithelia for experimental studies: New hair bundles on old tissue and implications for therapeutic interventions in ageing. *Neurobiol Aging* **36**:2068–2084. doi:10.1016/j.neurobiolaging.2015.02.013

Thomas ED, Raible DW. 2019. Distinct progenitor populations mediate regeneration in the zebrafish lateral line. *Elife* **8**:e43736. doi:10.7554/elife.43736

Uribe PM, Sun H, Wang K, Asuncion JD, Wang Q, Chen CW, Steyger PS, Smith ME, Matsui JI. 2013. Aminoglycoside-Induced Hair Cell Death of Inner Ear Organs Causes Functional Deficits in Adult Zebrafish (Danio rerio). *PLoS One* **8**. doi:10.1371/journal.pone.0058755

Vijayakumar S, Jones SM, Jones TA, Tian C, Johnson KR. 2019. Spontaneous mutations of the Zpld1 gene in mice cause semicircular canal dysfunction but do not impair gravity receptor or hearing functions. *Sci Rep* **9**. doi:10.1038/s41598-019-48835-5

Wan G, Corfas G, Stone JS. 2013. Inner ear supporting cells: Rethinking the silent majority. *Semin Cell Dev Biol* **24**:448–59. doi:10.1016/j.semcdb.2013.03.009

Wang T, Chai R, Kim GS, Pham N, Jansson L, Nguyen1 D-H, Kuo B, May L, Jian Z, Cunningham LL, Cheng AG. 2015. Lgr5+ Cells Regenerate Hair Cells via Proliferation and Direct Transdifferentiation in Damaged Neonatal Mouse Utricle. *Nat Commun* **6**:6613. doi:10.1038/ncomms7613.Lgr5

Warchol ME, Lambert PR, Goldstein BJ, Forge A, Corwin JT. 1993. Regenerative Proliferation in Inner Ear Sensory Epithelia from Adult Guinea Pigs and Humans. *Science (80-)* **259**:1619–1622. doi:10.1126/science.8456285

Warchol ME, Speck JD. 2007. Expression of GATA3 and tenascin in the avian vestibular maculae: Normative patterns and changes during sensory regeneration. *J Comp Neurol* **500**:646–657. doi:https://doi.org/10.1002/cne.21153

Weisleder P, Rubel EW. 1992. Hair cell regeneration in the avian vestibular epithelium. *Exp Neurol* **115**:2–6. doi:10.1016/0014-4886(92)90211-8

Weisleder P, Tsue TT, Rubel EW. 1995. Hair cell replacement in avian vestibular epithelium: Supporting

cell to Type I hair cell. *Hear Res* **82**:125–133. doi:10.1016/0378-5955(94)00169-Q

Wersall J. 1956. Studies on the structure and innervation of the sensory epithelium of the cristae ampulares in the guinea pig; a light and electron microscopic investigation. *Acta Otolaryngol Suppl* **126**:1–85.

White PM, Doetzlhofer A, Lee YS, Groves AK, Segil N. 2006. Mammalian cochlear supporting cells can divide and trans-differentiate into hair cells. *Nature* **441**:984–987. doi:10.1038/nature04849

White RM, Sessa A, Burke C, Bowman T, Ceol C, Bourque C, Dovey M, Goessling W, Burns E, Zon LI. 2008. Transparent adult zebrafish as a tool for in vivo transplantation analysis. *Cell Stem Cell* **2**:183–189. doi:10.1016/j.stem.2007.11.002

Wibowo I, Pinto-Teixeira F, Satou C, Higashijima SI, López-Schier H. 2011. Compartmentalized Notch signaling sustains epithelial mirror symmetry. *Development* **138**:1143–1152. doi:10.1242/dev.060566

Wilkerson BA, Zebroski HL, Finkbeiner CR, Chitsazan AD, Beach KE, Sen N, Zhang RC, Bermingham-McDonogh O. 2021. Novel cell types and developmental lineages revealed by single-cell RNA-seq analysis of the mouse crista ampullaris. *Elife* **10**:e60108. doi:10.7554/eLife.60108

Wolf FA, Hamey FK, Plass M, Solana J, Dahlin JS, Göttgens B, Rajewsky N, Simon L, Theis FJ. 2019. PAGA: graph abstraction reconciles clustering with trajectory inference through a topology preserving map of single cells. *Genome Biol* **20**:59. doi:10.1186/s13059-019-1663-x

Xu P, Balczerski B, Ciozda A, Louie K, Oralova V, Huysseune A, Crump JG. 2018. Fox proteins are modular competency factors for facial cartilage and tooth specification. *Development* **145**:dev165498. doi:10.1242/dev.165498

Xue J, Peterson EH. 2006. Hair Bundle Heights in the Utricle: Differences Between Macular Locations and Hair Cell Types. *J Neurophysiol* **95**:171–186. doi:10.1152/jn.00800.2005

Yamasoba T, Kondo K. 2006. Supporting cell proliferation after hair cell injury in mature guinea pig cochlea in vivo. *Cell Tissue Res* **325**:23–31. doi:10.1007/s00441-006-0157-9

Yan HY, Saidel WM, Chang JS, Presson JC, Popper AN. 1997. Sensory hair cells of a fish ear: evidence of multiple types based on ototoxicity sensitivity. *Proc R Soc London Ser B Biol Sci* **245**:133–138. doi:10.1098/rspb.1991.0099

Yang C-H, Cheng C-H, Chen G-D, Liao W-H, Chen Y-C, Huang K-Y, Hwang P-P, Hwang S-PL, Huang C-J. 2011. Zona Pellucida Domain-Containing Protein β-Tectorin is Crucial for Zebrafish Proper Inner Ear Development. *PLoS One* **6**:e23078.

Yang T, Hu N, Pangršič T, Green S, Hansen M, Lee A. 2018. Functions of CaBP1 and CaBP2 in the peripheral auditory system. *Hear Res* **364**:48–58. doi:https://doi.org/10.1016/j.heares.2018.04.001

Yao Q, Desmidt AA, Tekin M, Liu X, Lu Z. 2016. Hearing Assessment in Zebrafish during the First Week Postfertilization. *Zebrafish* **13**:79–86. doi:10.1089/zeb.2015.1166

Ye L, Robertson MA, Hesselson D, Stainier DYR, Anderson RM. 2015. Glucagon is essential for alpha cell transdifferentiation and beta cell neogenesis. *Dev* **142**:1407–1417. doi:10.1242/dev.117911

Yu R, Wang P, Chen X-W. 2020. The role of gfi1.2 in the development of zebrafish inner ear. *Hear Res* **396**:108055. doi:https://doi.org/10.1016/j.heares.2020.108055

Zeddies DG, Fay RR. 2005. Development of the acoustically evoked behavioral response in zebrafish to pure tones. *J Exp Biol* **208**:1363–1372. doi:10.1242/jeb.01534

Zhou W, Boucher RC, Bollig F, Englert C, Hildebrandt F. 2010. Characterization of mesonephric development and regeneration using transgenic zebrafish. *Am J Physiol - Ren Physiol* **299**:1040–1047. doi:10.1152/ajprenal.00394.2010

Zhu S, Chen Z, Wang H, McDermott BM. 2021. Tmc Reliance Is Biased by the Hair Cell Subtype and Position Within the Ear. *Front Cell Dev Biol* **8**:570486. doi:10.3389/fcell.2020.570486